

Portland State University

**PDXScholar**

---

Dissertations and Theses

Dissertations and Theses

---

6-13-1997

# Limitations of Methods for Determining the Position of The Center of Mass of a Human Subject Performing a Sit-up

Terrence Chadwick Smith  
*Portland State University*

Follow this and additional works at: [https://pdxscholar.library.pdx.edu/open\\_access\\_etds](https://pdxscholar.library.pdx.edu/open_access_etds)



Part of the [Mechanical Engineering Commons](#)

**Let us know how access to this document benefits you.**

---

## Recommended Citation


Smith, Terrence Chadwick, "Limitations of Methods for Determining the Position of The Center of Mass of a Human Subject Performing a Sit-up" (1997). *Dissertations and Theses*. Paper 6285.  
<https://doi.org/10.15760/etd.8145>

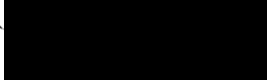
This Thesis is brought to you for free and open access. It has been accepted for inclusion in Dissertations and Theses by an authorized administrator of PDXScholar. Please contact us if we can make this document more accessible: [pdxscholar@pdx.edu](mailto:pdxscholar@pdx.edu).

## THESIS APPROVAL


The abstract and thesis of Terrence Chadwick Smith for the Master of Science in Mechanical Engineering were presented June 13, 1997, and accepted by the thesis committee and the department.

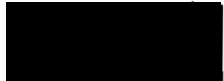
### COMMITTEE APPROVALS:

  
David A. Turcic, Chair

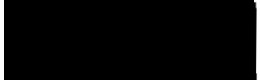
  
Paul J. Cordo

  
Gerald Recktenwald

  
Chien Wern

  
Gerardo Lafferriere  
Representative of the Office of  
Graduate Studies


### DEPARTMENT APPROVAL:

  
Graig Spolek, Chair  
Department of Mechanical Engineering

\*\*\*\*\*

ACCEPTED FOR PORTLAND STATE UNIVERSITY BY THE LIBRARY

by



on

Oct 30, 1997

## ABSTRACT

An abstract of the thesis of Terrence Chadwick Smith for the Master of Science in Mechanical Engineering presented June 13, 1997

Title: Limitations of Methods for Determining the Position of the Center of Mass of a Human Subject Performing a Sit-Up

The knowledge of the position of the center of mass of a human subject performing a sit-up could help us understand the coordination of the sit-up motion. This thesis investigates the limits in three methods of determining the center of mass of a human subject. The three methods are the anthropometric method, the dynamic method, and the static torque method. The anthropometric method is a standard method that uses measurements of the subject to estimate the mass properties of individual segments of the body. The center of mass of the body is calculated from the mass and positions of the center of mass of the segments. A Monte Carlo simulation was executed to calculate the uncertainty of using the anthropometric method. Estimated errors were introduced in the Monte Carlo simulation to determine the uncertainty of the center of mass calculation. The results of the analysis show that the uncertainty of the center of mass calculation is  $\pm 2.66$  cm for this model. The largest contribution of the uncertainty is the estimation of the mass of the segment. The dynamic method used the relations between the mass properties, the motion and ground reaction forces to solve the least squares approximation for the mass and moments

of inertia of the segments. The least squares approximation resulted negative masses and moments of inertia for some of the segments. The static method does not require separate knowledge of the mass and location of the center of mass. This method determines two coefficients per segment that combine the mass and its location. The center of mass of the body can be calculated from the location and angle of orientation of the segments. This method was determined to be limited by the precision of the force platform measurements.

LIMITATIONS OF METHODS FOR DETERMINING THE POSITION OF  
THE CENTER OF MASS OF A HUMAN SUBJECT  
PERFORMING A SIT-UP

by

TERRENCE CHADWICK SMITH

A thesis submitted in partial fulfillment of the  
requirements for the degree of

MASTER OF SCIENCE  
in  
MECHANICAL ENGINEERING

Portland State University  
1997

## TABLE OF CONTENTS

List of Tables .....	iv
List of Figures .....	v
Chapter 1	
Introduction .....	1
Chapter 2	
Equipment, Methods, and Error Description .....	13
Force Platform .....	13
Position Measurement .....	15
Anthropometric Measurements .....	15
Error Definition .....	16
Error Related to Measurement Devices .....	16
and Techniques	
Uncertainty Related to Segment .....	18
Mass Properties	
Chapter 3	
Error Analysis of Anthropometric Method .....	20
Applied to the Sit-up Motion	
Three Segment Model Description .....	22

Error Description .....	2 5
Analysis .....	2 8
Resulting Uncertainty .....	3 3
Conclusions .....	3 5

## Chapter 4

Dynamic Method .....	3 8
Theoretical Solution of a Multiple Segment Body .....	40
Application of the Theory to the .....	5 6
Sit-Up Experimental Data	
Conclusions .....	6 6

## Chapter 5

Static Torque Measurement Method .....	6 8
Theory .....	6 9
Solution of Shank and Thigh Segments .....	7 6
Analysis .....	7 9
Model Definition .....	8 0
Conclusions .....	8 4

## Chapter 6

Summary and Conclusions .....	8 6
-------------------------------	-----

Bibliography .....	90
Appendix A	
Force Platform .....	94
Appendix B	
Monte Carlo Simulation m-file 'stderror' .....	127



## LIST OF TABLES

Table 3-1	Average Male Mass Properties of the Three Segment Model Used for the Anthropometric Method Analysis	.....	2 3
Table 3-2	Uncertainties in the Mass Properties Used for the Anthropometric Method Analysis	...	2 8
Table 3-3	Standard Deviation of the Center of Mass Determined By Monte Carlo Analysis	.....	3 4
Table 4-1	Calculated Mass and Moments of Inertia for the Segments	.....	6 1
Table 5-1	Mass Properties of Thighs and Shanks	.....	8 1
Table 5-2	Actual Values of the Static Torque Constants	.....	8 2
Table 5-3	Leg Torque in Static Positions	.....	8 3
Table 5-4	Uncertainty in Static Coefficients	.....	8 4

## LIST OF FIGURES

Figure 1-1	First Stage of the Sit-up Movement .....	4
Figure 1-2	Second Stage of the Sit-up Movement .....	5
Figure 2-1	Forces measured by the force platform .....	14
Figure 3-1	The Three Segment Model Used for the Anthropometric Method Analysis .....	22
Figure 3-2	The Motion of the Three Segment Model .....	23
	Used for the Anthropometric Method Analysis	
Figure 3-3	Flow Chart of Monte Carlo Simulation .....	30
Figure 3-4	Convergence Plot of Monte Carlo .....	31
	Simulation	
Figure 3-5	Error Scatter of the Center of .....	32
	Mass of the Second Segment	
Figure 3-6	Location of the Center of Mass of the .....	35
	Model and the Two Standard Deviation Error	

Figure 4-1 The Three Segment Model Used for the Dynamic Method	.....	4 1
Figure 4-2 Free Body Diagram of Segment 1	.....	4 2
Figure 4-3 Free Body Diagram of Segment 2	.....	4 4
Figure 4-4 Free Body Diagram of Segment 3	.....	4 4
Figure 4-5 Platform Free Body Diagram	.....	5 0
Figure 4-6 Horizontal Reaction Force of the Force Platform	.....	5 7
Figure 4-7 Vertical Reaction Force of the Force Platform	.....	5 7
Figure 4-8 Reaction Torque of the Force Platform about the Reference Point	.....	5 8
Figure 4-9 Marker Position for Sit-up	.....	5 9
Figure 4-10 Horizontal Acceleration of a Torso Marker	.....	6 0

Figure 4-11	Horizontal Acceleration of a Torso Marker	60
Figure 4-12	Two Adjacent Trunk Segments	63
Figure 5-1	Position of the Center of Mass in a Supine Position	70
Figure 5-2	Force Platform Resultant and Reaction Forces	71
Figure 5-3	Position and Center of Mass of a Single Segment	73
Figure 5-4	Model Used to Solve for the Thigh and Shank Static Torque Coefficients	77
Figure 5-5	Adjusted Global Coordinate System	81

# Chapter 1

## Introduction

Sitting-up is a voluntary active movement of the body axis performed in two stages, flexion of the upper body followed by flexion of the hips. Many neuromuscular disorders affect the coordination of axial movement, yet most of our knowledge on motor coordination has come from studies of limb movement. It is hypothesized that, during the sit-up, the central nervous system controls the location of the body center of pressure to coordinate the two stages of sitting-up.

The center of pressure has static and dynamic components. To differentiate these two components, knowledge of the body center of mass is required. The goal of the project presented in this thesis was to identify an accurate method of determining the body center of mass. This study shows that the standard method using anthropometric measurement does not produce accurate results. Two other methods based on static and dynamic analysis were developed in the course of this study that also did not yield satisfactory results. The three methods have different approaches and different strengths, but the limitations of the mass estimates in the anthropometric method and measurement precision in the dynamic and static methods must be resolved before the accuracy is improved.

The separation of the static and dynamic contributions to the center of pressure will only be meaningful if the resolution of the center of mass is less than the resolution of the center of pressure. The distance between the center of pressure and the center of mass cannot be directly measured, but the magnitude of the static and dynamic forces can be estimated by comparing the magnitude of the force platform measurements to the weight of the subject. In an average sit-up of a subject weighing 740 N, the range of reaction forces acting on the table is 680-800 N. The contribution of the static forces to the center of pressure is significantly greater than the contribution of the dynamic forces, and the maximum deviation of the center of pressure from the center of mass due to the dynamic forces is approximately 3.5 cm. The resolution of the center of pressure is  $\pm 1.2$  cm, which is large in comparison to other measurements. The maximum range in of the center of pressure during the sit-up movement is 25-30 cm. Therefore, the uncertainty of the center of pressure is 4-5% of the range. The coordination of the sit-up movement involves timing of muscle activation. The precision of the muscle activation timing is obtained from eletromyogram (EMG) recordings, and it is significantly better than the uncertainty of the movement time of the center of pressure. Therefore, for the separation of the contributions of the dynamic and static components to be meaningful, the precision of the center of mass

should not be greater than the resolution of the center of pressure.

The goal of this study is to determine if the location of the center of mass of a subject performing a sit-up can be determined with a sufficient resolution. The location of the center of mass can be used to differentiate the contributions of the static and dynamic forces to the center of pressure. Therefore, the resolution of the center of mass should be less than the resolution of the center of pressure. Whole body motion involves a complex system of joints and muscles controlled by the central nervous system. The joints act as axes of rotation for the segments of the body. The muscles cause the segments to rotate about the joints. The forces on the segments are due to the internal forces of the muscles and joints, external ground reaction forces, force due to gravity, and inertial forces due to the acceleration of the segments. The sum of the forces over the segments of the body results in the total ground reaction force acting at the center of pressure. Assuming that all ground reaction forces act upward, the center of pressure must lie inside the points that are in contact with the ground.

Therefore, to lift a segment off the ground, the center of pressure must not be located under it. The central nervous system controls the motion of the body parts during a sit-up such that the center of pressure takes a series of favorable positions, the segments are lifted, and the sit-up succeeds. The initial position of the center of pressure is located between the pelvis and the

ribs. Therefore the sit-up requires two stages. The first stage, shown in Figure 1-1, is a series of upper body flexions that move the center of pressure (COP) through the hip joint.

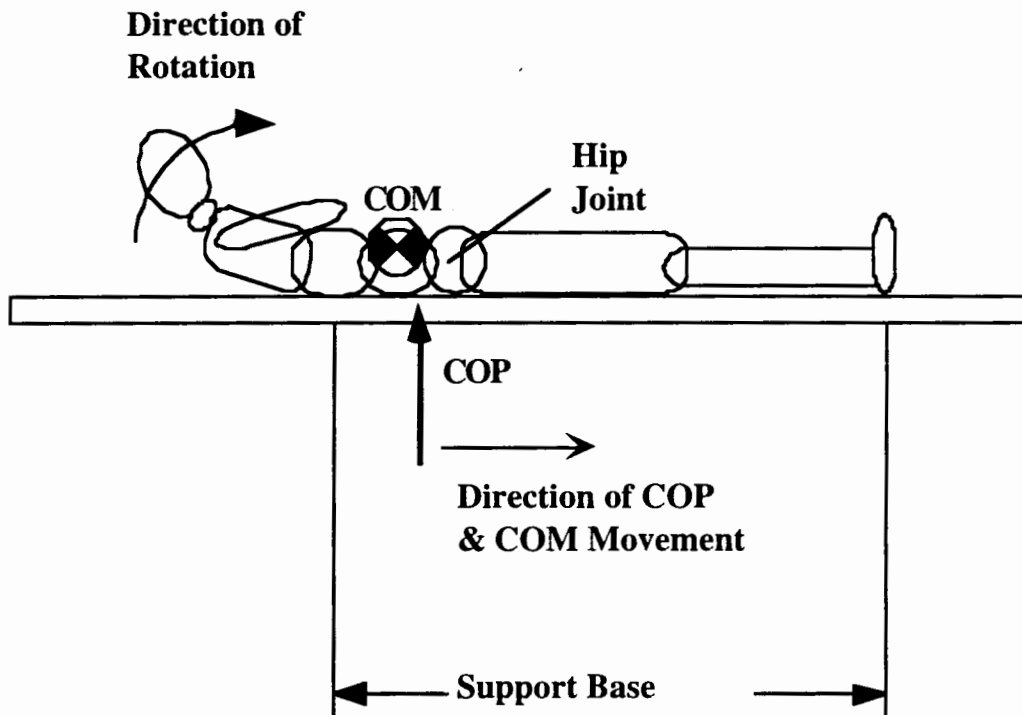


Figure 1-1 First Stage of the Sit-up Movement

The first stage of the sit-up begins with the head, which is lifted and rotated toward the feet. Head rotation causes the centers of mass and pressure to shift in the direction of the feet. After the head begins to rotate, the shoulders are lifted and rotated, again moving the centers of mass and pressure toward the feet. This sequence of body movements continues with the trunk until the center of pressure is moved through the hip joint. At this point the second phase, shown in Figure 1-2, of the sit-up begins.



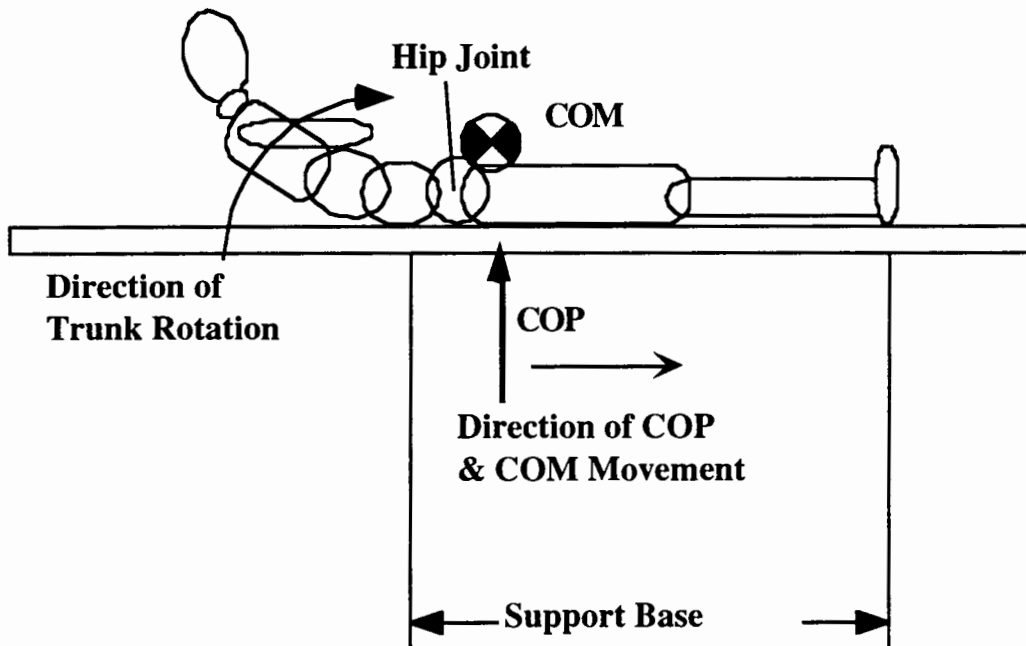


Figure 1-2 Second Stage of the Sit-up Movement

The center of pressure is in a favorable position to permit hip flexion, and the trunk is raised. The center of mass position has the largest influence over the position of the center of pressure, but the dynamic effects due to movements of the mass also contribute. The separation of the static and dynamic contributions to the location of the center of pressure could increase the understanding of how the central nervous system coordinates whole body motion. Therefore, this study attempts to define an accurate method of determining the position of the center of mass of a human subject performing a sit-up motion. The contributions of the static and dynamic forces to the location of the center of mass can be determined from knowledge of the position of the centers of mass and pressure and the weight of

the subject. Therefore, the calculation of the center of mass should not be worse than the measurement of the center of pressure.

Mathematical models of the human body are fundamental to the study of human movement dynamics. An accurate description of the position and motion of the center of mass, the mass distribution, and the moments of inertia of the body can contribute to the understanding of coordination. The study of the physical properties of the body has been the focus of research for the past 300 years [McConville 1980]. One of the most common methods of determining the position of the center of mass developed by Clauser et al. was reported in 1969. This method relates anthropometric measurements to segment mass properties in cadavers. The body was divided into segments that were assumed to have rigid body characteristics. The measurements related the cadaver's weight, height, and segment measurements to the mass, location of the center of mass, and moment of inertia of individual segments.

Biomechanists apply the anthropometric relationships to living subjects. The body is modeled with multiple rigid segments, and the joint and ground reaction forces can be predicted if the motion of the segments is known. The accuracy of this method is limited to the accuracy of the estimates of the physical properties of the segments and the resolution of the motion recording

system used to determine the positions and accelerations of the segments. The static and dynamic methods developed in this study investigate different ways of determining the mass properties of the segments using a force platform and motion recording system. The limitations of these methods are based on the measurement resolution. A description of the measurement equipment and their sources of uncertainty are discussed in Chapter 2.

The anthropometric method is commonly used to estimate reaction forces in the limbs and to perform gait analysis. The uncertainty associated with this method, which has not been well documented [Andrews 1996], is the focus of Chapter 3. This study investigated the accuracy of the anthropometric method applied to a human subject performing a sit-up. A simple three segment rigid body model was developed using the motion analysis software package Working Model 2D 4.0. The three segments of the model represented mass properties of the torso, thighs and shanks of an average male subject. The two joints were given torque inputs that cause the model to sit-up from a supine position. The motion and ground reaction forces were recorded similarly to the acquisition during a laboratory experiment with the exception that there were no errors in the model or the measured position and ground reaction forces. A Monte Carlo analysis was performed on the recorded data to determine the uncertainty range of the model's center of mass

calculation using MATLAB 5.0. The random noise and systematic errors of the hypothetical measurement systems and estimates of the segment mass properties were superimposed on 'clean' data and the resulting center of mass of the body was calculated.

Noise was added to the Working Model data to simulate the effects of normal laboratory conditions. One source of error produced by the external measurement system examined in this study is the resolution of the motion recording system. Sources of error (see Chapter 3) include estimates of the masses of the segments, locations of the centers of mass, estimations of the moments of inertia, and skin slippage relative to the skeletal structure. Sources of error not considered in this study are the movement of the internal organs and muscles relative to skeletal structure. This is a potentially large source of error especially in the torso region [Kingma 1995]. The sit-up motion requires large flexion of the torso, and therefore, it is prone to errors in the estimations of the mass properties. This uncertainty is difficult to model, and there has not been a significant amount of research investigating the effects of this error.

The results of the uncertainty analysis in the anthropometric method show that 95% of the results would lie within  $\pm 2.66$  cm of the actual center of mass of the model. The resolution of the center of pressure calculated from the force platform measurements is 1.2 cm. Therefore, the anthropometric model

does not satisfy the resolution requirements. The actual error in a human subject would be larger because the subject has more segments than the three modeled in this study. Movement of the soft tissues and muscles would also contribute error. The most significant source of error was due to the uncertainty in the estimate of the segment mass. The analysis of the three segment model that only superimposed the error due to the mass estimate predicted an uncertainty of  $\pm 2.56$  cm for a 95% confidence level. Therefore, this study shows that the largest reduction in the uncertainty could be achieved by reducing the uncertainty of the segment mass.

Chapter 4 of the study outlines a dynamic approach for determining the mass properties of individual segments of a human subject. The goal of this approach was to reduce the error due to the uncertainty of the masses of the segments that were found in the anthropometric model and increase the number of segments in the torso to better estimate the flexibility of the torso. First, a theoretical solution was formed that related the ground reaction forces, motion, and mass properties of three segment body performing a sit-up motion. The solution resulted in a set of linear equations written in matrix form, which can be solved using a least squares approximation approach. The generalized equations were written in matrix form and applied to a set of real motion and force platform data. The resulting solution for the masses and moments of inertia was found to be

unrealistic. The solution to the least squares fit of the data returned non-positive masses and moments of inertia for some of the segments. One of the sources of unrealistic results was attributed to the small magnitude of the terms of the relative accelerations of the segments in comparison to the precision of the measurement devices. The study shows that the independent terms that relate the mass and acceleration of the trunk segments have a maximum magnitude of 0.8 N. This is considerably smaller than the force platform precision of 2.5 N. The moment of inertia results are dependent on the angular accelerations and the resultant moments applied to the force platform. The maximum magnitude of the moment of inertia and angular acceleration product of the segments is 4.8 Nm applied by the thighs. This is only 2.5 times the 1.9 Nm precision of the force platform torque measurement. The smallest product, 0.03 Nm, is contributed by the trunk segments, and is considerably less than the precision of the platform. The resolution of the force platform and the small magnitude of the independent forces have a significant effect on the calculation of the mass properties. The magnitude of this error in comparison to other sources of error is not included in this study. Further investigation in this area is needed before this method is abandoned or successfully applied.

Chapter 5 outlines and evaluates the static torque method of determining the center of mass of a subject. The location of the

center of mass of the body can be determined by dividing the sum of the static torque of the segments by the sum of their weights. The position of the center of mass is not dependent on the dynamic motion and properties of the segments. Therefore, at each point in time, the center of mass can be determined if the position of the body segments are known. The advantage of the static approach over the anthropometric and dynamic approaches is that it does not require specific knowledge of the mass or the location of the center of mass of the segment. The disadvantage is the reliance on highly accurate force platform measurements which are not currently available. The static method uses force platform measurements of a subject in different static positions to determine the coefficients that relate the location and orientation of the segments to the static torque. The application of this technique to the two largest and most definable segments, the thighs and shanks, while considering the uncertainty of the force platform measurements as the only source of error, results in an uncertainty margin of  $\pm 2.7$  cm for the legs of the body. This margin is larger than that obtained from the three segment model of the whole body using the anthropometric method outlined in Chapter 3. The uncertainty of the static method could be reduced by increasing the precision of the force platform, but the errors increase dramatically when the method is applied to the trunk segments. The segments of the trunk are not well defined and the joint motion range is much smaller than the hip and knee joints. The conclusion of this section is that the

accuracy of the force platform limits the accuracy of the method to large segments with definite axes of rotation and large ranges of motion.

The final chapter of the thesis summarizes the analysis and limitations of the previously outlined methods of determining the location of the center of mass. The analysis shows that these three methods in the form presented result in an inadequate resolution of the center of mass of a human subject performing a sit-up.



## Chapter 2

### Equipment, Methods, and Error Description

The following section outlines the measurement devices used and description of the errors that will be discussed and analyzed in the following chapters. The goal of this chapter is to familiarize the reader with the terms and measurement devices that are used in the analysis of the three methods of determining the center of mass.

#### Force Platform

The ground reaction forces are recorded while a human subject performs a sit-up on a force platform. The force platform is a rigid 66 x 142 cm aluminum plate supported at the corners.

There are two end plates that are bolted on that increase the total support surface to 192 cm. The reaction forces are determined by strain gages attached to the load cells. The strain gages are arranged to measure the displacement and the proportionate force in the vertical and horizontal directions as shown in Figure 2-1.

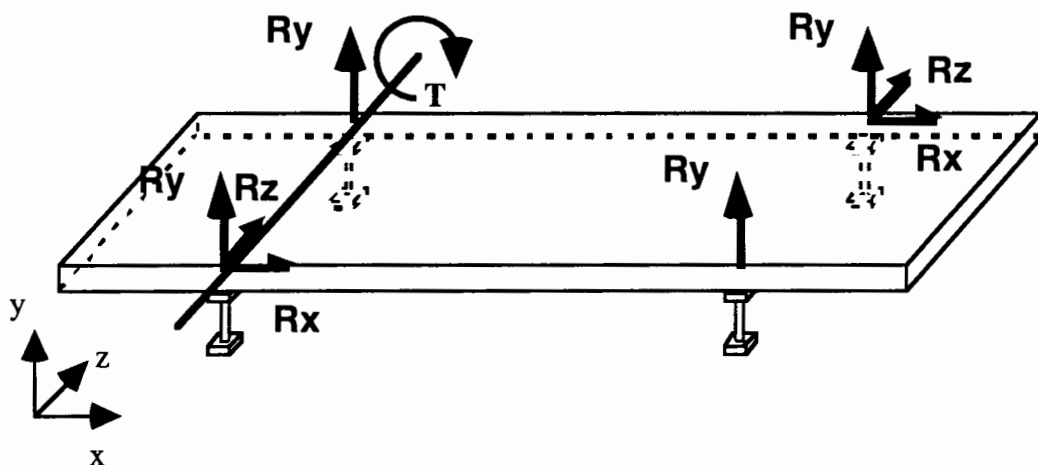


Figure 2-1 Forces measured by the force platform.

The voltages of the strain gages are sampled at 500 Hz and are used to determine the forces and torque acting on the platform. The forces and torques are calculated from the difference in the strain gage voltages of a known load and a reference load. For example, in a sit-up experiment the weight of the subject is measured independently of the force platform using a scale. The weight of the subject is used as the reference. Any changes in the forces applied to the platform are measured as changes in the strain gage voltages relative to the reference voltages when no dynamic forces are acting on the platform. The uncertainty in the horizontal and vertical force measurement is  $\pm 2.4$  N. The torque acting on the platform is defined about the z axis at the left end supports. The uncertainty of the torque measurements is  $\pm 1.9$  Nm. For more details on the construction and accuracy of the force platform refer to the Force Platform Appendix.

## Position Measurement

The position and motion of the subject are also measured. A motion analysis system (Elite manufactured by BTS, Milan, Italy) is used to record the position of reflective markers affixed to the subjects side. Infrared light is reflected off of the markers and captured by two cameras. The position is determined in three dimensional space. The motion of the markers for the duration of the sit-up is planar, and therefore, only the x and y coordinates are used. The software records the position of the markers within  $\pm 0.5$  mm in the xy plane at 50 Hz.

## Anthropometric Measurements

The use of anthropometric measurements is one of the most common methods of determining the center of mass of a subject. Total body weight, height, and segment dimensions of a subject can be directly measured. The anthropometric method developed by Clauser et al. uses these measurements to estimate the mass, location of the center of mass, and the moment of inertia for 19 segments of the body [McConville 1980]. The 19 segments include both the right and left side of the body. For sit-up analysis, the right and left halves of the body are considered to have identical mass properties and motion. Therefore, the number of segments is reduced. The analysis of this method is

the subject of Chapter 3, where the analysis is simplified by combining the mass properties and errors to produce three segments. The position and acceleration of the three resulting segments and their estimated mass properties are used to determine the position of the center of mass.

## Error Definition

### Uncertainty Related to Measurement Devices and Techniques

There are three sources of error considered in this study related to the measurement devices and techniques. The three errors are the marker position error, the force plate precision, and the skin slippage.

The marker position error referred to in the measurement methods section was reported to be 0.5 mm in the xy plane (Elite manufactured by BTS, Milan, Italy). This is an error in position that becomes significant when it is used to calculate the acceleration. The acceleration is the second derivative of the position. The error in the acceleration could be as large as twice the precision divided by the square of the sample interval or  $2.5 \text{ m/s}^2$ . The positional error and consequentially the acceleration error is reduced by smoothing the sampled position data using the low pass Butterworth filter described in Appendix A. The

error in marker position is considered in the analysis of the anthropometric method. The marker position error is added to the 'clean' marker location data and the filter characteristics are included as part of the analysis. The dynamic method also smoothes the position data before it is used to calculate the mass properties of the segments.

Force plate precision was also mentioned in the measurement methods section. The uncertainty in the force measurements is  $\pm 2.4$  N. The uncertainty of the torque measurements is  $\pm 1.9$  Nm. These errors contribute to the difficulties in the least squares approximation of the mass properties using the Dynamic Method described in Chapter 4. The uncertainty also defines the limits of the usefulness of the Static Torque Method described in Chapter 5 of this paper.

The measurement technique used to locate the joints is also a source of systematic error. Marker positions shift due to skin movement, as the body moves and the skin stretches. This error, referred to as skin slippage error, can cause a marker displacement as large as 20 mm [Cappozzo 1993]. The segments of the body are defined by the joints located at the extremes of the segment, and the center of mass of the segment is defined relative to the positions of the joints. Therefore, the skin slippage could cause an error in the location of the joint, and as a consequence, an error in the location of the center of mass of the

segment. Skin slippage error is used to determine the uncertainty of the center of mass of the body using anthropometric methods.

## Uncertainty Related to Segment Mass Properties

Estimations of the mass properties of the segments using the anthropometric measurement method also introduce some uncertainty. The anthropometric method uses the measurements of the body to estimate the mass, location of the center of mass and the moment of inertia of the segments. The estimation is based on cadaver studies performed by Clauser et al. in 1969 [McConville 1980]. The uncertainties associated with the estimates of the mass properties are not easily determined. To determine the actual properties of the segments, each segment would have to be separated from the rest of the body. Clauser (1969) reported the standard deviation of the sample used in his study, and this is commonly used as an estimate of the error. Several studies have attempted to increase the accuracy of segmental mass properties, but it is difficult to determine if the results of these studies achieved their goal. For the analysis presented in this study, the standard deviations of Clauser's results will be used to model the uncertainty as normally distributed error of the mass and moment of inertia. The uncertainty of the location of the center of mass of  $\pm 5\%$  of the segment length and width is used [Andrews 1996]. These

uncertainties are used to determine the uncertainty in the center of mass of a human subject performing a sit-up using the anthropometric method.

## Chapter 3

### Error Analysis of Anthropometric Method Applied to the Sit-up Motion

This section describes the use of anthropometric modeling to determine the position of the center of mass of a human subject performing a sit-up. The goal of this analysis was to determine if the accuracy of the anthropometric method is sufficient to determine the center of mass of a subject within the  $\pm 1.2$  cm precision of the center of pressure. The analysis uses a three segment rigid body model designed in Working Model 2D to generate a mathematical description of the motion and ground reaction forces of an average male subject performing a sit-up. An accurate mathematical model of the body allows the number and magnitude of the errors entering the system to be controlled. For example, the effect of the marker position error can be introduced as the only source of error without including the errors due to the uncertainties in the mass properties.

The errors considered in this investigation of the anthropometric model were due to the errors in the estimated mass properties and the measurement methods and devices. The human body consists of soft tissues enveloping a rigid skeleton. Therefore, movement of soft tissues relative to the skeleton hinders the definition of rigid segments and introduces errors in the rigid



body assumptions. Skin slippage error and joint characteristics combined make it difficult to define the segment axes of rotation and location of the center of mass. The location of the centers of rotation of the joints are also not easily defined, and in some joints there is no single point that can be considered the center of rotation [Leva 1996]. Therefore, for this analysis the joints of the body are modeled as simple mechanical joints.

Soft tissue characteristics are also responsible for the errors associated with the estimates in the location of the center of mass, the magnitude of the mass, and the moment of inertia. This is especially true in the torso. The model simplifies the problem by defining rigid segments, well defined joints, and eliminating measurement noise from the system. A Monte Carlo analysis is used to estimate the combined uncertainty in the center of mass of the body. The real environment is simulated by adding noise to the 'clean' signal as an approximation of the error associated with the uncertainties of the mass, location of the center of mass, moment of inertia, skin slippage, and segment marker position resolution. The center of mass is then calculated using the noisy data. This process is repeated until the standard deviation of the result converges.

## Three Segment Model Description

A three segment model of a body performing a sit up is used to analyze the effects of the previously mentioned uncertainties. The model was constructed using the motion simulation software Working Model 2D. The axial motion of the sit-up is considered to be symmetrical across the median plane of the body, and as a result, only planar motion is considered. Therefore, a two dimensional model is used. The three segments of the model represent the upper body, the thighs, and the shanks as shown in Figure 3-1.

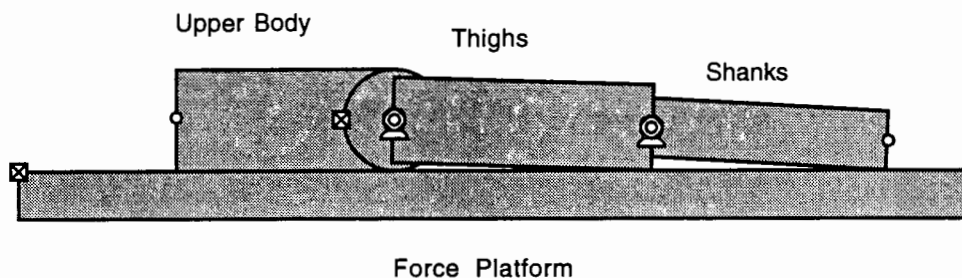


Figure 3-1 The Three Segment Model Used for the Anthropometric Method Analysis

To reduce the complexity of the model, the divisions used by the anthropometric method are combined into three segments. The upper body segment represents the mass and inertia properties of the head, neck, trunk, and torso. Divisions included in the upper body segment are assumed to be rigid and the joints are

locked. The model of the shanks includes the mass properties of the foot. The model assumes that the right and left leg have identical mass properties and movements, and therefore, both thighs are modeled as a single segment. The same assumption is used for the shanks. The mass properties, given in Table 3-1, of the model are similar to the mass properties of an average male [McConville 1980].

Table 3-1 Average Male Mass Properties of the Three Segment Model Used for the Anthropometric Method Analysis

Segment	Mass (kg)
Torso	45
Upper Leg	15
Lower Leg	8.8

The motion of the model is shown in Figure 3-2.

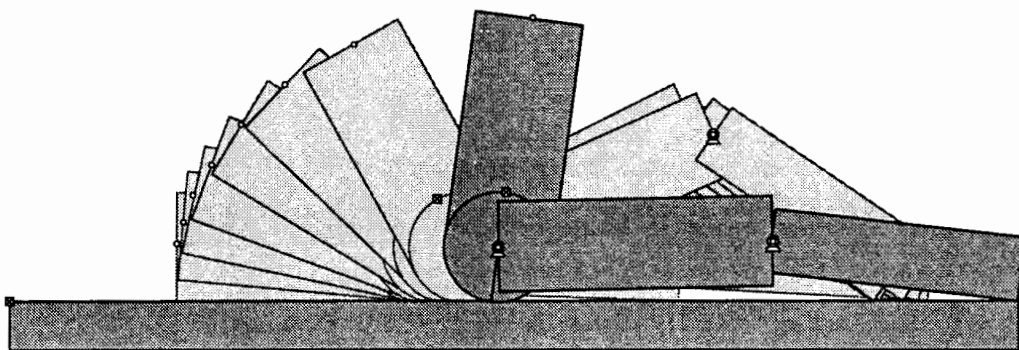


Figure 3-2 The Motion of the Three Segment Model Used for the Anthropometric Method Analysis

The motion of the three segment model is approximately the same as a subject performing the trunk rotation of the second phase of a sit-up. The second phase of the sit-up occurs after the center of pressure has passed through the hip joint and is in a favorable position for torso rotation. The trunk flexion of the first phase of the sit-up would require a more complex model and the model of the second phase is adequate to demonstrate the accuracy of the anthropometric method of determining the center of mass. Segment masses and joint torques were defined to give the range of segment motion, acceleration and ground reaction forces present in an average sit-up. The time required for the model to complete the second phase was two seconds. The knee joint applies a constant torque of 6.25 Nm which is less than the 15.5 Nm static torque of the lower leg, which allowed the model to use the lower leg as a counter balance. The joint at the hip was assigned a constant angular velocity of 45 deg/s. The vertical force, horizontal force and torque of the support surface were determined from the model. The motion of the markers at the extremities of the segments were also determined. This is equivalent to the data that is recorded during a sit-up experiment.

The numerical results of the forces and motion calculated using Working Model was 'clean', that is, there were no errors in the numerical results or the model. The joint location and axes of rotation were well defined. The segments are rigid, and

therefore, there are no errors in the model due to soft tissue movement or estimates of the mass, location of the center of mass, or moments of inertia. The resulting data was then used to add error in a controlled environment. The effects of individual errors were studied as well as the combined effects of all of the errors. The errors analyzed in this study are described in the following section.

## Error Description

This section outlines the errors that were considered in this study. The source, significance, and magnitude of each error is summarized in the following sections. The introduction of the error into the Monte Carlo simulation is also described.

The first error considered was the marker position error. The motion analysis systems commonly used have an error range of  $\pm 1.0$  mm in a viewing range of 1.0 m [Borget 1996]. The motion analysis system used in this analysis has an uncertainty of  $\pm 0.5$  mm (Elite manufactured by BTS, Milan, Italy). The marker position error becomes significant when it is differentiated to calculate the acceleration of the markers [Koopman et al. 1995; Kingma 1995]. The sampling rate of the marker position is 50 Hz. Therefore, the error in the acceleration calculation could be as high as  $\pm 2.5$  m/s<sup>2</sup>. The data is filtered using the low pass Butterworth filter in Appendix A to eliminate the noise due to the

marker position uncertainty. The marker position error is introduced into the model as normally distributed random noise, magnitude  $\pm 0.5$  mm, at each marker point for each sample. After the filter is applied the error has been reduced, but other errors may have entered the system due to the characteristics of the filter. Therefore, the filtered data has any error the filter introduced in addition to the attenuated original noise.

The second error considered is due to skin slippage. The skin is not firmly attached to the skeletal structure and moves relative to the bony landmarks used to define the segments. The skin slippage at the major joints is as large as 2.0 cm [Cappozzo 1993]. The magnitude of this slippage is related to the angle of joint rotation. It is assumed that the maximal error will occur at the maximal joint rotation. The error introduced in this study is defined as a uniformly random magnitude between 0 and 2.0 cm multiplied by the ratio of the joint angle to 90 degrees. Therefore, for each iteration in the Monte Carlo simulation the magnitude is a constant between 0 and 2.0 cm multiplied by the ratio of the angle. This accounts for the fact that the amount of skin slippage of specific a joint and person is unknown. So the random error is the magnitude of the slippage, and the systematic error is related to the joint angle. Since this error is systematic it does not introduce noise into the acceleration calculation.

The third set of errors relate to the physical properties of the segments. These properties include the mass and the location of the center of mass of each segment. For this analysis, the uncertainties reported by McConville et al. (1980) on the moment's of inertia, volume, and densities of Clauser's segments were used. The uncertainties in the density and volume are used to determine the uncertainty in the mass. For the three segments defined in this analysis, the error estimate must reflect the combined error of the parts that are included in the segment. For example, the torso's estimated error properties must include the error associated with the anthropometric method's torso, head, neck, arms and hands. In the same way the shanks must include the error estimates of the feet. Since divisions are set in a fixed orientation with respect to each other, the error estimates can also be combined to reflect the total error of the larger segment. The uncertainties of the mass properties for the three segments used in this analysis are shown in Table 3-2.

Table 3-2 Uncertainties in the Mass Properties Used for the  
Anthropometric Method Analysis

Segment	Mass	CoM	CoM
		Location	Location
		Long Axis	Short Axis
Torso	10.32%	5% x Length	5% x Width
Upper Legs	8.29	5% x Length	5% x Width
Lower Legs	7.65	5% x Length	5% x Width

The error in the location of the segment center of mass was assigned a deviation of  $\pm 5\%$  of the length and width of the segment along the long and short axis respectively [Andrews 1996]. The mass property errors were considered to be normally distributed because they are derived from the standard deviation of a sample population.

## Analysis

The analysis of the error propagation was done by comparing the actual measurements of the force platform reaction forces, and the center of mass to the calculated results after the error has been added. The force platform reaction forces were determined from the following equations.



### Vertical Forces

$$F_y = \sum_{i=1}^{\# \text{ of Segments}} m_i a_{y_i} \quad (\text{Eq 3-1})$$

### Horizontal Forces

$$F_x = \sum_{i=1}^{\# \text{ of Segments}} m_i a_{x_i} \quad (\text{Eq 3-2})$$

### Torque

$$T = \sum_{i=1}^{\# \text{ of Segments}} (m_i y_i a_{x_i} + m_i x_i a_{y_i} + I_i \alpha_i) \quad (\text{Eq 3-3})$$

The location of the center of mass along the x axis is determined by the following equation.

### Center of Mass

$$CoM = \frac{\sum_{i=1}^{\# \text{ of Segments}} m_i g x_i}{\sum_{i=1}^{\# \text{ of Segments}} m_i g} \quad (\text{Eq 3-4})$$

The direct calculation of the uncertainty of the center of mass, center of pressure, and the force platform reaction forces would be very laborious. Therefore, a Monte Carlo analysis was used to simulate the errors and calculate the uncertainty. The Monte Carlo analysis allows the errors to be introduced independently. The flow chart in Figure 3-3 shows the process used for each iteration in the analysis.

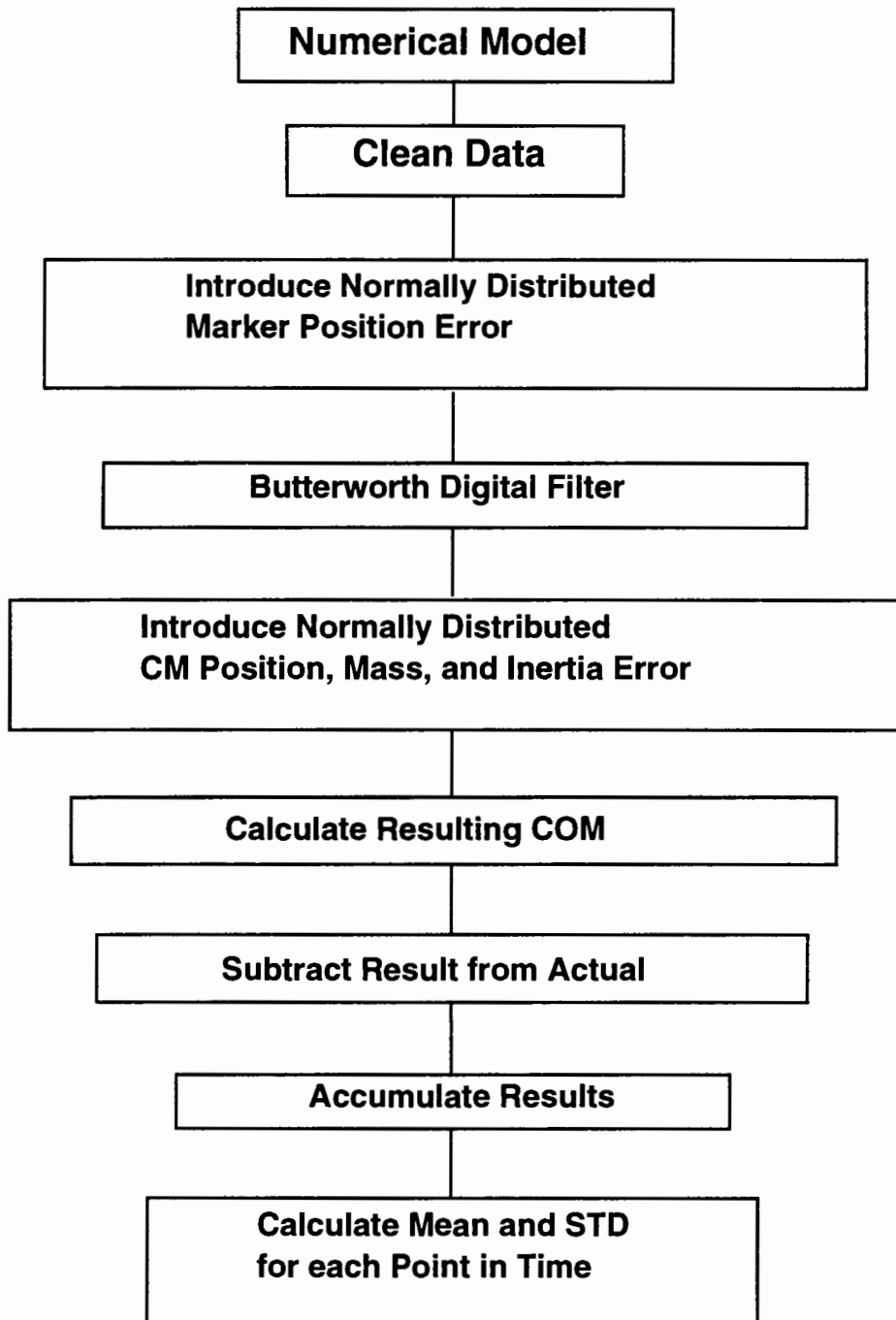


Figure 3-3 Flow Chart of Monte Carlo Simulation

The simulation kept track of the previous 100 iterations of the center of mass mean standard deviation. The maximum difference between iterations was used as a measure of the convergence. If the maximum difference in the standard deviation of the last 100 iterations was not greater than 0.001 cm then the simulation was considered to have converged. Figure 3-4 shows a plot of the convergence.

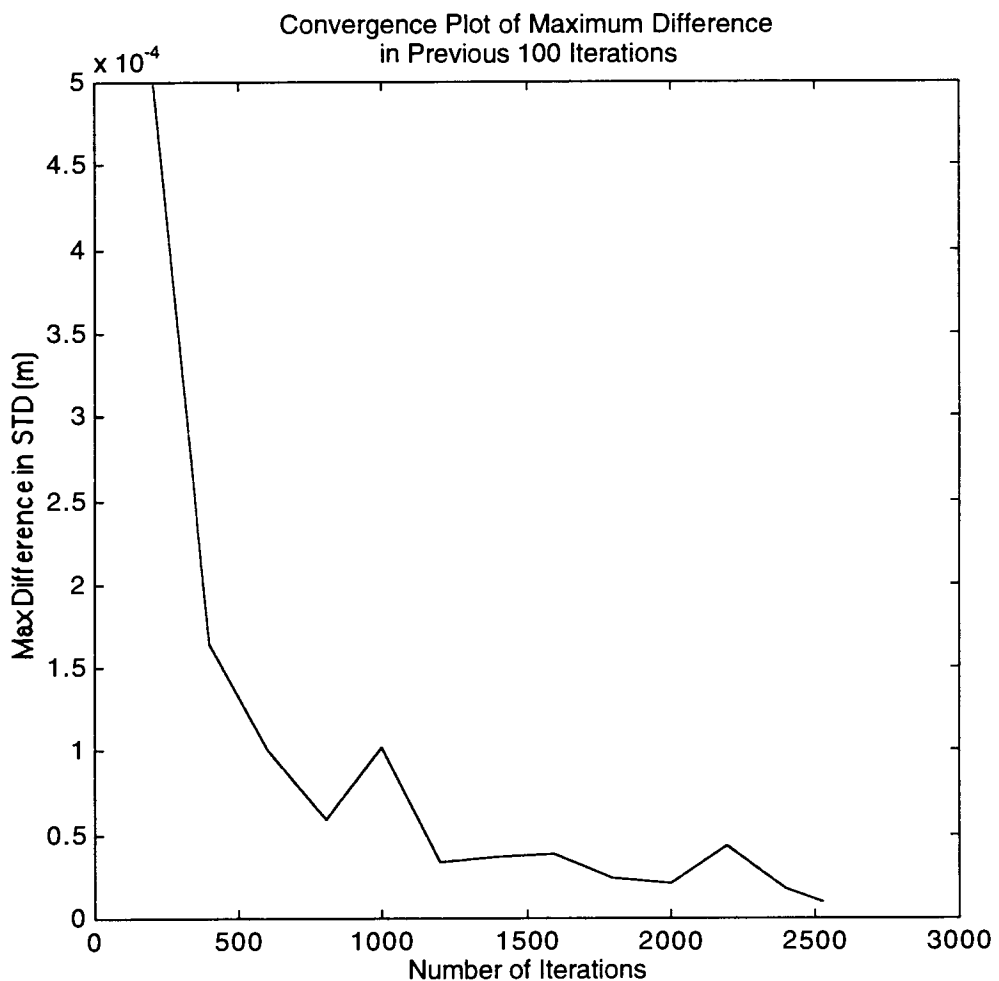


Figure 3-4 Convergence Plot of Monte Carlo Simulation

The error due to the skin slippage, marker position, and estimated center of mass caused a deviation from the actual center of mass of the segment. The scatter of the location of the center of mass of the thigh segment for 1000 iterations is shown in Figure 3-5.

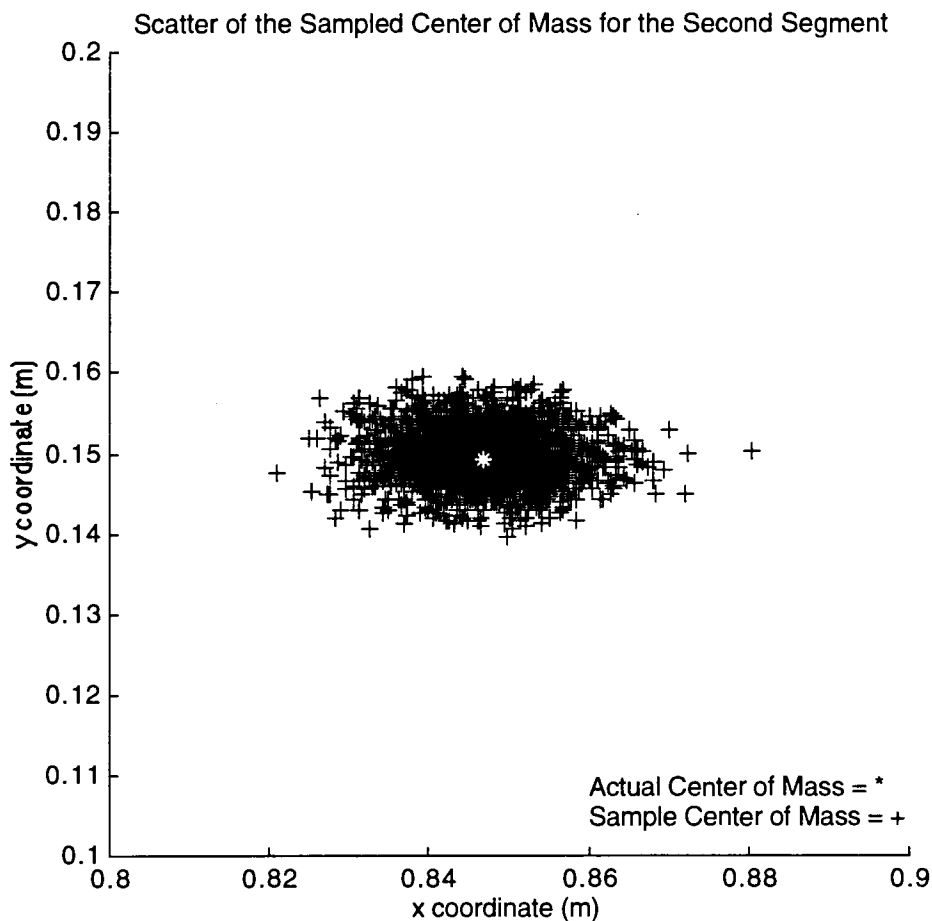


Figure 3-5 Error Scatter of the Center of Mass of the Second Segment

The Monte Carlo simulation was performed using MATLAB 5.0. The m-file is shown in Appendix B, includes the introduction of the error, the filtering of the marker position data, the calculation of the center of mass, and a comparison to the center of mass calculated from the 'clean' data. The program calculates the standard deviation of the error in the center of mass.

## Resulting Uncertainty

The total uncertainty in the position of the center of mass resulted in the following standard deviation of the error. The magnitude of the error was dependent on the orientation of the segments of the model. The projection of the error due to the location of the center of mass and the magnitude of the mass was much larger for a horizontally oriented segment than for a vertical segment. The skin slippage error also depends on the joint angle. Therefore, the error changed with the orientation of the segments. The average and range of the standard deviation is shown in the Table 3-3 for the duration of the sit-up.

Table 3-3 Standard Deviation of the Center of Mass  
Determined By Monte Carlo Analysis

	Mean STD (cm)	Min STD (cm)	Max STD (cm)
All Sources of Error	1.33	1.02	1.50
Mass Error Only	1.28	0.95	1.45
Segment CoM Error Only	0.34	0.26	0.38
Skin Slippage Error Only	0.16	0.00	0.30
Marker Position Error Only	0.00	0.00	0.01

The results show the average standard deviation of the center of mass calculation to be 1.33 cm when all of the errors are considered. Therefore a 95% confidence range of the uncertainty of the center of mass is  $\pm 2.66$  cm, or two standard deviations. The error due to the mass alone is  $\pm 2.56$  cm for the same confidence level. The error in the position of the center of mass of the individual segments also has a significant effect on the error of the location of the center of mass of the whole body. Figure 3-6 shows the center of mass bounded by the uncertainty margin of two standard deviations of the error due to all sources of uncertainty considered in this study.

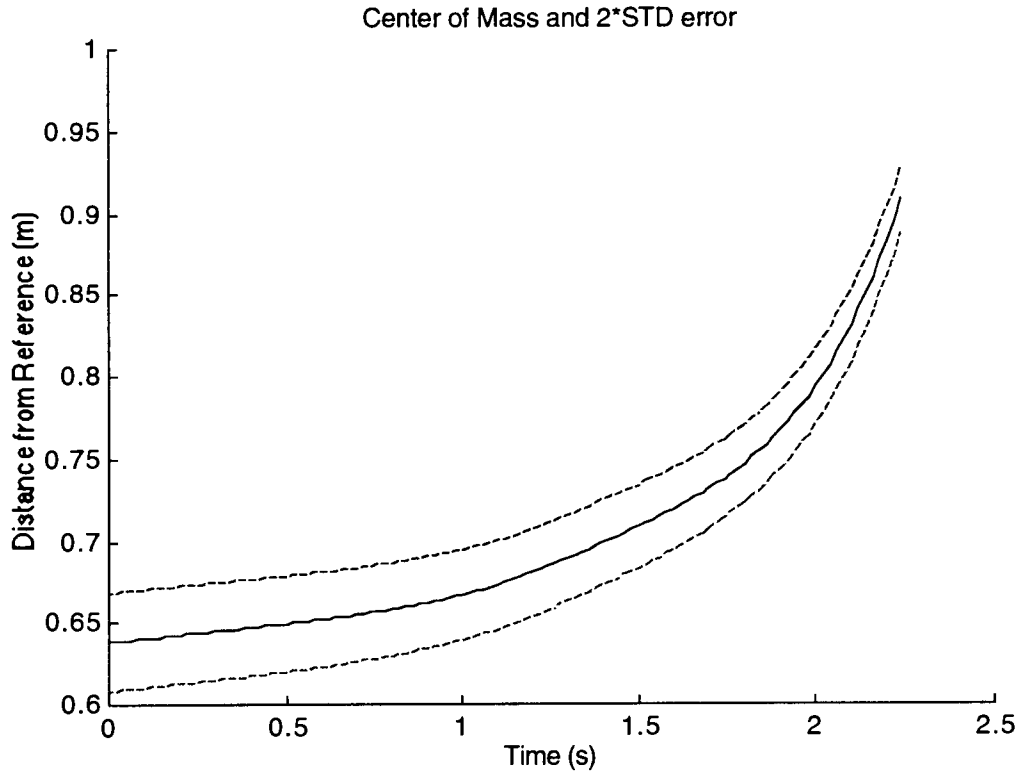


Figure 3-6 Location of the Center of Mass of the Model and the Two Standard Deviation Error Band

Figure 3-6 shows the change in the error margin as the sit-up progresses, demonstrating the effect of segment orientation on the magnitude of the error.

## Conclusions

The uncertainty in the marker position, skin slippage, location of the estimated center of mass, and mass of the segments results in a  $\pm 2.66$  cm average uncertainty in the body center of mass

location during the sit-up. The majority of this uncertainty is attributed to the uncertainty of the estimated mass of the segments. Improvement on the estimated mass of the segments would reduce the uncertainty of the body center of mass. Some studies have investigated more accurate methods of determining the mass properties of body segments. One study used magnetic resonance imaging to reduce the mass estimate to 6.9% for baboon segments [Martin et al. 1989], but this is only marginally better than the 7.7, 8.3, and 10.3% error used in this study. Another source of error that contributes to the error in the center of mass location is the estimation of the torso center of mass. The sit-up motion begins with near maximal torso flexion which distorts the soft tissues of the abdomen. Any error in the location of the center of mass of the torso would cause a significant error in the body center of mass [Kingma 1995]. The anthropometric method does not take this into consideration, and therefore, this error was not included in this study. The anthropometric method limits the division of the trunk into one or two segments. This is most likely inadequate to model the mass properties of the torso when large amounts of flexion are involved in the motion.

Thus, the anthropometric method would not result in an accurate estimate of the center of mass of a subject performing a sit-up. The analysis shows the majority of the error of this method results from inaccurate estimates of the mass of the segments. The anthropometric method estimates the masses of the



segments by using an average density of the cadaver segments used in Clauser's study (1969). The estimates are based on the average of a population. Therefore, there will always be an uncertainty associated with the standard deviation of the population. The accuracy needed for this application requires a much smaller uncertainty than the population data can provide. The mass properties used for this analysis must be subject specific to increase the certainty of the calculation of the center of mass.

## Chapter 4

### Dynamic Method

The previous chapter showed that the use of the anthropometric method to determine the center of mass of the body is not as accurate as the 1.2 cm precision of the center of pressure measurement. The largest source of error considered was due to the estimation of the mass of the segments. The dynamic method attempts to reduce this source of error by using ground reaction forces and segment motion to solve directly for the mass and moment of inertia of each segment. Another source of error mentioned, but not considered in the analysis of the anthropometric method, was the error due to the flexibility of the torso. The anthropometric model divides the torso into one or two segments that are assumed to be rigid, but this approximation of the flexible portion of the torso is prone to criticism when motions involving large flexion are analyzed [Kingma 1995]. The dynamic method does not limit the number of segments, and therefore, a higher order model of the torso is used to better approximate the flexion that occurs in the sit-up movement.

The goal of this chapter is to outline the theoretical solution of a set of linear equations relating the ground reaction forces, motion, and mass properties of a multiple segment body performing the

sit-up motion, and to define the limitations of applying this approach to a human subject performing a sit-up. A three segment rigid body model is used to demonstrate the theoretical solution, and the resulting equations are written in matrix form that can be solved for any number of segments using a least squares approach. This method is applied to existing human subject data collected at the Robert S. Dow Neurological Sciences Institute in the laboratory of Dr. Paul Cordo. The least squares approximation resulted in negative masses and moments of inertia for several segments. It is suggested that one of the reasons the results are unreliable is due to the small magnitude of the independent terms of the forces due to the acceleration of the segments in comparison to the precision of the force measurement devices. The independent force terms are defined as the forces due to segment motion with respect to the adjacent segments. The independent terms are especially small for the torso segments. The relative rotation of the segments of the torso are significant enough to cause errors in the static calculation of the center of mass, but they are not significant enough to be distinguished in the dynamic calculations. The small independent force to precision ratio is one source of error that leads to an inaccurate solution of the least squares approximation.

## Theoretical Solution of a Multiple Segment Body

The following is an outline to the solution of the mass properties of individual segments of a body that are subjected to the external forces of the ground, the force due to gravity, and the internal forces of the muscles. The results are used to determine the relations between the positions, accelerations, masses, moments of inertia of the segments, and the ground reaction forces. During a sit-up experiment, the ground reaction forces are measured, and the motion is recorded. Therefore, only the mass and inertia properties need to be determined in terms of the measured forces and motion. The force and moment balance equations are determined using the following equations.

$$\sum_{j=1}^{\text{\# of Supports}} F_{x_j} = \sum_{i=1}^{\text{\# of Segments}} m_i a_{x_i} \quad (\text{Eq 4 - 1})$$

$$\sum_{j=1}^{\text{\# of Supports}} F_{y_j} = \sum_{i=1}^{\text{\# of Segments}} m_i a_{y_i} \quad (\text{Eq 4 - 2})$$

$$\sum_{j=1}^{\text{\# of Supports}} M_{G_j} = \sum_{i=1}^{\text{\# of Segments}} I_i \alpha_i \quad (\text{Eq 4 - 3})$$

Where:

$i$  = Number of the segment

$m$  = The mass of the segment

$a$  = The absolute acceleration of the center of mass of the segment

$I$  = Moment of inertia about the center of mass of the segment

$\alpha$  = Angular acceleration fo the segment

The following section outlines the derivation of the equations of motion and force for a three segment body. Figure 4-1 shows the model.

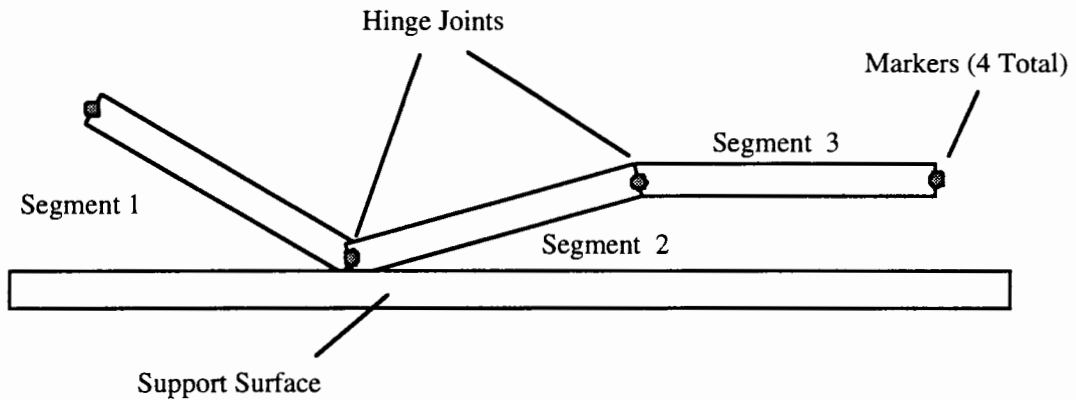


Figure 4-1 Three segment model used for the theoretical solution

The forces acting on each segment include the force due to gravitational acceleration, reaction forces from adjacent segments, active forces due to muscle contractions, and ground reaction forces (if applicable). For this model, all internal forces (i.e. muscle forces) are transferred between the segments as moments and joint reaction forces applied at the hinge joints. The ground reaction force is included at each end of the segment (it may be zero for joints not in contact with the ground). The segments are modeled as rigid bodies to simplify the derivation. The free body diagram of Segment 1 is shown in Figure 4-2.

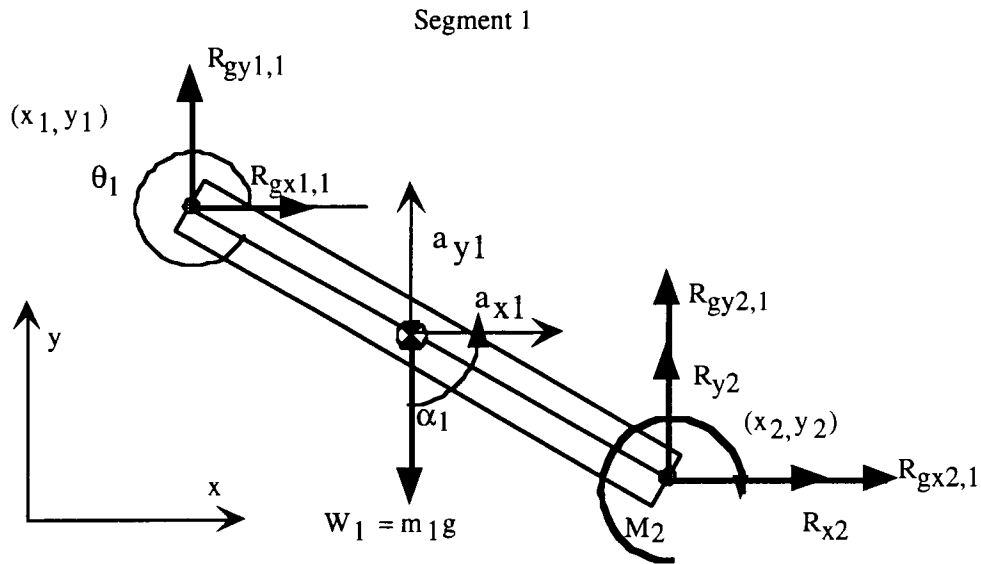


Figure 4-2 Free body diagram of Segment 1

Where:

$x_i, y_i$  = Position of joint i

$x_{cm}, y_{cm}$  = Position of segment centers of mass

$a_x, a_y$  = Acceleration of the centers of mass

$\theta$  = Angle of orientation

$\alpha$  = Angular acceleration

$W$  = Force due to the weight

$R_{gx1,1}, R_{gy1,1}$  = Ground reaction forces at joint 1 acting on segment 1

$R_{gx2,1}, R_{gy2,1}$  = Ground reaction forces at joint 2 acting on segment 1

$R_{yi}, R_{xi}, M_i$  = Internal reaction forces between segments at joint i

The force and moment balance equations for the first segment are as follows. The moments are summed about the segment center of mass.

$$\begin{aligned} \text{\# of Horz. Ground} \\ \text{Reaction Forces} \end{aligned} \sum_{j=1} F_{x_j} = \begin{aligned} \text{Segment \#} \\ \sum_i m_i a_{x_i} \end{aligned}$$

$$R_{gx1,1} + R_{gx2,1} + R_{x2} = m_1 a_{x1} \quad (\text{Eq 4 - 4})$$

$$\begin{aligned} \text{\# of Vert. Ground} \\ \text{Reaction Forces} \end{aligned} \sum_{j=1} F_{y_j} = \begin{aligned} \text{Segment \#} \\ \sum_i m_i a_{y_i} \end{aligned}$$

$$R_{gy1,1} + R_{gy2,1} + R_{y2} - m_1 g = m_1 a_{y1} \quad (\text{Eq 4 - 5a})$$

$$R_{gy1,1} + R_{gy2,1} + R_{y2} = m_1 (a_{y1} + g) \quad (\text{Eq 4 - 5b})$$

$$\begin{aligned} \text{\# of Moments} \\ \sum_{j=1} M_{G_j} \end{aligned} = \begin{aligned} \text{Segment \#} \\ \sum_i I_i \alpha_i \end{aligned}$$

$$R_{gy1,1}(x_1 - x_{cm1}) + R_{gy2,1}(x_2 - x_{cm1}) + R_{gx1,1}(y_1 - y_{cm1}) + R_{gx2,1}(y_2 - y_{cm1}) \quad (\text{Eq 4 - 6a})$$

$$+ R_{y2}(x_2 - x_{cm1}) + R_{x2}(y_2 - y_{cm1}) + M_2 = I_1 \alpha_1 \quad (\text{Eq 4 - 6b})$$

The second and third segments are shown in the following figures.

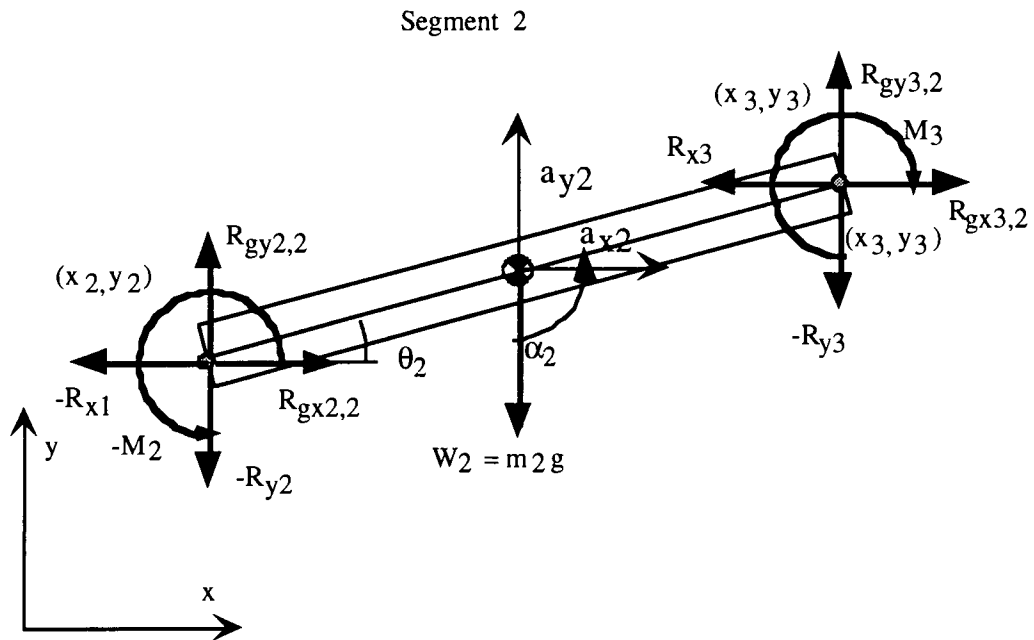


Figure 4-3 Free body diagram of Segment 2

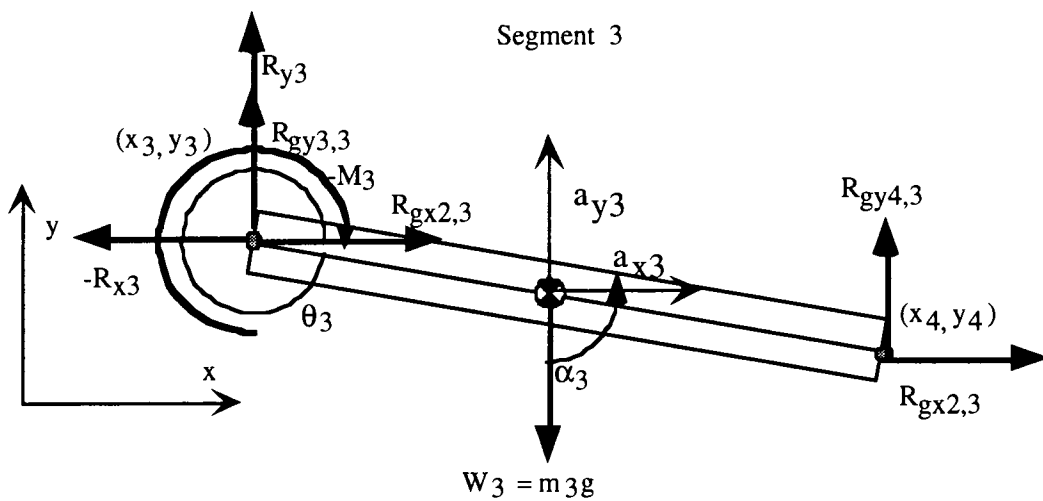


Figure 4-4 Free body diagram of Segment 3



Equations for Segments 2 and 3 can be generated similar to the equations generated for Segment 1.

## Segment 2

# of Horz. Ground  
Reaction Forces

$$\sum_{j=1} F_{x_j} = \sum_i m_i a_{x_i}$$

$$R_{gx2,2} + R_{gx3,2} - R_{x2} + R_{x3} = m_2 a_{x2} \quad (\text{Eq 4 - 7})$$

# of Vert. Ground  
Reaction Forces

$$\sum_{j=1} F_{y_j} = \sum_i m_i a_{y_i}$$

$$R_{gy2,2} + R_{gy3,2} - R_{y2} + R_{y3} - m_2 g = m_2 a_{y2} \quad (\text{Eq 4 - 8a})$$

$$R_{gy2,2} + R_{gy3,2} - R_{y2} + R_{y3} = m_2 (a_{y2} + g) \quad (\text{Eq 4 - 8b})$$

# of Moments

$$\sum_{j=1} M_{G_j} = \sum_i I_i \alpha_i$$

$$\begin{aligned} R_{gy2,2}(x_2 - x_{cm2}) + R_{gy3,2}(x_3 - x_{cm2}) + R_{gx2,2}(y_2 - y_{cm2}) + R_{gx3,2}(y_3 - y_{cm2}) \\ - R_{y2}(x_2 - x_{cm2}) - R_{x2}(y_2 - y_{cm2}) + R_{y3}(x_3 - x_{cm2}) + R_{x3}(y_3 - y_{cm2}) \\ - M_2 + M_3 = I_2 \alpha_2 \end{aligned} \quad (\text{Eq 4 - 9})$$

### Segment 3

# of Horz. Ground  
Reaction Forces

$$\sum_{j=1} F_{x_j} = \sum_i m_i a_{x_i}$$

$$R_{gx3,3} + R_{gx4,3} - R_{x3} = m_3 a_{x3} \quad (\text{Eq 4-10})$$

# of Vert. Ground  
Reaction Forces

$$\sum_{j=1} F_{y_j} = \sum_i m_i a_{y_i}$$

$$R_{gy3,3} + R_{gy4,3} - R_{y3} - m_3 g = m_3 a_{y3} \quad (\text{Eq 4-11a})$$

$$R_{gy3,3} + R_{gy4,3} - R_{y3} = m_3 (a_{y3} + g) \quad (\text{Eq 4-11b})$$

# of Moments

$$\sum_{j=1} M_{G_j} = \sum_i I_i \alpha_i$$

$$R_{gx3,3}(x_3 - x_{cm3}) + R_{gy4,3}(x_4 - x_{cm3}) + R_{gx3,3}(y_3 - y_{cm3}) + R_{gx4,3}(y_4 - y_{cm3}) - R_{y3}(x_3 - x_{cm3}) - R_{x3}(y_3 - y_{cm3}) - M_3 = I_3 \alpha_3 \quad (\text{Eq 4-12})$$

The total forces and torques are obtained by adding the equations for each link. The sum of the horizontal force equations, 4-4, 4-7, 4-10, results in equation 4-13a.

$$\begin{array}{c} \# \text{ of Horz. Ground} \\ \text{Reaction Forces} \end{array} \sum_{j=1} F_{x_j} = \begin{array}{c} \# \text{ of Segments} \\ \sum_{i=1} m_i a_{x_i} \end{array}$$

$$R_{gx1,1} + R_{gx2,1} + R_{x2} = m_1 a_{x1} \quad (\text{Eq 4 - 4})$$

$$R_{gx2,2} + R_{gx3,2} - R_{x2} + R_{x3} = m_2 a_{x2} \quad (\text{Eq 4 - 7})$$

$$R_{gx3,3} + R_{gx4,3} - R_{x3} = m_3 a_{x3} \quad (\text{Eq 4 - 10})$$

$$R_{gx1,1} + (R_{gx2,1} + R_{gx2,2}) + (R_{gx3,2} + R_{gx3,3}) + R_{gx4,3} + (R_{x2} - R_{x2}) + (R_{x3} - R_{x3}) = m_1 a_{x1} + m_2 a_{x2} + m_3 a_{x3} \quad (\text{Eq 4 - 13a})$$

$$R_{gx1,1} + (R_{gx2,1} + R_{gx2,2}) + (R_{gx3,2} + R_{gx3,3}) + R_{gx4,3} = m_1 a_{x1} + m_2 a_{x2} + m_3 a_{x3} \quad (\text{Eq 4 - 13b})$$

The internal joint reaction force cancel, and the result is equation 4-13b. The vertical force balance equations, 4-5, 4-8, 4-11, are summed in a similar manner resulting in equations 4-14 a and b. Again the internal reaction forces cancel.

$$\begin{array}{c} \# \text{ of Vert. Ground} \\ \text{Reaction Forces} \end{array} \sum_{j=1} F_{y_j} = \begin{array}{c} \# \text{ of Segments} \\ \sum_{i=1} m_i a_{y_i} \end{array}$$

$$R_{gy1,1} + (R_{gy2,1} + R_{gy2,2}) + (R_{gy3,2} + R_{gy3,3}) + R_{gy4,3} + (R_{y2} - R_{y2}) + (R_{y3} - R_{y3}) - m_1 g - m_2 g - m_3 g = m_1 a_{y1} + m_2 a_{y2} + m_3 a_{y3} \quad (\text{Eq 4 - 14a})$$

$$R_{gy1,1} + (R_{gy2,1} + R_{gy2,2}) + (R_{gy3,2} + R_{gy3,3}) + R_{gy4,3} = m_1 (a_{y1} + g) + m_2 (a_{y2} + g) + m_3 (a_{y3} + g) \quad (\text{Eq 4 - 14b})$$

The sum of equations 4-6b, 4-9b, 4-12b, results in the sum of the moments in equation 4-15 a and b. The internal reaction

moments applied at the joints cancel in equation 4-15a to result in equation 4-15b.

$$\begin{matrix} \# \text{ of Moments} \\ \sum_{j=1} \end{matrix} M_{G_j} = \begin{matrix} \# \text{ of Segments} \\ \sum_{i=1} \end{matrix} I_i \alpha_i$$

$$\begin{aligned} & x_1(R_{gy1,1}) + y_1(R_{gx1,1}) + x_2(R_{gy2,1} + R_{gy2,2} + R_{y2} - R_{y2}) + y_2(R_{gx2,1} + R_{gx2,2} + R_{x2} - R_{x2}) \\ & + x_3(R_{gy3,2} + R_{gy3,3} + R_{y3} - R_{y3}) + y_3(R_{gx3,2} + R_{gx3,3} + R_{x3} - R_{x3}) + x_4(R_{gy4,3}) \\ & + y_4(R_{gx4,3}) - x_{cm1}(R_{gy1,1} + R_{gy2,1} + R_{y2}) - y_{cm1}(R_{gx1,1} + R_{gx2,1} + R_{x2}) \\ & - x_{cm2}(R_{gy2,2} + R_{gy3,2} - R_{y2} + R_{y3}) - y_{cm2}(R_{gx2,2} + R_{gx3,2} - R_{x2} + R_{x3}) \\ & - x_{cm3}(R_{gy3,3} + R_{gy4,3} - R_{y3}) - y_{cm3}(R_{gx3,3} + R_{gx4,3} - R_{x3}) + M_2 - M_2 + M_3 - M_3 \\ & = I_1 \alpha_1 + I_2 \alpha_2 + I_3 \alpha_3 \end{aligned} \quad (\text{Eq 4-15a})$$

$$\begin{aligned} & x_1(R_{gy1,1}) + y_1(R_{gx1,1}) + x_2(R_{gy2,1} + R_{gy2,2}) + y_2(R_{gx2,1} + R_{gx2,2}) + x_3(R_{gy3,2} + R_{gy3,3}) \\ & + y_3(R_{gx3,2} + R_{gx3,3}) + x_4(R_{gy4,3}) + y_4(R_{gx4,3}) \\ & - x_{cm1}(R_{gy1,1} + R_{gy2,1} + R_{y2}) - y_{cm1}(R_{gx1,1} + R_{gx2,1} + R_{x2}) \\ & - x_{cm2}(R_{gy2,2} + R_{gy3,2} - R_{y2} + R_{y3}) - y_{cm2}(R_{gx2,2} + R_{gx3,2} - R_{x2} + R_{x3}) \\ & - x_{cm3}(R_{gy3,3} + R_{gy4,3} - R_{y3}) - y_{cm3}(R_{gx3,3} + R_{gx4,3} - R_{x3}) = I_1 \alpha_1 + I_2 \alpha_2 + I_3 \alpha_3 \end{aligned} \quad (\text{Eq 4-15b})$$

The summation of moments can be simplified using the following equations.

$$R_{gx1,1} + R_{gx2,1} + R_{x2} = m_1 a_{x1} \quad (\text{Eq 4 - 4})$$

$$R_{gx2,2} + R_{gx3,2} - R_{x2} + R_{x3} = m_2 a_{x2} \quad (\text{Eq 4 - 7})$$

$$R_{gx3,3} + R_{gx4,3} - R_{x3} = m_3 a_{x3} \quad (\text{Eq 4 - 10})$$

$$R_{gy1,1} + R_{gy2,1} + R_{y2} = m_1 (a_{y1} + g) \quad (\text{Eq 4 - 5b})$$

$$R_{gy2,2} + R_{gy3,2} - R_{y2} + R_{y3} = m_2 (a_{y2} + g) \quad (\text{Eq 4 - 8b})$$

$$R_{gy3,3} + R_{gy4,3} - R_{y3} = m_3 (a_{y3} + g) \quad (\text{Eq 4 - 11b})$$

$$\begin{aligned} & x_1 (R_{gx1,1}) + y_1 (R_{gx1,1}) + x_2 (R_{gy2,1} + R_{gy2,2}) + y_2 (R_{gx2,1} + R_{gx2,2}) + x_3 (R_{gy3,2} + R_{gy3,3}) \\ & + y_3 (R_{gx3,2} + R_{gx3,3}) + x_4 (R_{gy4,3}) + y_4 (R_{gx4,3}) \\ & - x_{cm1} m_1 (a_{y1} + g) - y_{cm1} m_1 a_{x1} - x_{cm2} m_2 (a_{y2} + g) \\ & - y_{cm2} m_2 a_{x2} - x_{cm3} m_3 (a_{y3} + g) - y_{cm3} m_3 a_{x3} \\ & = I_1 \alpha_1 + I_2 \alpha_2 + I_3 \alpha_3 \end{aligned} \quad (\text{Eq 4 - 16})$$

The remaining terms involving the reaction forces can be related to the measured reaction forces by determining the force balance equations of the force platform. The following figure shows the forces exerted by the body on the top of the platform and the reaction forces of the supports under the platform.

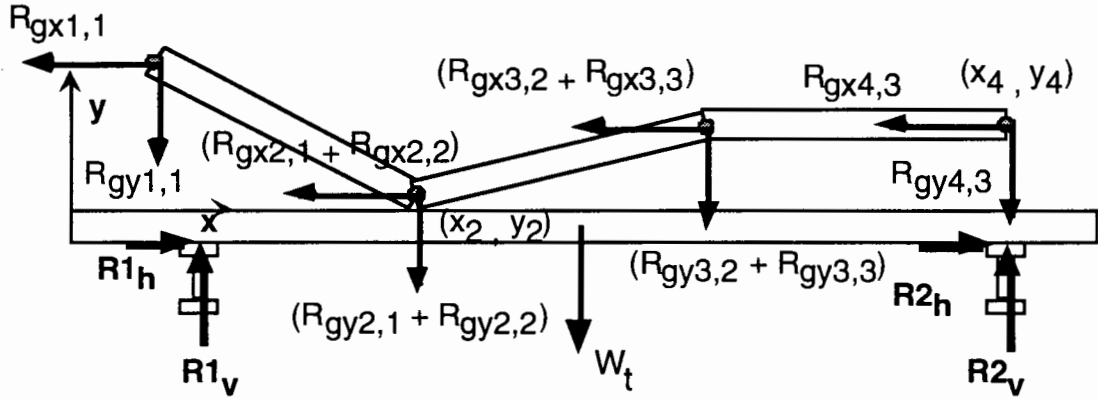


Figure 4-5 Platform Free Body Diagram

Where:

$R1_h, R1_v$  = Horizontal and vertical reaction forces of the first supports

$R2_h, R2_v$  = Horizontal and vertical reaction forces of the second supports

$W_t$  = Weight of the table acting at  $x_{t,cm}$

$x_{t,cm}$  = Location of the center of mass of the table

$R_{gx1,1}, R_{gy1,1}, \dots$  = Ground reaction forces at joint 1 acting on segment 1

$R_{gx2,1}, R_{gy2,1}, \dots$  = Ground reaction forces at joint 2 acting on segment 1

The previous figure shows the ground reaction forces for all of the joints. The joints that are not in contact with the table would not have a reaction force associated with them, but they are included in the derivation for completeness.

The force balance equations of the platform are as follows.

$$\begin{matrix} \# \text{ of Horiz. Forces} \\ \sum_{j=1} F_{x_j} = 0 \end{matrix}$$

$$R_{1h} + R_{2h} - (R_{gx1,1} + R_{gx2,1} + R_{gx2,2} + R_{gx3,2} + R_{gx3,3} + R_{gx4,3}) = 0 \quad (\text{Eq 4-17a})$$

$$R_{1h} + R_{2h} = R_{gx1,1} + R_{gx2,1} + R_{gx2,2} + R_{gx3,2} + R_{gx3,3} + R_{gx4,3} \quad (\text{Eq 4-17b})$$

$$\begin{matrix} \# \text{ of Vert. Forces} \\ \sum_{j=1} F_{y_j} = 0 \end{matrix}$$

$$R_{1v} + R_{2v} - (R_{gy1,1} + R_{gy2,1} + R_{gy2,2} + R_{gy3,2} + R_{gy3,3} + R_{gy4,3} + W_t) = 0 \quad (\text{Eq 4-18a})$$

$$R_{1v} + R_{2v} - W_t = R_{gy1,1} + R_{gy2,1} + R_{gy2,2} + R_{gy3,2} + R_{gy3,3} + R_{gy4,3} \quad (\text{Eq 4-18b})$$

$$\begin{matrix} \# \text{ of Moments} \\ \sum_{j=1} M_j = 0 \end{matrix}$$

$$\begin{aligned} x_{R1}R_{1v} + x_{R2}R_{2v} + y_{R1}R_{1h} + y_{R2}R_{2h} - (x_1(R_{gy1,1}) + y_1(R_{gx1,1}) + x_2(R_{gy2,1} + R_{gy2,2}) \\ + y_2(R_{gx2,1} + R_{gx2,2}) + x_3(R_{gy3,2} + R_{gy3,3}) + y_3(R_{gx3,2} + R_{gx3,3}) + x_4(R_{gy4,3}) \\ + y_4(R_{gx4,3}) + x_{tcm}W_t) = 0 \end{aligned} \quad (\text{Eq 4-19a})$$

$$\begin{aligned} x_{R1}R_{1v} + x_{R2}R_{2v} + y_{R1}R_{1h} + y_{R2}R_{2h} - x_{tcm}W_t = x_1(R_{gy1,1}) + y_1(R_{gx1,1}) + x_2(R_{gy2,1} + R_{gy2,2}) \\ + y_2(R_{gx2,1} + R_{gx2,2}) + x_3(R_{gy3,2} + R_{gy3,3}) \\ + y_3(R_{gx3,2} + R_{gx3,3}) + x_4(R_{gy4,3}) + y_4(R_{gx4,3}) \end{aligned} \quad (\text{Eq 4-19b})$$

The total forces measured by the force platform can be combined into three components, the horizontal reaction force ( $R_x$ ), the vertical reaction force ( $R_y$ ), and the torque ( $T$ ). These are shown in the following equations. The constant terms in the force and moment balance equations involving the weight of the platform

are accounted for when the reaction forces are calculated from the load cell voltages (see Appendix A).

$$R_x = R_{1h} + R_{2h} \quad (\text{Eq 4-20})$$

$$R_y = R_{1v} + R_{2v} - W_t \quad (\text{Eq 4-21})$$

$$T = x_{R1}R_{1v} + x_{R2}R_{2v} + y_{R1}R_{1h} + y_{R2}R_{2h} - x_{tcm}W_t \quad (\text{Eq 4-22})$$

The previous equations relate the body reaction forces to the forces measured by the force platform. These equations are substituted into equations 4-13b, 4-13b, and 4-16 to result in a relation between the masses, centers of mass, accelerations of the centers of mass of the segments, and the measured reaction forces of the force platform.

For the horizontal forces the left hand side of equation 4-13b is equivalent to the right hand side of equation 4-17b. Therefore, the left hand side of equation 4-13b is replaced by the left hand side of equation 4-17b. Then equation 4-20 is used to relate the total horizontal force to the sum of the masses times the horizontal acceleration in equation 4-23b.

#### Horizontal Forces

$$R_{gx1,1} + (R_{gx2,1} + R_{gx2,2}) + (R_{gx3,2} + R_{gx3,3}) + R_{gx4,3} = m_1a_{x1} + m_2a_{x2} + m_3a_{x3} \quad (\text{Eq 4-13b})$$

$$R_{1h} + R_{2h} = R_{gx1,1} + R_{gx2,1} + R_{gx2,2} + R_{gx3,2} + R_{gx3,3} + R_{gx4,3} \quad (\text{Eq 4-17b})$$



$$R_{1h} + R_{2h} = m_1 a_{x1} + m_2 a_{x2} + m_3 a_{x3} \quad (\text{Eq 4 - 23a})$$

$$R_x = R_{1h} + R_{2h} \quad (\text{Eq 4 - 20})$$

$$R_x = m_1 a_{x1} + m_2 a_{x2} + m_3 a_{x3} \quad (\text{Eq 4 - 23b})$$

The verical forces are derived in a similar way using equations 4-14b, 4-18b, and 4-21.

### Vertical Forces

$$R_{1v} + R_{2v} - W_t = m_1(a_{y1} + g) + m_2(a_{y2} + g) + m_3(a_{y3} + g) \quad (\text{Eq 4 - 24a})$$

$$R_y = m_1(a_{y1} + g) + m_2(a_{y2} + g) + m_3(a_{y3} + g) \quad (\text{Eq 4 - 24b})$$

Moment equations are related to the torque using equations 4-16, 4-19b, and 4-22.

## Moments about the origin

$$\begin{aligned}
 x_{R1}R_{1v} + x_{R2}R_{2v} + y_{R1}R_{1h} + y_{R2}R_{2h} - x_{tcm}W_t - x_{cm1}m_1(a_{y1} + g) - y_{cm1}m_1a_{x1} \\
 - x_{cm2}m_2(a_{y2} + g) - y_{cm2}m_2a_{x2} - x_{cm3}m_3(a_{y3} + g) - y_{cm3}m_3a_{x3} \\
 = I_1\alpha_1 + I_2\alpha_2 + I_3\alpha_3 \quad (\text{Eq 4 - 25a})
 \end{aligned}$$

$$\begin{aligned}
 x_{R1}R_{1v} + x_{R2}R_{2v} + y_{R1}R_{1h} + y_{R2}R_{2h} - x_{tcm}W_t = x_{cm1}m_1(a_{y1} + g) + y_{cm1}m_1a_{x1} \\
 + x_{cm2}m_2(a_{y2} + g) + y_{cm2}m_2a_{x2} + x_{cm3}m_3(a_{y3} + g) + y_{cm3}m_3a_{x3} \\
 + I_1\alpha_1 + I_2\alpha_2 + I_3\alpha_3 \quad (\text{Eq 4 - 25b})
 \end{aligned}$$

$$\begin{aligned}
 T = x_{cm1}m_1(a_{y1} + g) + y_{cm1}m_1a_{x1} + x_{cm2}m_2(a_{y2} + g) + y_{cm2}m_2a_{x2} + x_{cm3}m_3(a_{y3} + g) \\
 + y_{cm3}m_3a_{x3} + I_1\alpha_1 + I_2\alpha_2 + I_3\alpha_3 \quad (\text{Eq 4 - 25c})
 \end{aligned}$$

The equations 4-23b, 4-24b, and 4-25c can be written as follows.

$$R_x = \sum_{j=1}^{\# \text{ of Segments}} m_j a_{xj} \quad (\text{Eq 4 - 26})$$

$$R_y = \sum_{j=1}^{\# \text{ of Segments}} m_j (a_{yj} + g) \quad (\text{Eq 4 - 27})$$

$$T = \sum_{j=1}^{\# \text{ of Segments}} x_{cmj}m_j(a_{yj} + g) + y_{cmj}m_ja_{xj} + I_j\alpha_j \quad (\text{Eq 4 - 28})$$

And written in matrix form as:

$$\begin{bmatrix} a_{x_1} & \cdots & a_{x_n} & 0 & \cdots & 0 \\ (a_{y_1} + g) & \cdots & (a_{y_n} + g) & 0 & \cdots & 0 \\ ((a_{y_1} + g)x_{cm_1} + a_{x_1}y_{cm_1}) & \cdots & ((a_{y_n} + g)x_{cm_n} + a_{x_n}y_{cm_n}) & \alpha_1 & \cdots & \alpha_n \end{bmatrix} \begin{bmatrix} m_1 \\ \vdots \\ m_n \\ I_1 \\ \vdots \\ I_n \end{bmatrix} = \begin{bmatrix} R_x \\ R_y \\ T \end{bmatrix}$$

(Eq 4 - 29)

The resulting matrix form of the equations shows that the number of segments is not limited by the theory of the dynamic method, nor is the number of equations.

The location of the center of mass of a segment was defined relative to the markers used to define the segment ends. The acceleration of the center of mass was calculated from the position data of the markers associated with the segment. The location of the centers of mass of the segments had to be determined before the equations could be solved. The previous chapter showed that errors associated with the estimate of the location of the center of mass were less significant than the errors associated with the estimation of the mass of the segment in the anthropometric method. Therefore, the anthropometric estimates of the locations of the center of mass of the segments were used. The anthropometric measurements can be used with confidence for the head and limb segments in comparison to the location of the center of mass of the torso [Kingma 1995]. The torso in this model has been divided into several segments in comparison to

the two used in most anthropometric models. The center of mass of each of the torso segments is assumed to be located midway between the markers.

## Application of the Theory to the Sit-Up Experimental Data

The sit-up data used in this analysis was provided by the Robert S. Dow Neurological Sciences Institute. The sit-ups were performed on the force platform and the motion was recorded using the Elite motion analysis system described in Chapter 2. The sampling rate of the motion analysis system was 50 Hz, and a horizontal, vertical and torque balance equation was written for each sample frame. Therefore, a total of 600 equations were written from the data collected during a four second sit-up. The experimental recording of a human performing a sit-up used 17 markers to define 16 body segments resulting in 16 unknown masses and 16 unknown moments of inertia. A least squares fit algorithm was used to solve for the unknown mass and inertia properties. Figures 4-6, 4-7, and 4-8 show the reaction forces of the force platform for a sample trial.

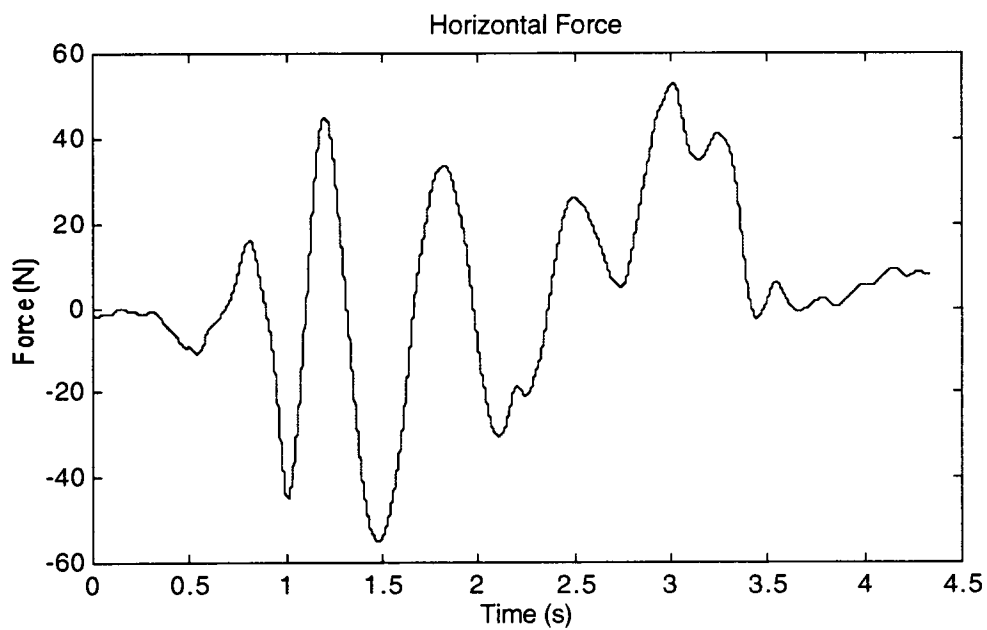


Figure 4-6 Horizontal reaction force of the force platform.

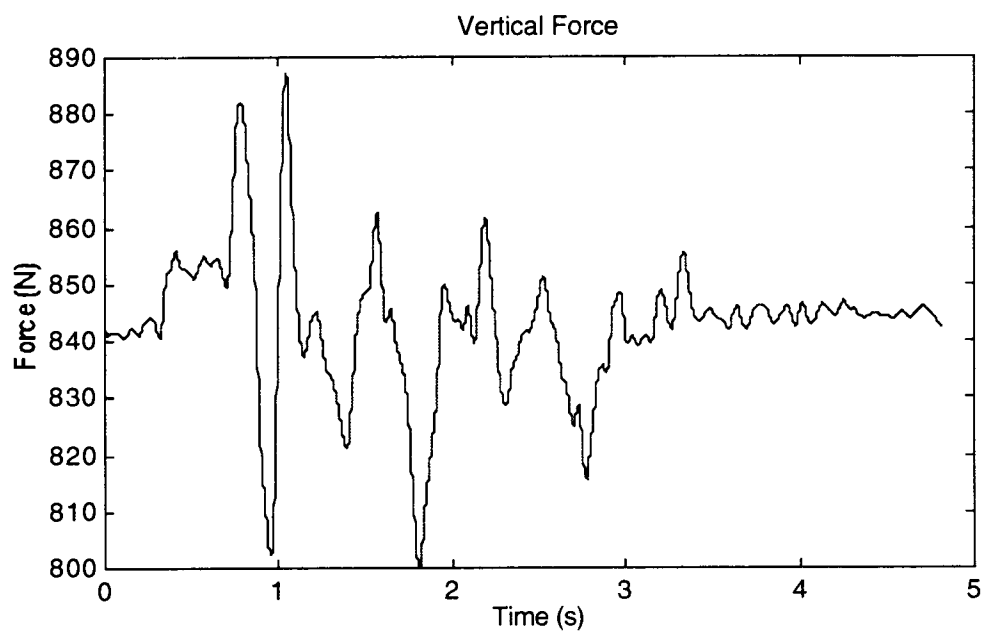


Figure 4-7 Vertical reaction force of the force platform.

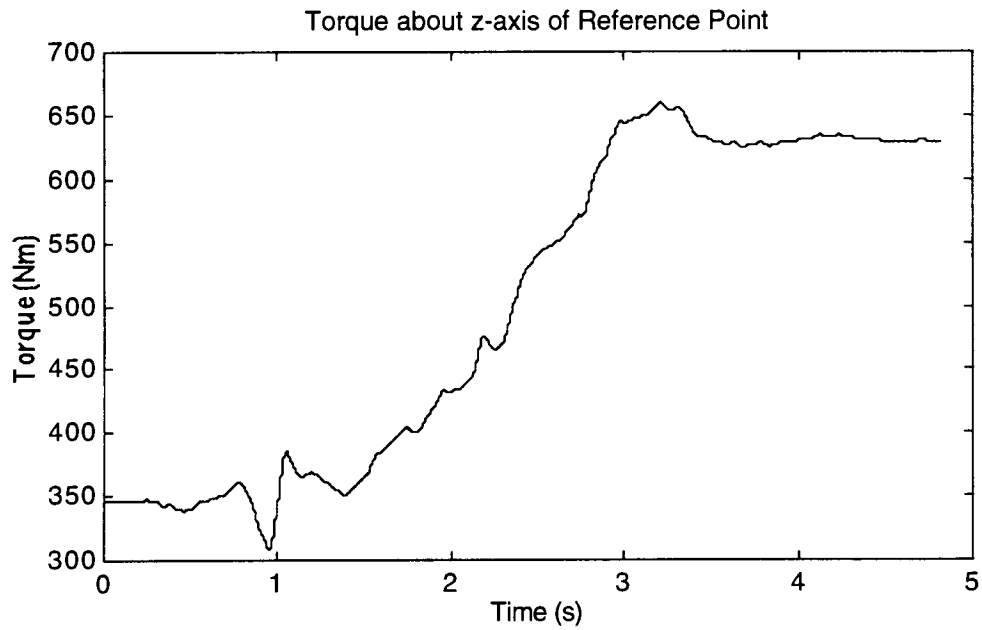


Figure 4-8 Reaction torque of the force platform about the reference point.

The motion of the subject is recorded by the reflective markers. Figure 4-9 shows the motion of the individual markers.

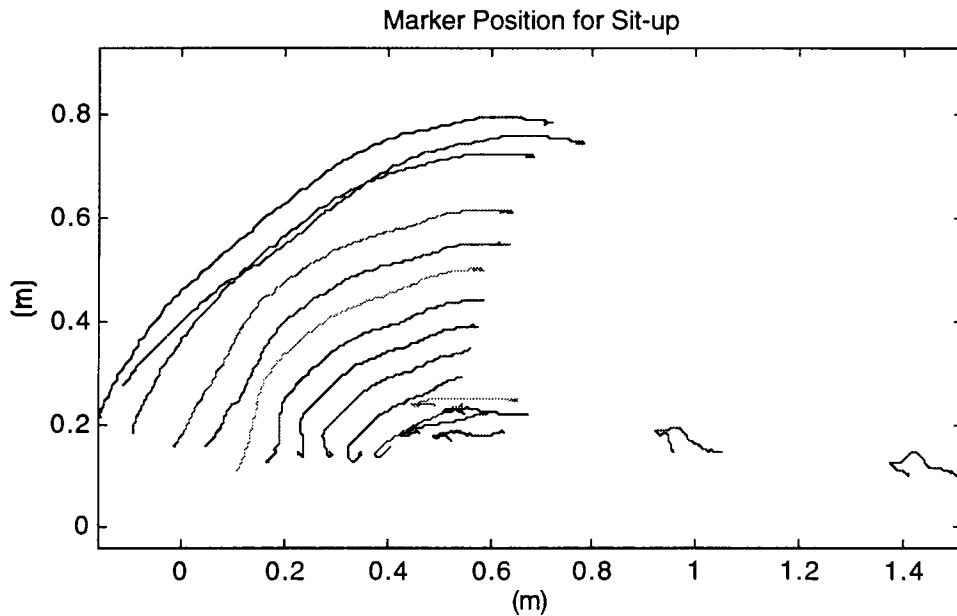


Figure 4-9 Marker position for sit-up.

The marker data is used to determine the vertical, horizontal and angular accelerations of the segments. These accelerations are used to build the matrix on the left hand side of equation 4-29, and are shown in Figures 4-10 and 4-11.

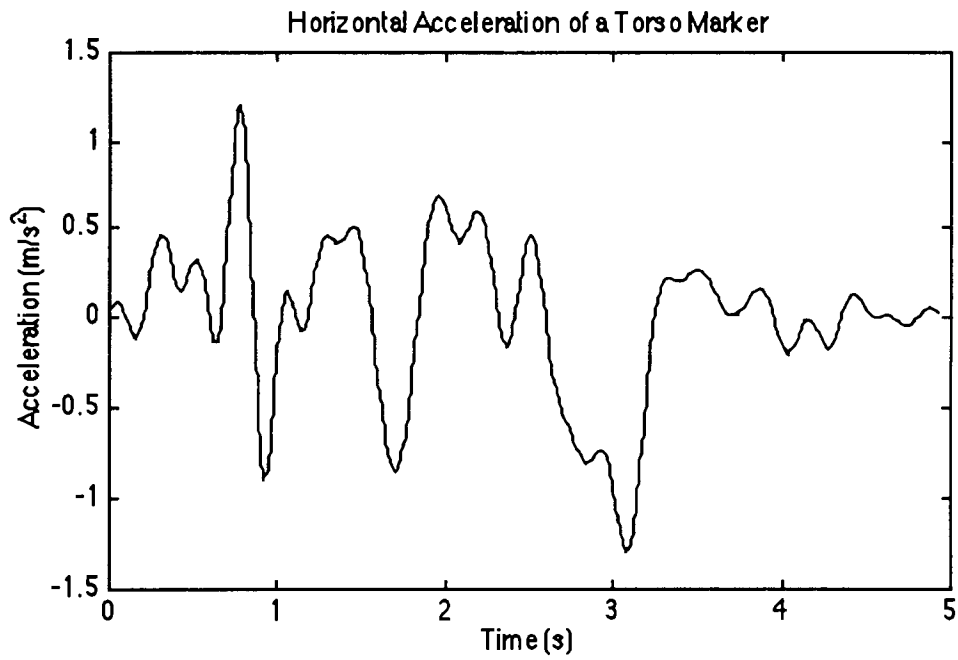


Figure 4-10 Horizontal Acceleration of a Torso Marker

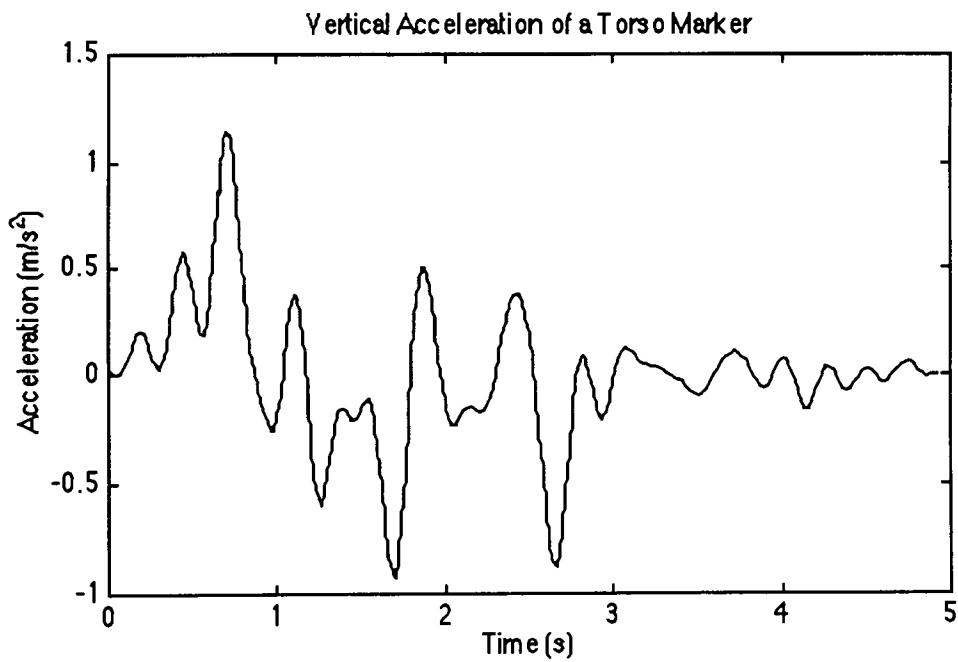


Figure 4-11 Vertical Acceleration of a Torso Marker



The vector on the right hand side of the equation is built using the reaction forces of the force platform. Once the matrix and the vector have been built the vector containing the masses and moments of inertia are calculated using a least squares approximation. The results are shown in the following table.

Table 4-1 Calculated Mass and Moments of Inertia  
for the Segments.

Segment	Mass (kg)	Moment of Inertia (kg m <sup>2</sup> )
Head	9.1	-0.76
Neck	7.0	0.33
Torso 1	7.3	0.01
Torso 2	3.2	-0.71
Torso 3	6.7	-0.58
Torso 4	6.9	-0.82
Torso 5	2.1	0.44
Torso 6	-0.8	0.63
Torso 7	1.2	0.66
Torso 8	2.7	0.37
Pelvis 1	4.2	0.76
Pelvis 2	4.2	0.63
Pelvis 3	9.7	-0.70
Thighs	13.2	-5.36
Shanks	9.4	-2.96

The application of the theoretical solution using data collected from a real sit-up experiment resulted in unreliable magnitudes of mass and moments of inertia. The previous sample shows that some of the properties have negative values which are obviously an inaccurate description of the mass properties of a subject. One possible source of the inaccuracy is attributed to the relatively small deviation of the trunk from rigid body dynamic characteristics. One of the goals of this approach was to reduce the error associated with trunk flexion. The model attempts to reduce the error by dividing the trunk into several segments from the shoulder to the pelvis instead of the one or two segments used in Clauser's anthropometric model [McConville 1980]. One result of partitioning the torso into more segments is the reduction of relative motion between the segments. The relative rotation of the torso segments is significant enough to cause an error in the static calculation of the center of mass, but the relative angular acceleration is not significant enough to determine the segment mass properties using the dynamic method. The result of the small relative angular acceleration was a small magnitude of the independent terms of the forces in comparison to the precision of the force platform measurements.

The accuracy of the least squares fit solution of the segment mass properties relies on the accuracy and magnitude of the terms used in the approximation. For the sit-up, the accuracy of the force platform and the magnitude of the independent

relationships between the translational and angular accelerations of the segments are significant factors in the calculation of the mass properties. This is demonstrated in the following section. Figure 4-12 shows the angular orientation ( $\theta$ ), velocity ( $\omega$ ) and acceleration ( $\alpha$ ) of two adjacent segments.

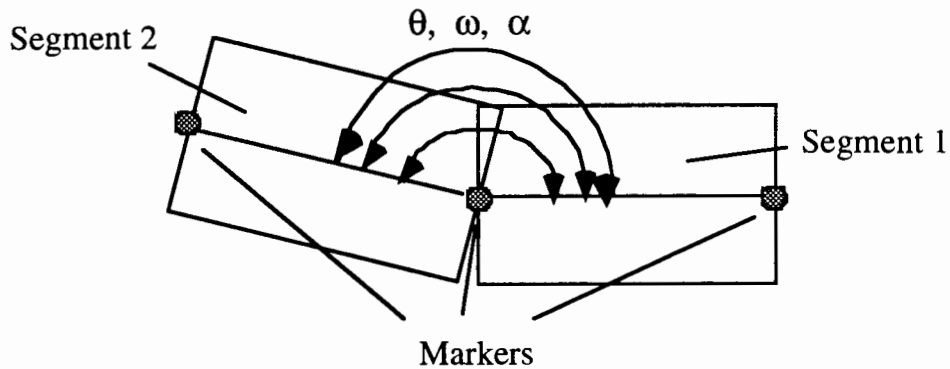


Figure 4-12 Two Adjacent Trunk Segments

The vertical reaction forces of the two link model results in the following equations.

$$F = \sum_{i=1}^{\text{\# of Segments}} m_i a_i = m_1 r_1 (\alpha_1 + \omega_1^2) + m_2 ((\alpha_1 + \omega_1^2 + \alpha_2 + \omega_2^2) r_2 + \alpha_1 l_1) \quad (\text{Eq 4 - 30})$$

$$F = m_1 r_1 (\alpha_1 + \omega_1^2) + m_2 (\alpha_1 + \omega_1^2) (l_1 + r_2) + m_2 r_2 (\alpha_2 + \omega_2^2) \quad (\text{Eq 4 - 31})$$

Where:

$F$  = Force

$m_1$  = Mass of Segment 1

$m_2$  = Mass of Segment 2

$\alpha_1$  = Angular acceleration of Segment 1 relative to the ground

$\alpha_2$  = Angular acceleration of Segment 2 relative to Segment 1

$\omega_1$  = Angular velocity of Segment 1 relative to the ground

$\omega_2$  = Angular velocity of Segment 2 relative to Segment 1

$r_1$  = Distance from marker to center of mass of Segment 1

$r_2$  = Distance from marker to center of mass of Segment 2

$l_1$  = Length of Segment 1

If the two segments were rigidly joined, the equation would be as follows.

$$F = m_1 r_1 (\alpha_1 + \omega_1^2) + m_2 (\alpha_1 + \omega_1^2) (l_1 + r_2) \quad (\text{Eq 4 - 32})$$

The difference of the rigid and non-rigid equations is equal to the magnitude of the force of the independent term.

$$-(F = m_1 r_1 (\alpha_1 + \omega_1^2) + m_2 (\alpha_1 + \omega_1^2) (l_1 + r_2)) \quad (\text{Eq 4 - 30})$$

$$+(F = m_1 r_1 (\alpha_1 + \omega_1^2) + m_2 (\alpha_1 + \omega_1^2) (l_1 + r_2) + m_2 r_2 (\alpha_2 + \omega_2^2)) \quad (\text{Eq 4 - 31})$$

$$\Delta F = m_2 r_2 (\alpha_2 + \omega_2^2) \quad (\text{Eq 4 - 33})$$

Therefore the deviation from the rigid body is due to the angular velocity and acceleration of the second segment relative to the first segment. The data shows that the relative angular velocity is less than 0.4 rad/sec and the maximum relative angular acceleration is 2 rad/sec<sup>2</sup>. The maximum force due to the non-rigid term is 0.8 N. This is less than the 2.5 N precision of the force platform.

The term that relates the moment of inertia to the torque is also not significantly greater than the 1.9 Nm precision of the torque measurement. The thigh segment has the largest moment due to the product of the moment of inertia and angular acceleration. The approximate moment of inertia is 1.21 kgm<sup>2</sup> for the two thighs, and the maximum angular acceleration is 4 rad/sec<sup>2</sup>. Therefore the largest product is 4.8 Nm and only 2.5 times the precision of the force platform. The smallest moment would be the product of the moment of inertia and the angular acceleration of one of the torso segments. The moment of inertia for one of these segments is approximately 0.00602 kgm<sup>2</sup>. The maximum angular acceleration is approximately 4.5 rad/s<sup>2</sup>. Therefore the maximum moment of a torso segment due to angular acceleration is 0.03 Nm. The magnitude of the independent terms is not significantly greater than the precision of the force platform measurements. This is likely the source of the unreliable results of the least squares problem. Further investigation would be necessary to prove that this was the most significant source.

## Conclusions

The magnitude of the forces and moments resulting from the dynamic motion of the body are not significantly greater than the resolution of the force platform measurements. This is one source of uncertainty that is significant and could be the cause of the inaccurate solution to the least squares approximation. Other sources of error that would contribute to the inaccuracy include the errors in the position of the segment center of mass, marker position errors that result in acceleration errors, and the error due to the skin slippage at the marker locations.

The analysis of the dynamic method is somewhat inconclusive due to the inaccuracy of the results. One likely source of the inaccuracy has been outlined, but further investigation would be necessary to determine if this was the only dominant source of error. The dynamic method would have some advantages over the anthropometric method if the least squares approximation was improved. The mass properties estimated using the dynamic method are subject specific and not based on population samples. The largest source of uncertainty found in the analysis of the anthropometric method was due to the estimation of the mass properties using population samples. Another advantage of the dynamic method is that the mass properties are directly calculated. The anthropometric method required calculating the

mass properties of the segments based on 248 dimensions of the subject. Therefore, the dynamic method does have some significant advantages, but further investigation into the inaccuracy of the least squares approximation of the mass properties is necessary before the feasibility of this approach can be determined.

## Chapter 5

### Static Torque Measurement Method

This section outlines and evaluates a method of determining the center of mass of a subject using the static torque of the segments of the body. The location of the center of mass can be determined by dividing the sum of the static torques of the segments by the sum of the weights. Static torque is related to the constant physical properties of the segments. These include the mass of the segment and its location and orientation with respect to the supporting platform. The constant terms are combined into two coefficients. The two constant coefficients combined with the orientation of the segment define the static torque. The orientation of the segment can be measured by the motion recording system. Therefore, the two coefficients can be determined for the segments of the body by placing the body into numerous static positions and measuring the resulting torque on the force platform. The advantage of this method is that it does not require specific knowledge of the mass or the location of the center of mass of the segment. One disadvantage of this method is that it relies on highly accurate force measurements. A rigid body model of the thighs and shanks of a human subject is used to evaluate this technique. Application of this technique to the two largest and most definable masses, the thighs and the shanks, and considering only the measurement uncertainty of the force



platform and the motion recording system, results in a larger uncertainty than the anthropometric model analyzed in Chapter 3.

## Theory

The body is divided into segments defined by the location of the markers attached to the subject's side. Each segment has a definable center of mass and moment of inertia. If the body is not moving relative to the force platform, then the measured center of pressure is coincident with the center of mass.

Therefore, the center of mass position relative to the platform can be determined by summing the static torques and dividing by the sum of the weights. Figure 5-1 shows the position of the center of masses of individual segments and the body center of mass.

Where  $m_1$  is the mass of the first segment, etc. and  $g$  is the gravitational acceleration. The reaction forces of the platform are denoted by  $R_{1h}$  and  $R_{2h}$  for the horizontal and  $R_{1v}$  and  $R_{2v}$  for the vertical.

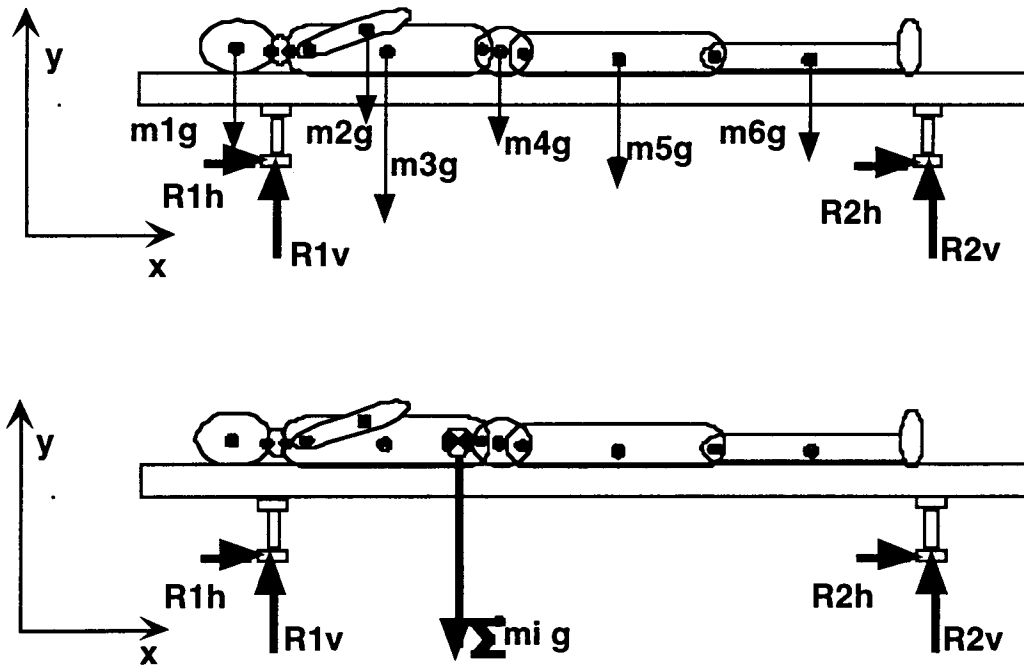


Figure 5-1 Position of the Center of Mass in a Supine Position

The center of pressure of the platform is calculated in the global coordinate system using the reaction forces at the four corners of the platform. The origin of the global coordinate system is located on the surface of the platform at the head of the force platform. The location of the center of pressure is calculated as follows.

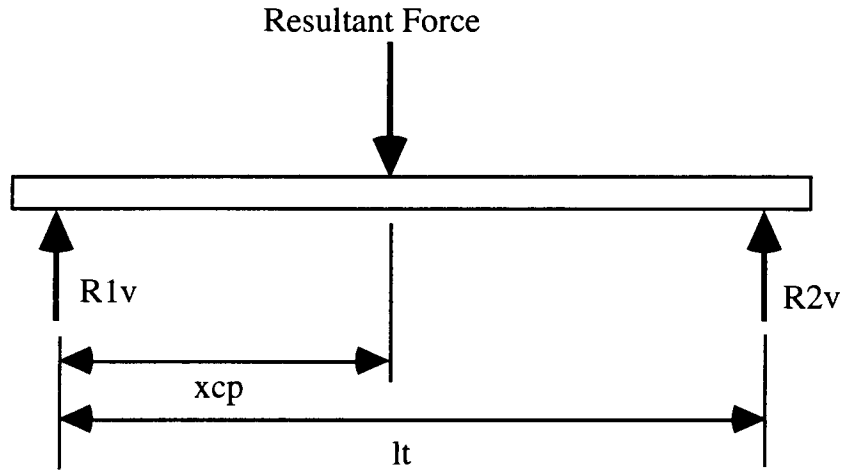


Figure 5-2 Force platform resultant and reaction forces.

$$x_{cp} = \frac{R2_v l_t}{R1_v + R2_v} \quad (\text{Eq 5-1})$$

Where:

$x_{cp}$  = Location of platform center of pressure in global coordinates

$R2_v$  = Vertical reaction force at the foot of the force platform

$R1_v$  = Vertical reaction force at the head of the force platform

$l_t$  = Distance between reaction forces

The location of the center of mass of the whole body in the global coordinate system is the sum of the static torques of the body segments divided by the sum of their weights.

$$x_{cm} = \frac{\sum_{i=1}^n x_i m_i g}{\sum_{i=1}^n m_i g} \quad (\text{Eq 5 - 2})$$

Where:

$x_{cm}$  = Location of body center of mass in global coordinates

$x_i$  = Location of segment center of mass in global coordinates

$m_i$  = Mass of segment

$g$  = Acceleration due to gravity

$n$  = Number of segments

In static conditions the center of pressure and the center of mass are coincident. Therefore, these two equations can be combined and reduced as follows.

$$x_{cp} = x_{cm} \quad \text{and} \quad R1_h + R2_h = \sum_{i=1}^n m_i g \quad (\text{Eq 5 - 3})$$

Therefore,

$$\frac{R2_h l_t}{R1_h + R2_h} = \frac{\sum_{i=1}^n x_i m_i g}{\sum_{i=1}^n m_i g} \quad (\text{Eq 5 - 4})$$

$$R2_h l_t = \sum_{i=1}^n x_i m_i g \quad (\text{Eq 5 - 5})$$

The previous equation can also be described as the sum of the moments about the axis that intersects the supports at the head gages. The moment due to the reaction force will be referred to as the static torque of the platform, T.

$$\sum M = 0$$

$$R2_h l_i - \sum_{i=1}^n x_i m_i g = 0 \quad (\text{Eq 5-6})$$

$$T = R2_h l_i \quad (\text{Eq 5-7})$$

The position of the center of mass of each segment can be described relative to a local coordinate system defined by two markers fixed to the segment. The position in the local coordinate system is defined by  $\theta_{cm}$  and  $r_{cm}$ . The local coordinate system is defined in the global coordinate system by the location of one of the markers  $(x_p, y_p)$  and the angle  $\theta_g$ . Figure 5-3 shows the position of the center of mass of a single segment.

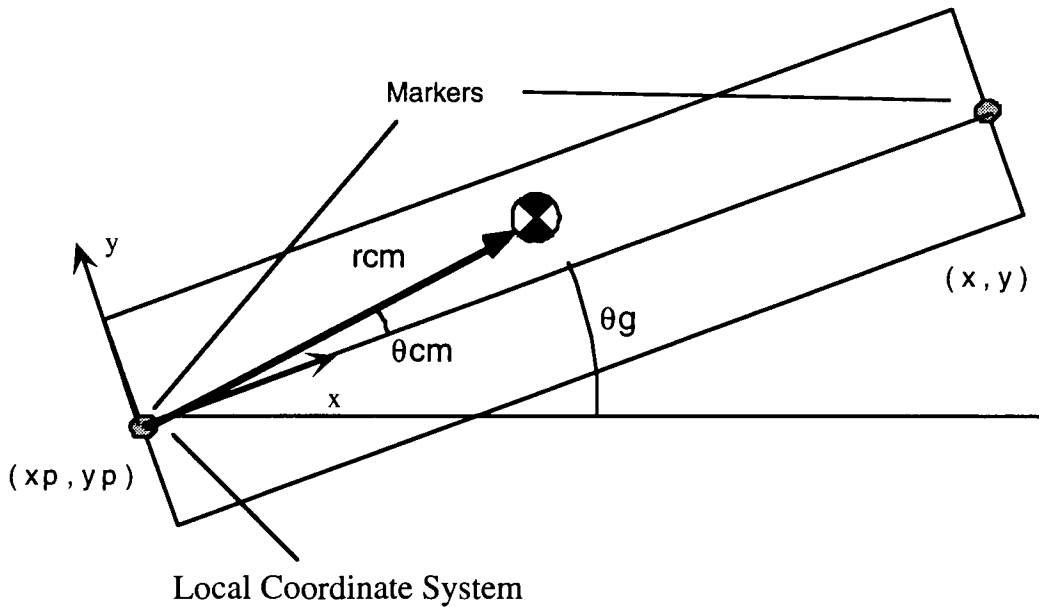


Figure 5-3 Position and Center of Mass of a Single Segment

The location of the center of mass in the global coordinate system is as follows.

$$x_{cm,g} = x_{p,g} + r_{cm} \cos(\theta_g + \theta_{cm}) \quad (\text{Eq 5-8})$$

$$y_{cm,g} = y_{p,g} + r_{cm} \sin(\theta_g + \theta_{cm}) \quad (\text{Eq 5-9})$$

Where:

$y_{cm,g}$  = Vertical position of center of mass in global coordinates

$x_{cm,g}$  = Horizontal position of center of mass in global coordinates

$y_{p,g}$  = Vertical position of the marker in global coordinates

$x_{p,g}$  = Horizontal position of the marker in global coordinates

$r_{cm}$  = Distance to the center of mass from the marker

$\theta_{cm}$  = Angle of center of mass in local coordinates

$\theta_g$  = Angle of Segment in global coordinates

Therefore, the resulting torque due to each segment in reference to the global coordinate system is:

$$T_i = x_i m_i g \quad (\text{Eq 5-10})$$

$$x_i = x_p + r_i \cos(\theta_{g_i} + \theta_{cm_i}) \quad (\text{Eq 5-11})$$

$$T_i = (x_p + r_i \cos(\theta_{g_i} + \theta_{cm_i})) m_i g \quad (\text{Eq 5-12})$$

$$T = \sum_{i=1}^n T_i = \sum_{i=1}^n (x_p + r_i \cos(\theta_{g_i} + \theta_{cm_i})) m_i g \quad (\text{Eq 5-13})$$

In the previous set of equations the location of the marker, ( $x_m$ ,  $y_m$ ), and the angle,  $\theta_g$ , are determined from the marker position data and are therefore considered as known variables. The variables that describe the location of the center of mass in the

local coordinate system,  $\theta_{cm}$  and  $r_{cm}$ , and the mass of the segment,  $m$ , are unknowns. The previous equation can be expanded to give the following result.

*Substituting*

$$\cos(\theta_{g_i} + \theta_{cm_i}) = \cos(\theta_{g_i})\cos(\theta_{cm_i}) - \sin(\theta_{g_i})\sin(\theta_{cm_i}) \quad (\text{Eq 5-14})$$

$$T_i = \left( x_p + r_i \left( \cos(\theta_{g_i})\cos(\theta_{cm_i}) - \sin(\theta_{g_i})\sin(\theta_{cm_i}) \right) \right) m_i g \quad (\text{Eq 5-15})$$

$$T_i = x_p m_i g + r_i m_i g \cos(\theta_{cm_i})\cos(\theta_{g_i}) - r_i m_i g \sin(\theta_{cm_i})\sin(\theta_{g_i}) \quad (\text{Eq 5-16})$$

The previous equation can be simplified by defining the following two constants that contain the three unknowns,  $m$ ,  $r$ , and  $\theta_{cm}$ .

The static torque of a segment is defined by these two constants and the orientation of the segment.

$$C_1 = r_i m_i g \cos(\theta_{cm_i}) \quad (\text{Eq 5-17})$$

$$C_2 = r_i m_i g \sin(\theta_{cm_i}) \quad (\text{Eq 5-18})$$

The center of mass of the body is defined as follows.

$$x_{cm} = \frac{T}{W} \quad (\text{Eq 5-19})$$

$$x_{cm} = \frac{\sum_{i=1}^n x_i m_i g + C_1 \cos(\theta_{g_i}) - C_2 \sin(\theta_{g_i})}{\sum_{i=1}^n m_i g} \quad (\text{Eq 5-20})$$

The resulting equation contains three unknown terms,  $C_1$ ,  $C_2$ , and  $m$ , for each segment. If these unknowns can be determined  $\theta_{cm}$  and  $r_{cm}$  can be calculated using the following relationships.

$$\theta_{cm} = \arctan\left(\frac{C_2}{C_1}\right) \quad (\text{Eq 5-21})$$

$$r = \frac{C_1}{mg \cos(\theta_{cm})} \quad (\text{Eq 5-22})$$

However, the three unknowns cannot be determined for each segment because the terms that relate them are not linearly independent, but the constants  $C_1$  and  $C_2$  can be determined for a single segment. The following section outlines the method for determining these values.

## Solution of Shank and Thigh Segments

The coefficients  $C_1$  and  $C_2$  can be determined if there are three linearly independent equations per link. To demonstrate the process to determine these coefficients the linked body model will be used. A model representing the trunk, thighs and shanks is shown in Figure 17 below.



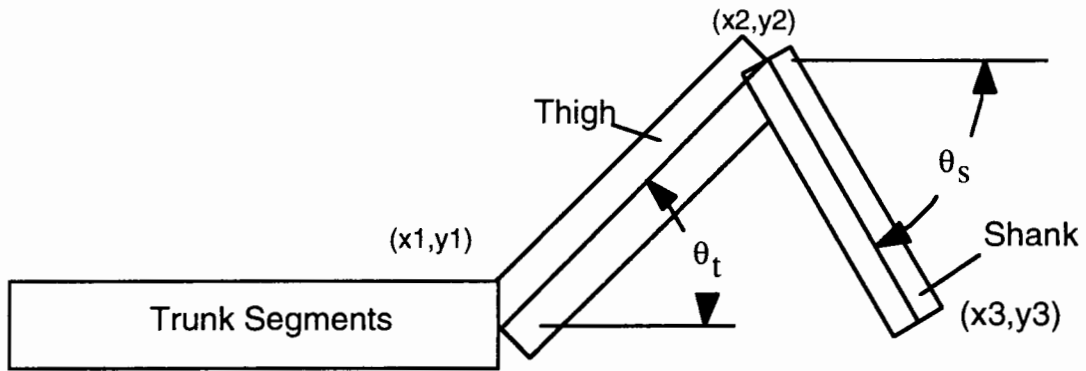


Figure 5-4 Model Used to solve for the Thigh and Shank Static Torque Coefficients

To simplify the procedure only the links representing the thighs and shanks will be allowed to move. In these positions the only change in the torque will be due to the change in orientation of the leg segments. Therefore two equations can be created by subtracting the equations defined by placing the body in three different positions. The result is two equations with two unknowns. This is shown in the following equations. The first subscript on  $\theta$  represents the segment ( $s$  = shank and  $t$  = thigh). The second subscript represents the position number. The first subscript on the constants,  $C_1$  and  $C_2$ , represents the segment. The subscript on the torque,  $T$ , represents the position number.

$$T_1 - T_2 = C_{s,1}(\cos(\theta_{s,1}) - \cos(\theta_{s,2})) - C_{s,2}(\sin(\theta_{s,1}) - \sin(\theta_{s,2})) \quad (\text{Eq 5 - 23})$$

$$T_1 - T_3 = C_{s,1}(\cos(\theta_{s,1}) - \cos(\theta_{s,3})) - C_{s,2}(\sin(\theta_{s,1}) - \sin(\theta_{s,3})) \quad (\text{Eq 5 - 24})$$

The previous equations are used to determine  $C_1$  and  $C_2$  for the shank. The results are shown in the following equations.

$$C_{s,1} = \frac{(T_1 - T_2) + C_{s,2}(\sin(\theta_{s,1}) - \sin(\theta_{s,2}))}{(\cos(\theta_{s,1}) - \cos(\theta_{s,2}))} \quad (\text{Eq 5-25})$$

$$C_{s,2} = \frac{(T_1 - T_3)(\cos(\theta_{s,1}) - \cos(\theta_{s,2})) - (T_1 - T_2)(\cos(\theta_{s,1}) - \cos(\theta_{s,3}))}{(\sin(\theta_{s,1}) - \sin(\theta_{s,2}))(\cos(\theta_{s,1}) - \cos(\theta_{s,3})) + (\sin(\theta_{s,1}) - \sin(\theta_{s,3}))(\cos(\theta_{s,1}) - \cos(\theta_{s,2}))} \quad (\text{Eq 5-26})$$

The static torque of the shank can now be determined relative to the marker located at the knee. A similar method is used to determine the constants relating to the static torque of the thigh. Again the orientation of the trunk is held constant and its effects are eliminated when the difference of two positions is considered. The difference in torque of two positions includes the terms relating to the translation of the thigh center of mass as it rotates about the hip joint, the shank center of mass as it rotates about the knee, and the shank as the knee translates with the thigh rotation. If the shank is held at a constant angle relative to the platform the change in the static torque due to its rotation will also be eliminated. Assuming the trunk and the rotation of the shank are constant the equation relating the difference in torque will be as follows.

$$\Delta T = C_{t,1}(\Delta \cos(\theta_t)) - C_{t,2}(\Delta \sin(\theta_t)) + m_s g l_t (\Delta \cos(\theta_t)) \quad (\text{Eq 5-27a})$$

The terms relating  $C_1$  of the thigh and the mass of the shank are not linearly dependent and therefore cannot be separately determined. Therefore, they are combined into a single constant  $C_1$  as is shown in the following equations.

$$\Delta T = (C_{t,1} + m_s g l_t)(\Delta \cos(\theta_t)) - C_{t,2}(\Delta \sin(\theta_t)) \quad (\text{Eq 5-27b})$$

Redefine  $C_{t,1}$  to be

$$C_{t,1} = m_t g r_t \cos(\theta_{cm,t}) + m_s g l_t \quad (\text{Eq 5-28})$$

$$\Delta T = C_{t,1}(\Delta \cos(\theta_t)) - C_{t,2}(\Delta \sin(\theta_t)) \quad (\text{Eq 5-27c})$$

The solution for the two constants is the same as the solution determined for the shank segment. Three additional positions are needed to determine the two constants.

$$C_{t,1} = \frac{(T_4 - T_5) + C_{t,2}(\sin(\theta_{t,4}) - \sin(\theta_{t,5}))}{(\cos(\theta_{t,4}) - \cos(\theta_{t,5}))} \quad (\text{Eq 5-29})$$

$$C_{t,2} = \frac{(T_4 - T_6)(\cos(\theta_{t,4}) - \cos(\theta_{t,5})) - (T_4 - T_5)(\cos(\theta_{t,4}) - \cos(\theta_{t,6}))}{(\sin(\theta_{t,4}) - \sin(\theta_{t,5}))(\cos(\theta_{t,4}) - \cos(\theta_{t,6})) + (\sin(\theta_{t,4}) - \sin(\theta_{t,6}))(\cos(\theta_{t,4}) - \cos(\theta_{t,5}))} \quad (\text{Eq 5-30})$$

## Analysis

The previous section outlines the method for determining the constants relating the orientation of the leg segments to the static

torque and center of mass. This section outlines the method used to determine the accuracy of this approach. The model is limited to the thighs and shanks of the body. These segments have the largest masses and most definable geometries, and therefore have the least amount of error. Consideration of uncertainties is limited to the accuracy of the force platform and the motion recording system. The uncertainty of the force platform torque measurements is 1.9 Nm. The uncertainty associated with the marker locations determined by the motion analysis system is 0.5 mm. Errors associated with changing mass properties due to soft tissue movement and skin slippage are not considered.

## Model Definition

The model consists of two ideal links representing the thighs and the shanks. Since the movement associated with a sit-up is considered to be symmetrical the properties include both legs. The mass properties of the links shown in Table 5-1 are for an average male [Kingma 1996; Andrews 1996].

Table 5-1 Mass Properties of Thighs and Shanks

	Thighs	Lower Legs
Mass	14.80 kg	8.40 kg
$\theta_{cm}$	7.5 deg.	5 deg.
$r_{cm}$	0.27 m	0.26 m
Length	0.54 m	0.52 m

For this analysis the trunk does not move and therefore, the torque due to the trunk is constant for each position, and can therefore be eliminated from the total torque calculations. For convenience, the coordinate system can be moved to the location of the hip joint.

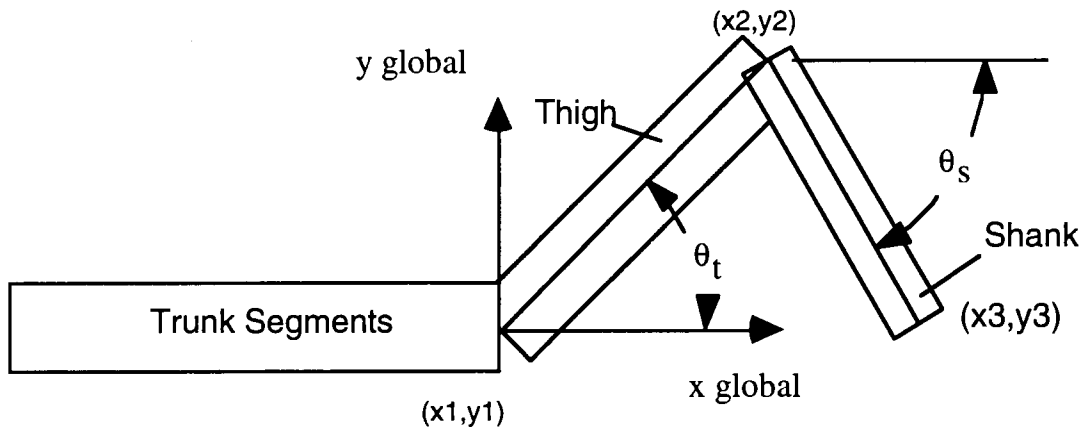


Figure 5-5 Adjusted Global Coordinate System

The actual values of the constants are calculated from the following equations, and shown in the Table 5-2 below.

$$C_{s,1} = r_s m_s g \cos(\theta_{cm,s}) \quad (\text{Eq 5-17})$$

$$C_{s,2} = r_s m_s g \sin(\theta_{cm,s}) \quad (\text{Eq 5-18})$$

$$C_{t,1} = m_t g r_t \cos(\theta_{cm,t}) + m_s g l_t \quad (\text{Eq 5-28})$$

$$C_{t,2} = r_t m_t g \sin(\theta_{cm,t}) \quad (\text{Eq 5-18})$$

Table 5-2 Actual Values of the Static Torque Constants

Constant	Actual Value
Cs,1	21.3 Nm
Cs,2	1.9 Nm
Ct,1	83.3 Nm
Ct,2	5.1 Nm

The total torque of the legs can be calculated from the following equation, and the total torque of the legs in six different positions is shown in Table 5-3.

$$T_i = C_{t,1} \cos(\theta_{t,i}) - C_{t,2} \sin(\theta_{t,i}) + C_{s,1} \cos(\theta_{s,i}) - C_{s,2} \sin(\theta_{s,i}) \quad (\text{Eq 5-31})$$

Table 5-3 Leg Torque in Static Positions

Position	Angle of Thighs (deg)	Angle of Lower Legs (deg)	Total Torque of Legs (Nm)
1	45	0	76.6
2	45	-60	67.6
3	45	-90	57.2
4	0	0	104.7
5	60	0	58.6
6	90	0	16.2

The uncertainty in the calculation of the constants is determined from the following equation.

$$U_c = \sqrt{\sum \left( \frac{\delta C}{\delta x_i} Ux_i \right)^2} \quad (\text{Eq 5-32}) \quad (\text{Figliola and Beasley pg. 180})$$

The resulting uncertainties in the calculation of the constants, the torque and the center of mass of the legs are shown in Table 5-4.

Table 5-4 Uncertainty in Static Coefficients

Constant	Uncertainty
Cs,1	4.6 Nm
Cs,2	3.8 Nm
Ct,1	4.6 Nm
Ct,2	3.8 Nm
T	7.1 Nm
x <sub>cm</sub>	3.1 cm

## Conclusions

The results show that the uncertainty in the position of the center of mass of the two most accurate segments of the body is  $\pm 3.1$  cm. This is larger than the three link analysis of the current measurement methods in chapter 3 of this study. Therefore, this method does not present an improvement to the existing methods. If this method were applied to the trunk segments of the body that have smaller masses and less flexibility the margin of error would increase. In this study improvements on this method are limited by the accuracy of the force platform. There are other sources of error that are not considered in this study, that would also limit the effectiveness of this method. One of the sources of error would be the location of the markers. The ideal marker location would be at the point of the joint rotation, but



several studies have shown that defining these joint centers can result a large source of error [Leva 1996; Hinrichs 1990]. Skin slippage changes the marker position relative to the skeleton by as much as 2.0 cm [Cappozzo 1993]. Another source of error would be caused by the soft tissue movement relative to the skeleton [Kingma 1995]. Given the known uncertainty due to the precision of the force platform and the additional sources of error this method does not result in an improved estimate of the mass properties.

## Chapter 6

### Summary and Conclusions

When the center of pressure passes through the hip joint the subject can contract the hip flexor muscles and lift the torso into a sitting position. One of the goals of the sitting-up experiments in Dr. Cordo's laboratory is to show that the timing of the hip flexor activity is coordinated with the coincidence of the center of pressure and the hips. It is also important to distinguish the static and dynamic components of the center of pressure to account for the contribution of the forces on the sitting-up motion.

The goal of this study was to determine if the location of the center of mass of a subject performing a sit-up can be determined with a sufficient resolution. This study shows that the anthropometric, dynamic, and static methods investigated in this study, as they are presented, cannot be used to calculate the position of the center of mass with the same precision as the center of pressure is measured. In a sit-up, the center of pressure and mass move about 25 cm in an individual with average dimensions. Approximately 75% of this distance or about 18 cm lies between the starting location (i.e. mid torso) and the hip joint. The center of pressure measurements have a relatively large uncertainty of  $\pm 1.2$  cm, which represents 5-10% of the total

distance moved to the hips. The most precise center of mass calculations have an uncertainty twice as large (10-20%). In a sit-up where the center of pressure took 2 seconds to reach the hips, the timing uncertainty related to the location of the center of mass would be 10-20% of the total time, or 200-400 ms. This amount of uncertainty would make it impossible to identify a correlation between the timing of muscle activation and the coincidence of the center of mass and the hip joint.

The anthropometric model uses measurements of the subject's height, weight and segment dimensions to calculate the mass properties of the segments. The analysis of the uncertainty in using the anthropometric method resulted in an average uncertainty of  $\pm 2.66$  cm. The investigation showed that the largest source of error was due to the uncertainty of the estimation of the segment masses. The error due to the uncertainty of the mass alone resulted in an average center of mass location uncertainty of  $\pm 2.56$  cm.

The dynamic method used a different approach to solve for the mass properties of the segments. This method attempted to solve for the mass properties of the segments from the motion of the segments and the ground reaction forces. The force and torque balance equations written in matrix form and solved using a least squares approach. The motion and ground reaction forces of a real experiment were used to solve for the mass and moments of

inertia of the subject. The results were found to be unreliable. The solution contained negative values for the mass and moment of inertia for some of the segments. The most likely source of the inaccuracies is due to the small magnitude of the independent force terms in comparison to the precision of the force platform. Verification of this hypothesis would require further investigation and it is beyond the scope of this thesis.

The final method discussed in this thesis is the static method. This approach used static relationships to determine the coefficients of the static torque of the individual segments. The coefficients relate the position and orientation of the segments to the static torque. The center of mass can be determined by dividing the sum of the static torque by the weight of the subject. This method is limited by the precision of the force platform. The application of this method to a rigid body model of the thighs and shanks resulted in an uncertainty of 3.1 cm which is larger than the whole body model analyzed for the anthropometric method uncertainty. The uncertainty using the static method would increase if it was applied to all of the segments of the body.

The study has shown that the uncertainty of the mass property estimates and the measurement devices limit the accuracy of the location of the center of mass. Improvements in the estimates of the mass properties would decrease the uncertainty using the anthropometric method, and improvements in the measurement

devices would improve the accuracy in the static and dynamic methods. However, there is another source of error that is not considered in this study or addressed in the literature. All of the efforts to determine the center of mass model the segments as rigid bodies. During movement the soft tissues of the body move and change the distribution of the mass within the segments. The effect of these changes is unknown, and should be investigated before the results are relied upon to give an accurate estimate of the center of mass location.

# Bibliography

Andrews, J.G. and Mish, S.P. (1996) Methods for investigating the sensitivity of joint resultants to body segment parameter variations. *Journal of Biomechanics* V29,5 651-654

Ball, K.A. and Pierrynowski, M.R. Classification of errors in locating a rigid body. *J-Biomech.* Volume 29, Issue 9, September 1996 page 1213-1217

Bevington, Philip R., *Data reduction and error analysis for the physical sciences.* McGraw-Hill Inc., New York, 1992

Borget, A.J. van den, Read, L., and Nigg, B.M. (1996) A method for determining inverse dynamic analysis using accelerometry. *Journal of Biomechanics* V29,7 949-954

Cappozzo, A., Catani, F. and Leardini, A. (1993) Skin movement artefacts in human movement photogrammetry. *Proc. XIVth Congress of the Int. Society of Biomechanics.*

Clauser, C.E., McConville, J.T. and Young, J.W. (1969) Weight, volume, and center of mass of segments of the human body. AMRL Technical Report 69-70, Wright-Patterson Air Force Base, Ohio (NTIS No. AD-710-622)

Cordo, P.J., Verschueren, S.M.P., Smith, T.C., Gurfinkel, E.V., and Gurfinkel, V.S. Coordination of Sitting-up. Posture and Gait Symposium Paris, France 1997

Figliola, R.S. and Beasley, D.E. *Theory and Design for Mechanical Measurements*. John Wiley and Sons, Inc. New York 1995

Hall, M.G., Fleming, M.J. Dolan, Millbank, S.F.D., and Paul, J.P. (1996) Static in situ calibration of force plates. Journal of Biomechanics V29,5 659-665

Hinrichs, R.N. (1990) Adjustments to the center of mass proportions of Clauser et al. (1969). Journal of Biomechanics V23,9 949-951

Kalos, M.H. and Whitlock, P.A. Monte Carlo Methods, Volume 1: Basics. John Wiley and Sons, Inc. New York 1986

Kingma, I.M., Toussaint, H.M., De Looze, M.P., and Van Dieen, J.H. Segment inertial parameter evaluation in two anthropometric models by application of a dynamic linked segment model Journal of Biomechanics v.29,5 pp693-704 1996

Kingma-I. Toussaint-H-M. Commissaris-D-A. Hoozemans-M-J., Ober-M-J. Optimizing the determination of the body center of mass. J-Biomech. 1995 Sep. 28(9). P 1137-42.

Koopman, B., Grootenboer, H.J., and Jongh, H.J. (1995) An inverse dynamics approach for the analysis, reconstruction and prediction of bipedal walking. Journal of Biomechanics V28,11 1369-1376

Leva, P. (1996) Joint center longitudinal positions computed from a selected subset of Chandler's data. Journal of Biomechanics V29,9 1231-1233

Martin-P-E. Mungiole-M. Marzke-M-W. Longhill-J-M. The use of magnetic resonance imaging for measuring segment inertial properties. J-Biomech. 1989. 22(4). P 367-76.

McConville, J. T., Churchill, T. D., Kaleps, I., Clauser, C. E. and Cuzzi, J. (1980) Anthropometric relationships of body and body segment moments of inertia. Report No. AFAMRL-TR-80-119, Wright-Patterson Air Force Base, OH.

Robinson, Enders A. *Least Squares Regression Analysis in Terms of Linear Algebra*. Goose Pond Press, Houston, Texas. 1981



Wei, Chen and Jensen, Robert K. (1995) The application of segment axial density profiles to a human body inertia model. Journal of Biomechanics V 28,1 103-108

MATLAB 5.0, The MathWorks, Inc., Natick, MA

Working Model 2D 4.0, Knowledge Revolution, San Mateo, CA

# Appendix A

## Force Platform

### Force Platform Reaction Forces

The force platform is designed to measure the reaction forces in three directions. This allows us the calculation of the perpendicular and parallel forces, and the relative torques.

Figure A1 shows the platform and the measurement recorded at each support.

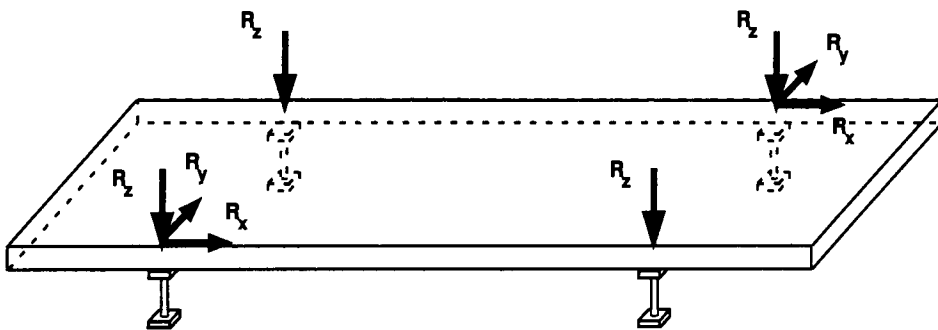


Figure A1 Force platform force measurements.

The force platform is designed to measure the voltages of Wheatstone bridges located on each of the four corners of the platform. The figure above shows the corresponding reaction forces. The upper right and lower left corners have gages that measure force in three directions. The other two corners only

measure the force in the vertical direction. The four supports are machined aluminum columns with strain gages attached.

The platform is made of aluminum. The top surface is flat and smooth and the underside is a web of 5 cm flanges designed for rigidity. The length of the platform is 192 cm including two end plates, each 25 cm, and the width is 66 cm. The distance between the supports is 117 cm. The rigid plate is designed to resist bending, but it is expected that there will still be a very small amount of deflection in the plate. This is one of the properties of the system that influences the accuracy.

The force is transferred through the supports at the four corners of the platform. Strain gages are attached to these machined aluminum columns. Figure A2 shows the column located at the lower left corner of the platform.

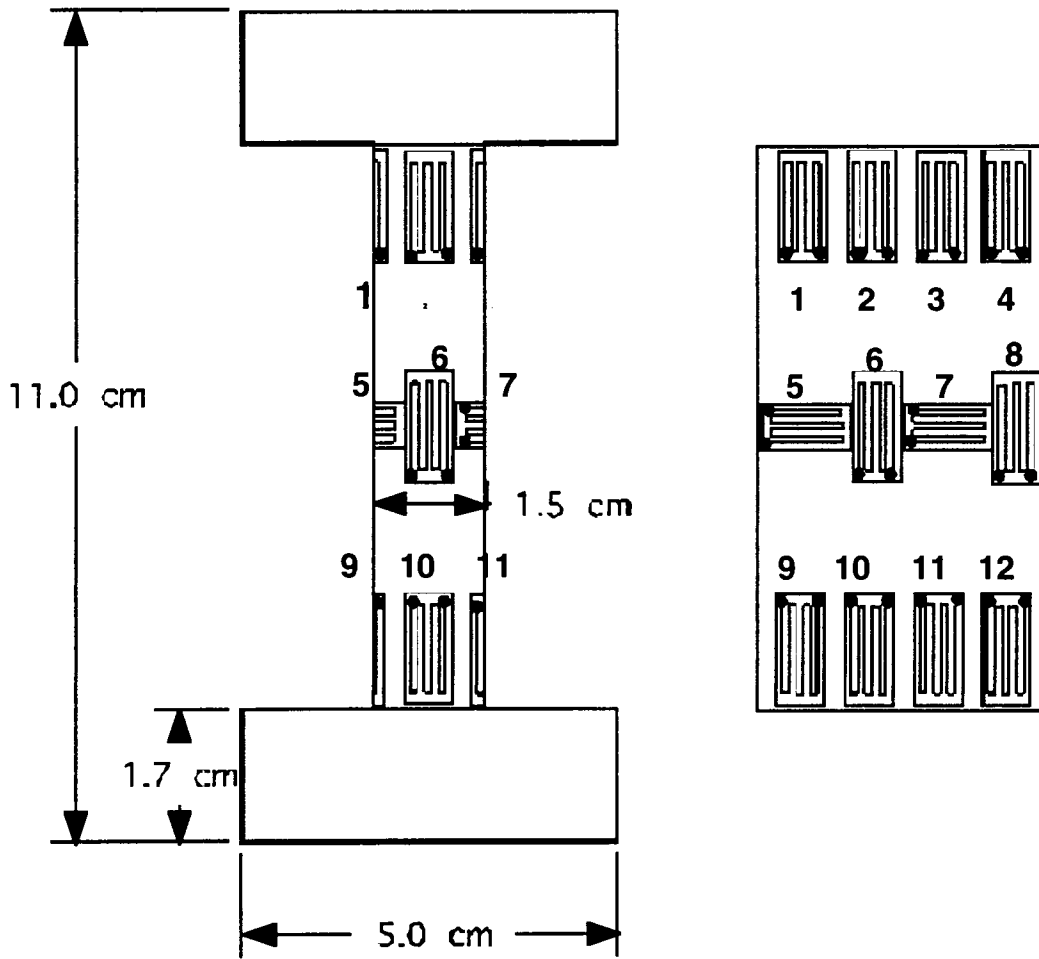


Figure A2 Support Column

The dimensions of the four columns are identical.

## Strain Gage Readings

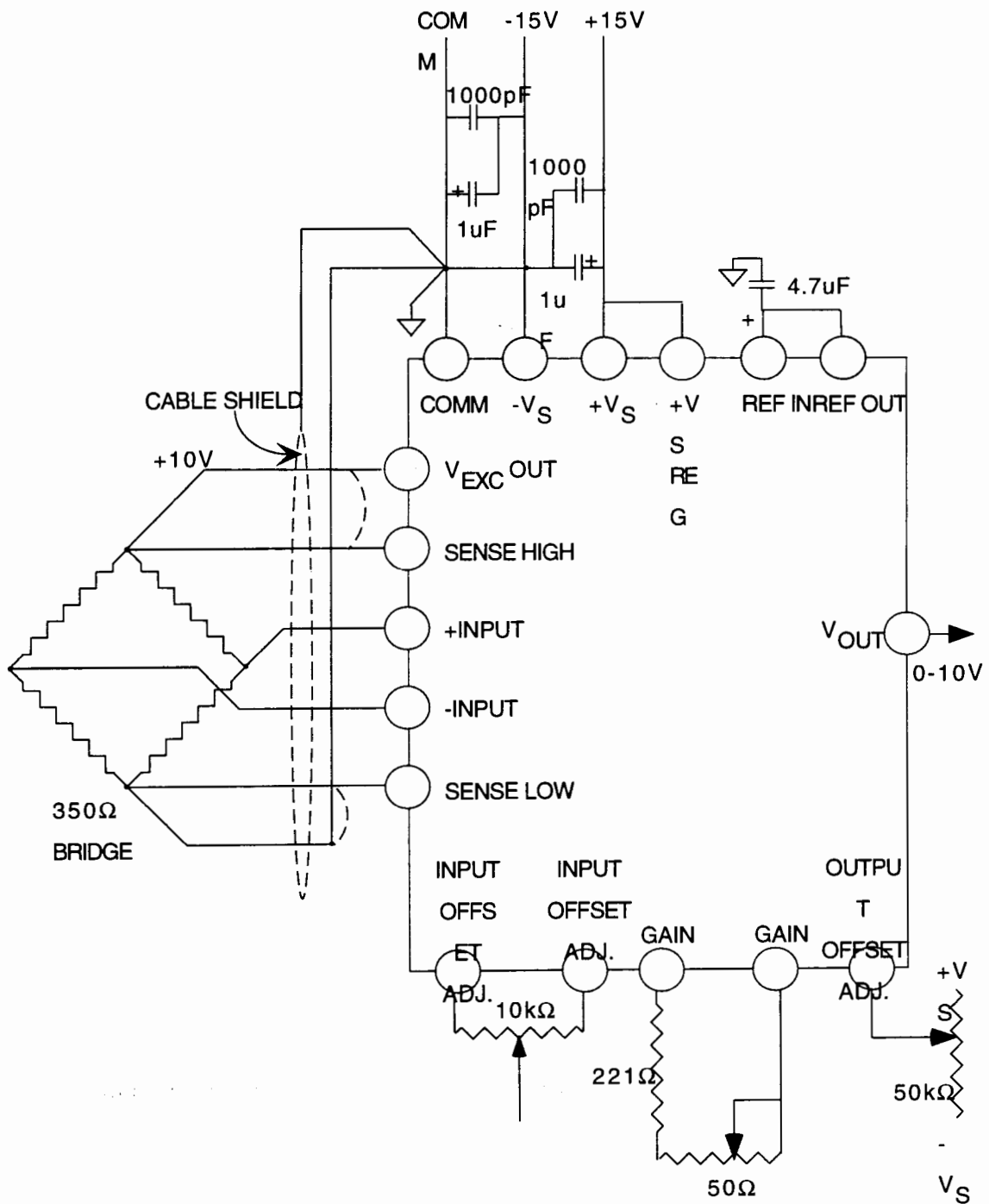
The strain gage locations are identical for the diagonal corners. Figure A1 shows that the upper right and lower left corners measure force in three directions and the strain gages are oriented as shown in the previous figure. The opposite two corners only measure the force in the vertical direction and only

have the center set of gages. The strain gages are wired into a Wheatstone bridge. The gages are specified as linear for the region that this platform operates in.

## Strain Gage Conditioners

Figure A3, on the following page, shows the strain gage conditioner wiring. The wide bandwidth strain gage signal conditioner, 1B31AN, is used.

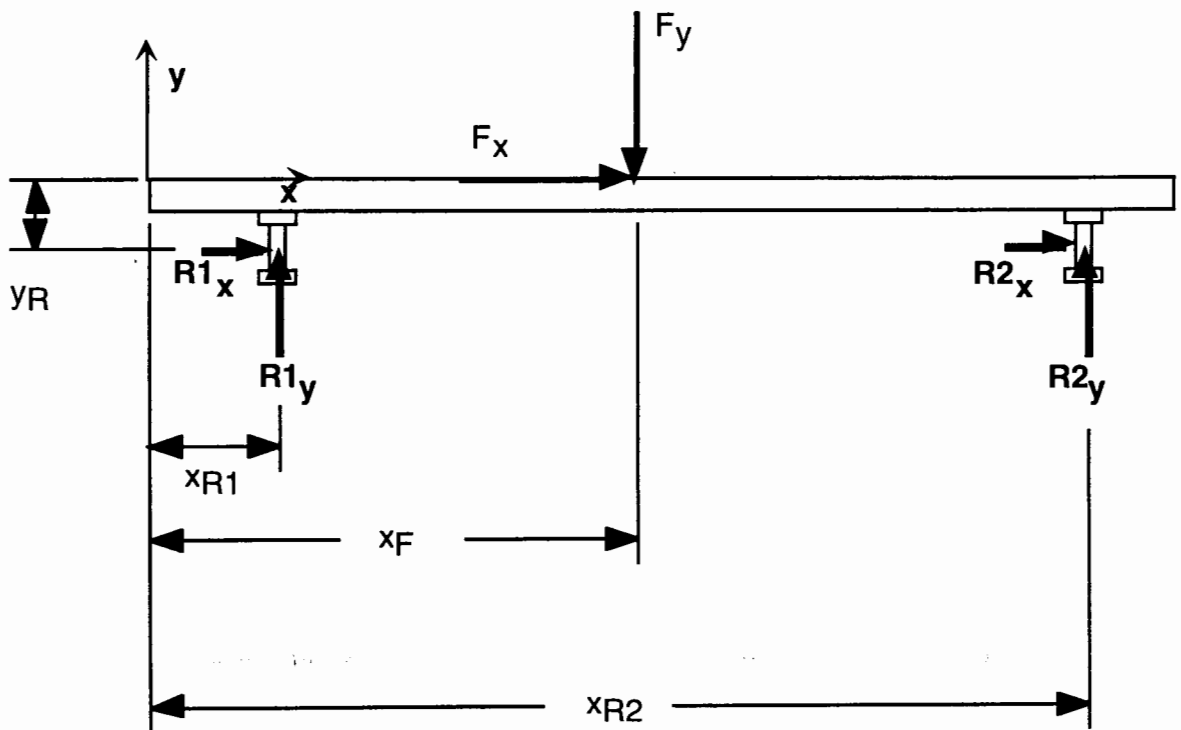
# Wide Bandwidth Strain Gage Signal Conditioner 1B31AN



The figure shows the configuration used for this set up. The advantages of using this set up is that the offset can be eliminated by adjusting the  $10\text{k}\Omega$  potentiometer wired to the INPUT OFFSET ADJ. terminal. The output offset can be adjusted as well using the  $50\text{k}\Omega$  potentiometer wired across the OUTPUT OFFSET ADJ. terminals. This allows us to eliminate the effect of the weight of the platform. The configuration also includes a low pass filter set at  $1\text{KHz}$  to eliminate noise. The resulting output voltage range is set to 0 to 10 volts corresponding to 0 to 400 N force. This gives a 40 N/V resolution.

# Calibration

We are interested in three table reaction forces, the vertical force, the horizontal force, and the torque. Therefore, the table must be calibrated such that the appropriate gains can be determined to translate the output voltages of the load cells into the three reaction forces. The following figure shows a two dimensional side view of the forces acting on the platform. The platform reaction forces ( $R1_x$ ,  $R1_y$ ,  $R2_x$ ,  $R2_y$ ) are shown at the center of the load cells where they are measured.





Where:

$F_y$  = vertical force applied to the surface of the platform

$F_x$  = horizontal force applied to the surface of the platform

$R_{1x}$ ,  $R_{1y}$  = reaction forces measured at the load cells closest to  
the reference point

$R_{2x}$ ,  $R_{2y}$  = reaction forces measured at the load cells farthest  
from the reference point

The force balance equations for the platform are as follows.

$$\sum F_x = 0$$

$$F_x - (R_{1x} + R_{2x}) = 0$$

$$F_x = R_{1x} + R_{2x}$$

$$\sum F_y = 0$$

$$F_y - (R_{1y} + R_{2y}) = 0$$

$$F_y = R_{1y} + R_{2y}$$

$$\sum M = 0$$

$$-x_F F_y + y_R (R_{1x} + R_{2x}) + x_{R1} R_{1y} + x_{R2} R_{2y} = 0$$

$$x_F F_y = y_R (R_{1x} + R_{2x}) + x_{R1} R_{1y} + x_{R2} R_{2y}$$

The output of the force table is the voltages of the strain gage bridges attached to the support beams. These output voltages are processed by a digital Butterworth filter. The filtered voltage data is translated into force data. In order to apply

this conversion the transformation gains have to be determined. The transformation gains relate the table output voltages to the vertical forces, the horizontal forces along the length of the table, and the torques about the axis perpendicular to the measured forces. There are a total of six outputs from the table, four vertical bridge voltages, and two horizontal bridge voltages. The transformation matrix composed of the gains is designed such that when it is multiplied by the six voltages measured from the table it results in the vertical force, the horizontal force, and the torque. The equation in matrix form is shown below.

$$\begin{bmatrix} v_{y1} & v_{y2} & v_{y3} & v_{y4} & v_{x1} & v_{x2} \end{bmatrix} \begin{bmatrix} g_{y1} & 0 & g_{T1} \\ g_{y2} & 0 & g_{T2} \\ g_{y3} & 0 & g_{T3} \\ g_{y4} & 0 & g_{T4} \\ 0 & g_{x1} & g_{T5} \\ 0 & g_{x2} & g_{T6} \end{bmatrix} = \begin{bmatrix} F_y & F_x & T \end{bmatrix}$$

Where:

$F_y$  = the total vertical force

$F_x$  = the total horizontal force

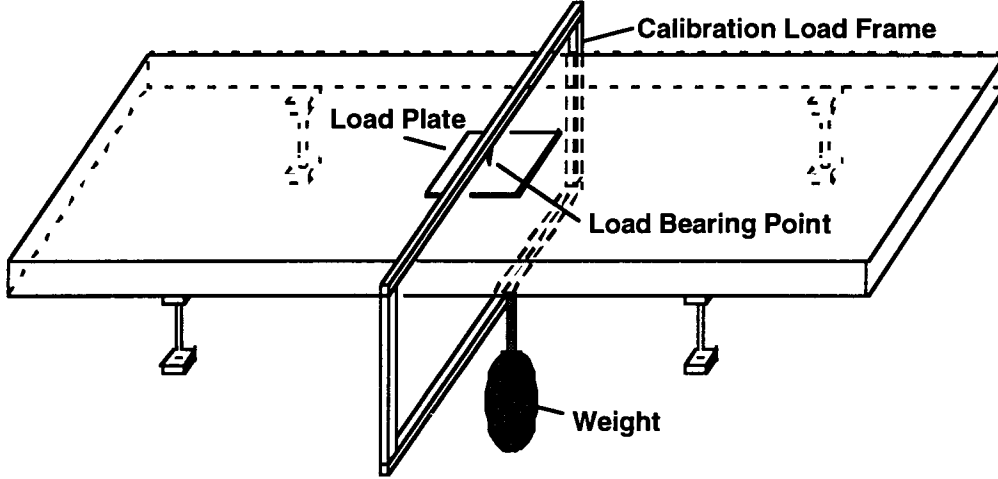
$T$  = the total torque

$v$  = the bridge output voltages

$g$  = the gains

A series of fifteen loads are used to determine the gains. The horizontal loads are applied using a pulley fixture attached to the end of the table. The table is vertically loaded using the

calibration frame. This frame as shown in the following figure allows the weight to be precisely applied to a specific point.



The loads are translated to their total horizontal forces, vertical forces, and torques, and the corresponding voltages are measured. A set of equations is now formulated that relates the differences in torque and load. These equations are of the following form.

$$\begin{aligned}
 T_1 - T_2 &= (v_{y1,1} - v_{y1,2})g_{T1} + (v_{y2,1} - v_{y2,2})g_{T2} + (v_{y3,1} - v_{y3,2})g_{T3} + (v_{y4,1} - v_{y4,2})g_{T4} \\
 &\quad + (v_{x1,1} - v_{x1,2})g_{T5} + (v_{x2,1} - v_{x2,2})g_{T6} \\
 F_{y1} - F_{y2} &= (v_{y1,1} - v_{y1,2})g_{y1} + (v_{y2,1} - v_{y2,2})g_{y2} + (v_{y3,1} - v_{y3,2})g_{y3} + (v_{y4,1} - v_{y4,2})g_{y4} \\
 F_{x1} - F_{x2} &= (v_{x1,1} - v_{x1,2})g_{x1} + (v_{x2,1} - v_{x2,2})g_{x2}
 \end{aligned}$$

For the calibration procedure the maximum number of difference equations are formulated from the set of fifteen loads. A least squares method is used to solve these equations for the gains.

The difference equations eliminates the need for a zero offset, and it eliminates the effects of the constant weight of the platform. Each of the gains relates the change in volts of a channel to the corresponding change in the reaction load. Therefore, a known load at a known voltage can be used instead of a zero load. The reference voltage and load are used in conjunction with the gain matrix to calculate the total load on the platform.

$$\begin{bmatrix} v_{y1} - vr_{y1} & v_{y2} - vr_{y2} & v_{y3} - vr_{y3} & v_{y4} - vr_{y4} & v_{x1} - vr_{x1} & v_{x2} - vr_{x2} \end{bmatrix} \begin{bmatrix} g_{y1} & 0 & g_{T1} \\ g_{y2} & 0 & g_{T2} \\ g_{y3} & 0 & g_{T3} \\ g_{y4} & 0 & g_{T4} \\ 0 & g_{x1} & g_{T5} \\ 0 & g_{x2} & g_{T6} \end{bmatrix} + \begin{bmatrix} Fr_y & Fr_x & Tr \end{bmatrix} = \begin{bmatrix} F_y & F_x & T \end{bmatrix}$$

Where:

$Fr_y$  = the reference vertical force

$Fr_x$  = the reference horizontal force

$T$  = the reference torque

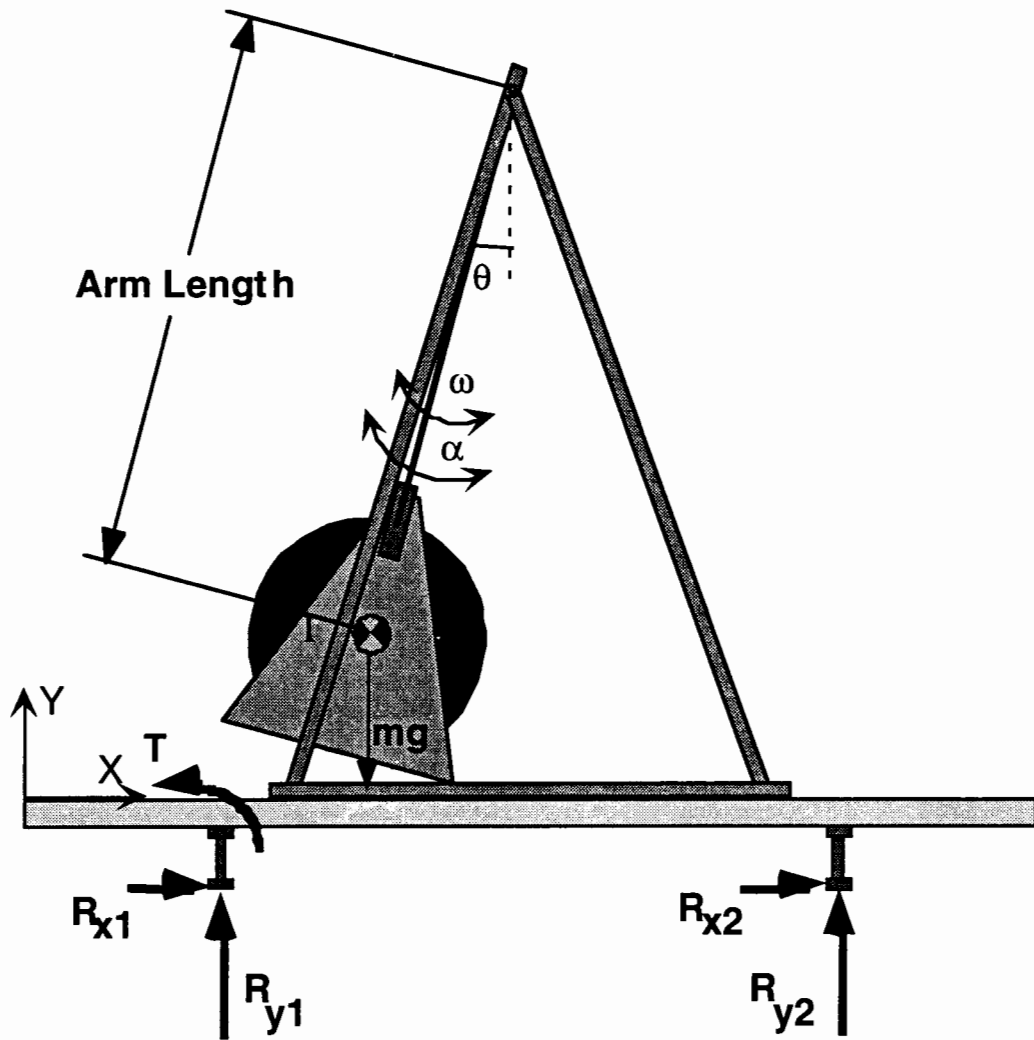
$vr$  = the reference output voltages

The accuracy of the static calibration is determined calculating the standard deviation of the difference between the known force load and the calculated force load using the gain matrix and the fifteen calibration trials. Two standard deviations is considered to be the accuracy of the calibration. The following table shows the accuracy of the static calibration.

	Uncertainty
Horizontal Force	$\pm 2.4 \text{ N}$
Vertical Force	$\pm 2.4 \text{ N}$
Torque	$\pm 1.9 \text{ Nm}$

## Dynamic Verification

To verify that the table also records accurate information for dynamic movement it is required that a known dynamic force be applied to the table. To accomplish this a pendulum of known mass and arm length was attached to the table and the forces and torque were measured. The following figure shows the pendulum used.



The pendulum is described by the following differential equation.

$$\frac{d^2\theta}{dt^2} + \frac{cl}{(ml^2 + I)} \frac{d\theta}{dt} + \frac{mgl}{(ml^2 + I)} \sin(\theta) = 0$$

Where:

$\theta$  = Angular Displacement

$\frac{d\theta}{dt}$  = Angular Velocity

$\frac{d^2\theta}{dt^2}$  = Angular Acceleration

$c$  = Damping Constant (due to friction and air resistance)

$m$  = Mass of Pendulum

$I$  = Moment of Inertia

$l$  = Length of Pendulum Arm

$g$  = Acceleration due to Gravity

The previous equation is solved for the angular displacement. The angular velocity, and angular acceleration are calculated from the result. The initial conditions are a known initial displacement and zero initial angular velocity. Once the motion is determined the resulting forces and torque can be calculated using the following equations.

$$F_z = m \left( g + l \frac{d^2\theta}{dt^2} \cos(\theta) - \left( \frac{d\theta}{dt} \right)^2 r \sin(\theta) \right)$$

$$F_y = m \left( l \frac{d^2\theta}{dt^2} \sin(\theta) - \left( \frac{d\theta}{dt} \right)^2 r \cos(\theta) \right)$$

$$T = m \left( g + l \frac{d^2\theta}{dt^2} \cos(\theta) - \left( \frac{d\theta}{dt} \right)^2 r \sin(\theta) \right) (l \sin(\theta)) \\ + m \left( l \frac{d^2\theta}{dt^2} \sin(\theta) - \left( \frac{d\theta}{dt} \right)^2 r \cos(\theta) \right) (h - l \cos(\theta))$$

Where

$h$  = Height of Pivot Point

The results show that the dynamic measurements are within the uncertainty of the static measurements.

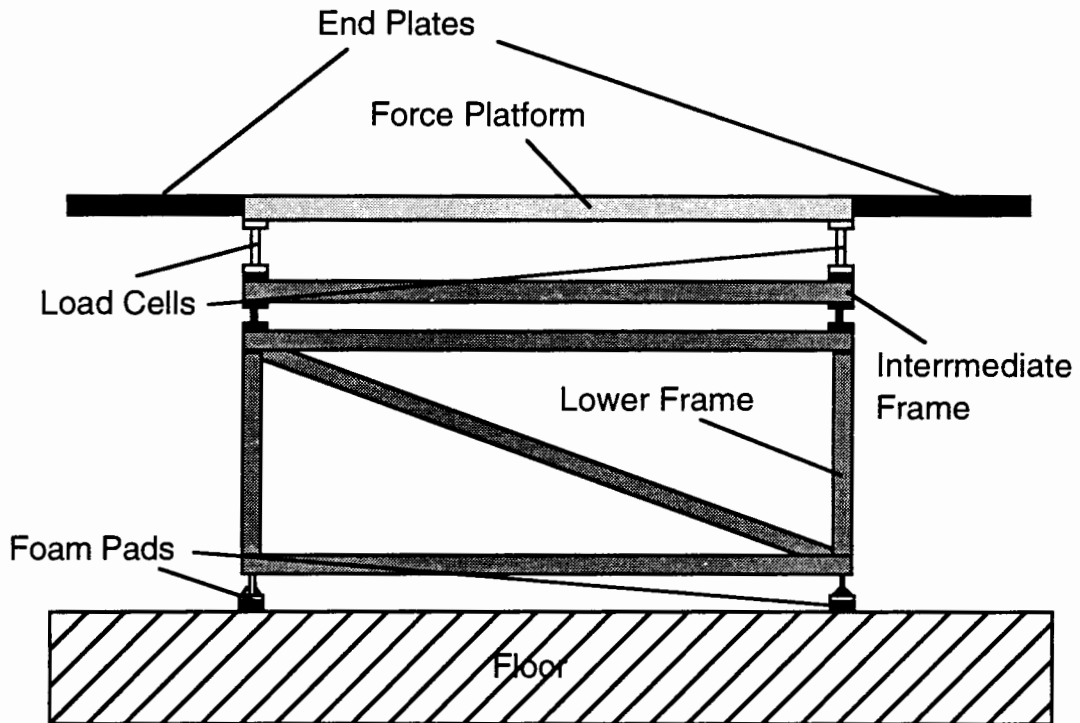


# Table Vibrations

## Introduction

We are interested in ensuring that the natural frequencies of the force platform are above the measured forces. To determine the natural frequencies we excite the platform in with an impact force and record the load cell voltage measurements after the impact. The resonant frequencies are determined by performing a spectral analysis of the voltage outputs. An accelerometer is used to determine if the voltage output from the load cells correspond to actual vibrations of the surface of the platform. Resonant frequencies are the result of the mechanical and electrical characteristics of the system.

Sources of vibration that could interfere with measurements include the force platform, the two end plates, the two supporting frames, the foam pads, the floor, and the electronics. The pads are designed to filter out the high frequency oscillations of the building.



The forces of interest applied by a human subject are present below 15 Hz. Therefore, any resonant frequencies below 15 Hz are of concern. The spectral analysis is used to determine the frequencies at which the platform is oscillating. Comparison between spectra for this experiment is limited to the frequencies at which there is a signal. The magnitude of the power should not be relied on for comparison because it changes with factors that are not sufficiently controlled in this experiment, such as the length of time in the trial after the impact and intensity of the impact. So the frequencies of the signals of two trials can be compared, but not the magnitudes of the signals at those frequencies.

## Experiment

The goal of the experiment is to excite the natural frequencies of the platform and record the voltage outputs of the load cells and the accelerometer. A power spectrum analysis of the outputs reveals the natural frequencies of the platform. The vertical platform excitation was achieved by dropping a 0.5 kg elastic ball from a height of approximately 1.25 m. A device used to measure point of contact was used to record the end of the impact time. The platform was excited horizontally by hitting the end of the table with the same ball. The reaction forces of the table and the accelerometer were recorded for five seconds. After the recorder was started, the ball was dropped onto the surface or tossed at the end of the platform. The contact device shows the end of the impact time for the vertical impact. The end of the horizontal impact was determined to be after the voltage has returned to its pre-impact magnitude. A frequency analysis was performed on the accelerometer and strain gage voltage outputs for the portion of the trial after the ball had left the table.

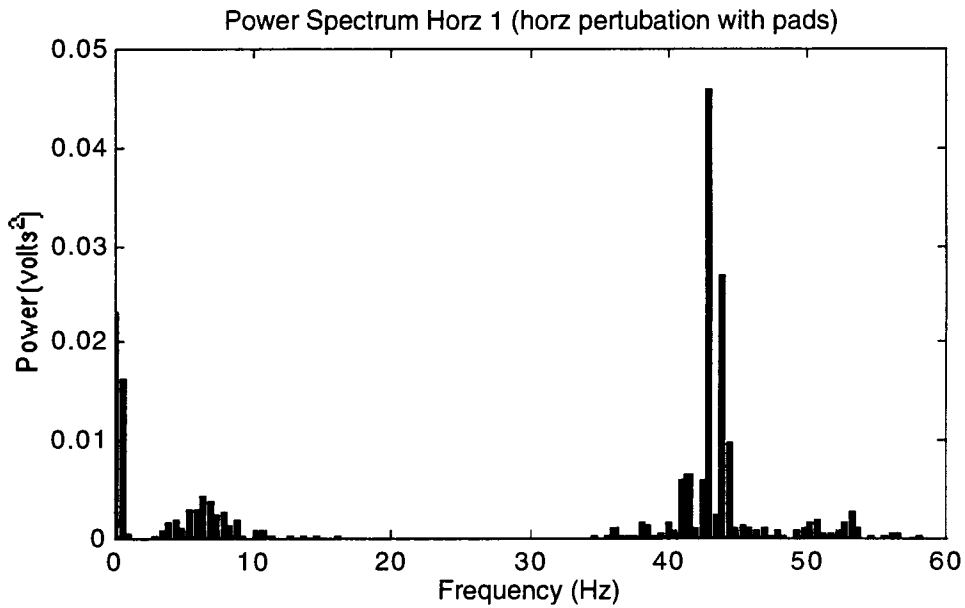
## Results

The first observations showed that the power spectrum is consistent for all four vertical supports. This was determined by

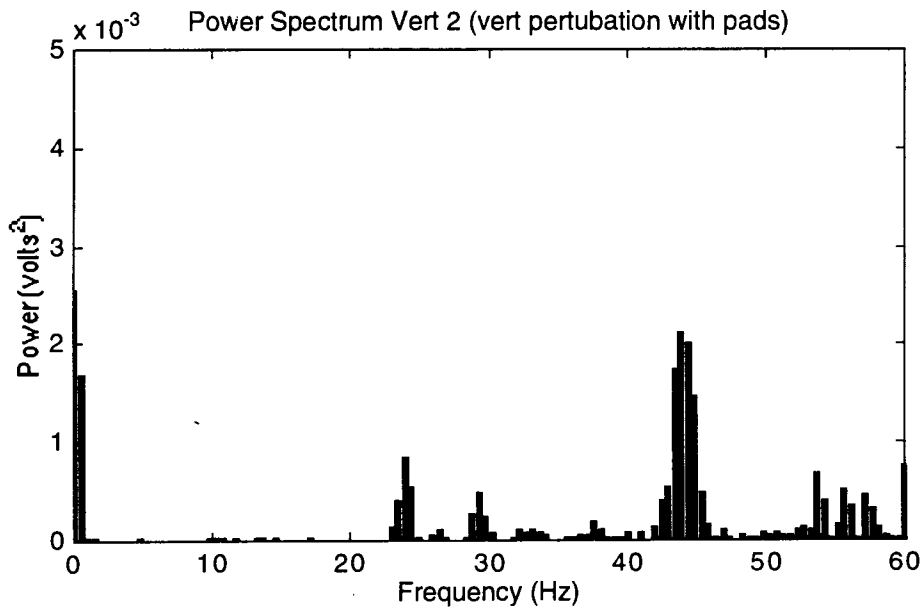
evaluating the power spectrum of the four voltage outputs from the strain gage configurations on the load cells. A similar result was found when the horizontal voltages were analyzed. The accelerometer was used to determine if the voltage readings corresponded to actual accelerations of the platform. To test this it was attached to the surface of the platform directly above one of the load cells. The result showed a very strong correlation between the voltage signal of the load cells and the accelerometer for both the vertical and horizontal directions.

The analysis showed that there are resonant frequencies in the system below 15 Hz when the platform is fully assembled and the pads are placed under the feet.

The following two figures show the horizontal and vertical natural frequencies present in the strain gage readings with the pads in place.

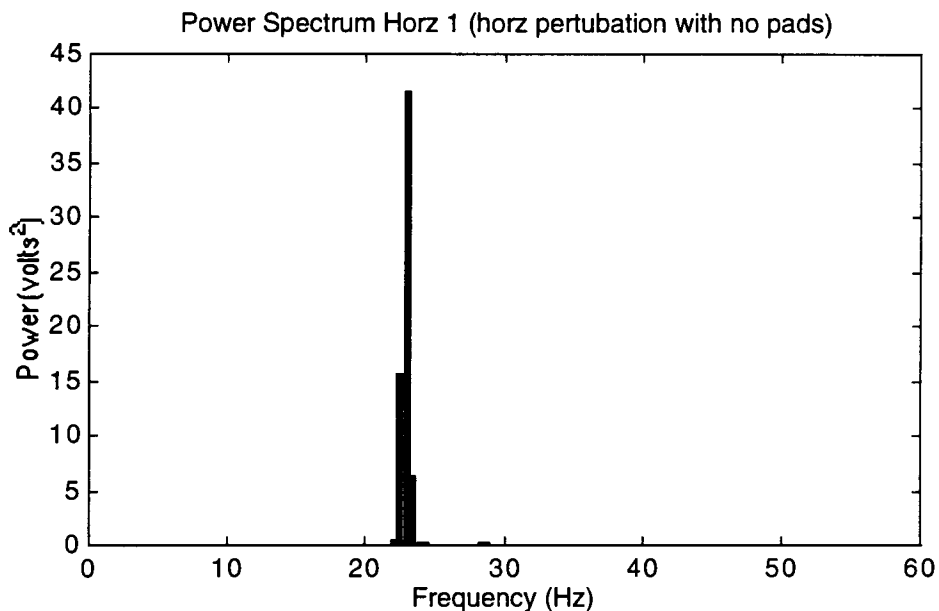


The previous figure shows that there is a signal at approximately 7 Hz in the horizontal strain gage recordings.

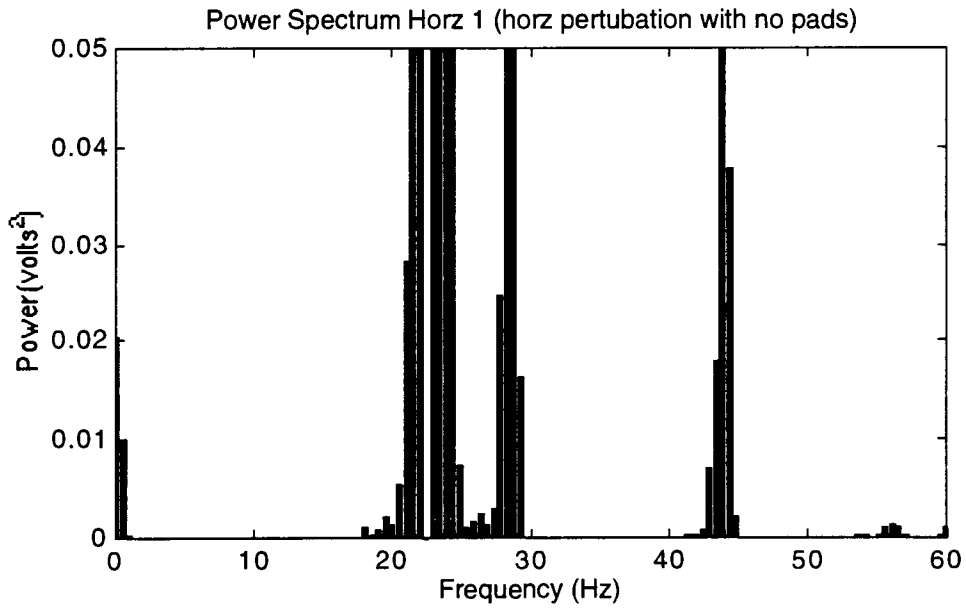


There are no signals below 20 Hz in the vertical direction.  
Further investigation revealed that the recorded low frequency

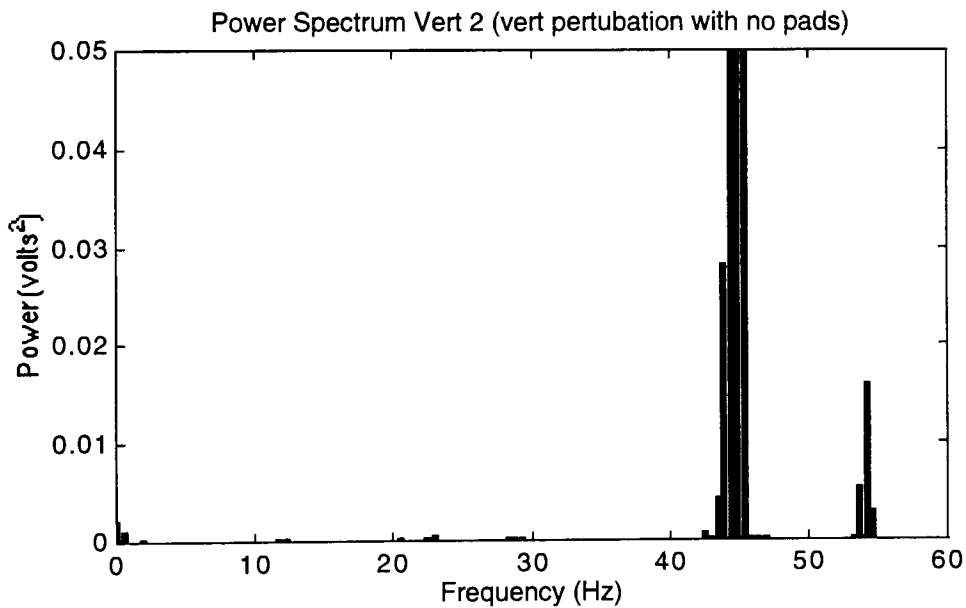
vibrations in the horizontal direction are the result of the foam pads placed under the feet of the lower frame. These pads are designed to filter out the higher frequency signals in the building, but the elastic properties of the pads introduce a new low natural frequency characteristic into the system. Therefore, the pads were removed from the feet and the platform was reevaluated. The following figures show the power spectrums after the pads were removed.



The previous figure shows that there is a significant signal at 24 Hz in the horizontal channel. The following figure magnifies the y-axis to see if there are any other signals of significance below 15 Hz.



The previous figures show that there is a significant signal at 24 Hz that appears when the pads are removed. However, the signal at 7 Hz. has been eliminated. The vertical power spectrum shows that no low frequency vibrations appear in this case.



## Conclusion

The results show that the removal of the pads eliminates all resonant frequencies below 20 Hz. It does, however, allow vibration from the floor to enter into the system at just above 20 Hz. Therefore the pads can be removed and a digital filter can be designed to eliminate all frequencies above 15 Hz.



# Filter Design

The system needs a digital filter to eliminate the higher frequency components in the output signals. The analysis of the frequency response of the system shows that there is a significant signal in the horizontal channels at 24 Hz. The measurement requirements state that it is desirable to preserve the signals below 15 Hz. Therefore, the digital filters requirements are to preserve the signal below 15 Hz and eliminate the signal above 20 Hz.

The voltage measurement range of the amplified strain gage signals is  $\pm 5$  V. The error resulting from the static calibration of the table is currently greater than 1.0 cm in terms of the center of pressure measurement. The error associated with 1.0 cm center of pressure measurement corresponds to 0.1 V in the strain gage voltage. Therefore, the attenuation in the pass band should be no greater than  $\pm 0.05$  V. This is equivalent to 0.086 dB. Further improvements in the calibration procedure may call for a revision of this value.

In the stop band the attenuation should be large enough to reduce the signals above 20 Hz to less than 0.05 V. The signal in the horizontal channels at 24 Hz has a magnitude of approximately 0.6 V when the table is unloaded. However, when the table is loaded with 300 N, the magnitude of the signal is

reduced to 0.08 V. Therefore, the signal must be reduced by a factor of 0.625, which is equivalent to 4.1 dB of attenuation in the stop band.

A classic Butterworth filter was chosen for two reasons. The first reason is that it has a very smooth and flat pass band, and the second reason is that it has a smooth and steep cutoff slope. Also to preserve the time sequence a double filtering technique is used that has zero phase distortion.

Pass Band: 0-15 Hz

Stop Band: 20- $\infty$  Hz

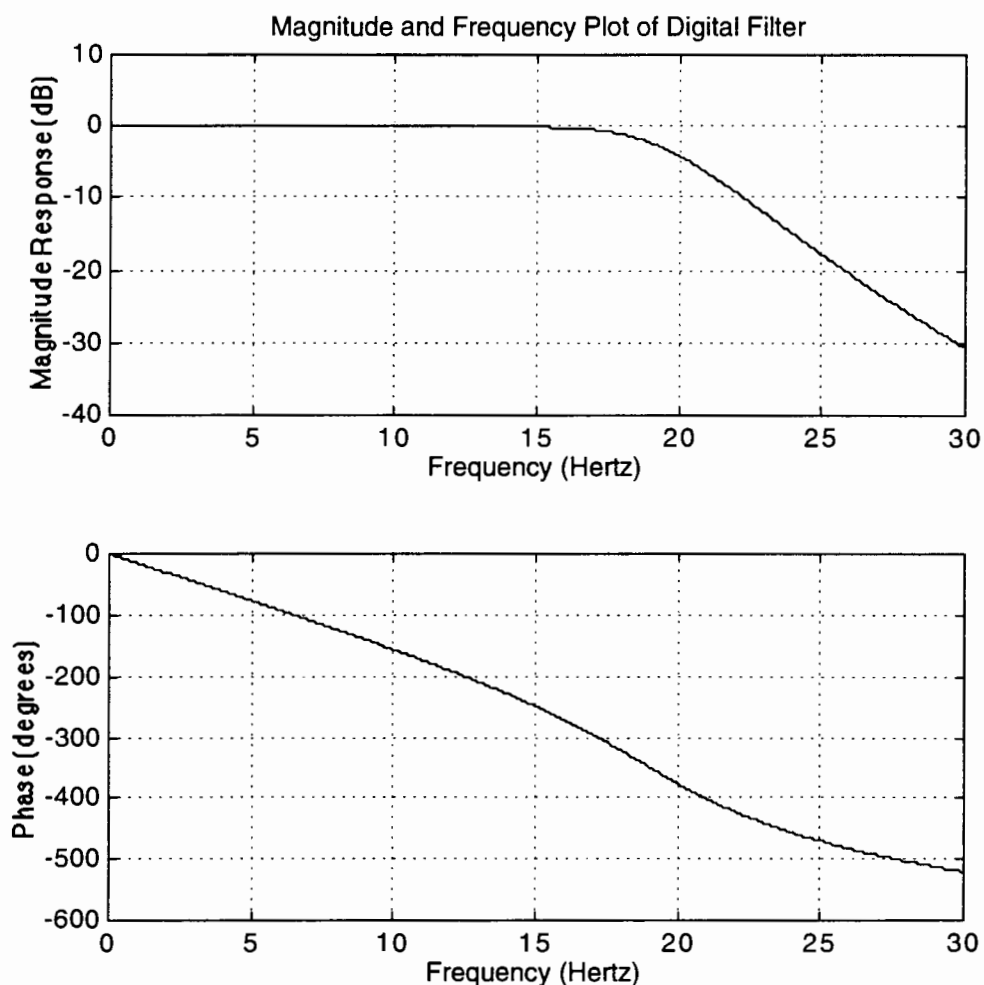
Maximum Attenuation in Pass Band: 0.086 dB

Minimum Attenuation in Stop Band: 4.1 dB

Filter Order: 8

Filter Natural Frequency: 19.4 Hz

The following figure shows the magnitude and frequency plots of the filter.



The filter is applied using the following difference equation in the forward direction and then the data is reversed and the filter is applied again. This eliminates all phase distortion in the filtered signal.

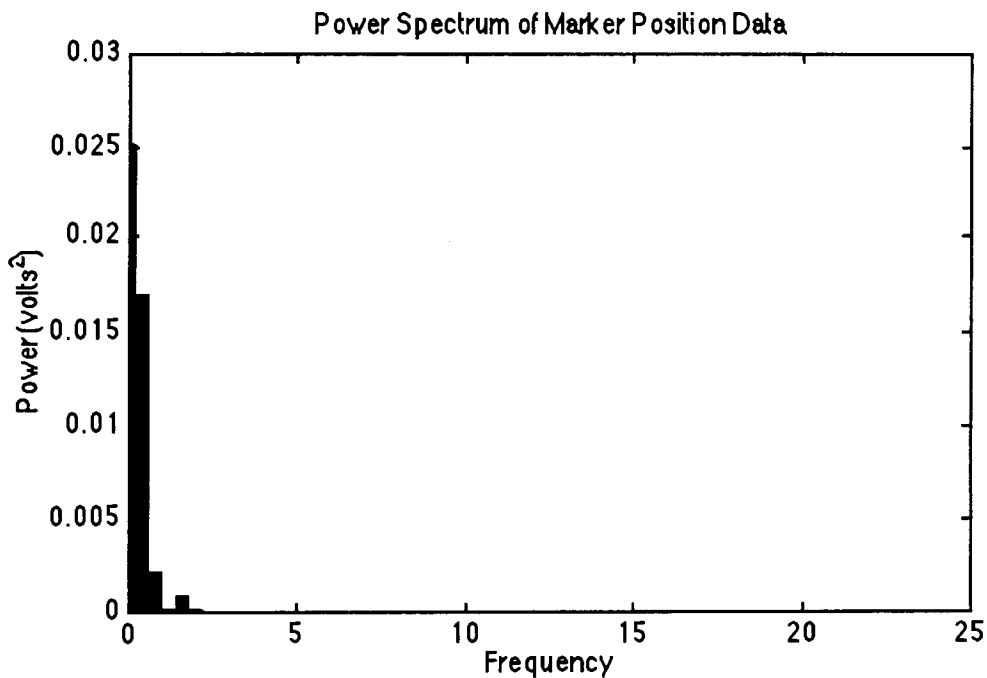
$$y(n) = b(1)*x(n) + b(2)*x(n-1) + \dots + b(nb+1)*x(n-nb) \\ - a(2)*y(n-1) - \dots - a(na+1)*y(n-na)$$

The coefficients used in this filter are shown in the following table.

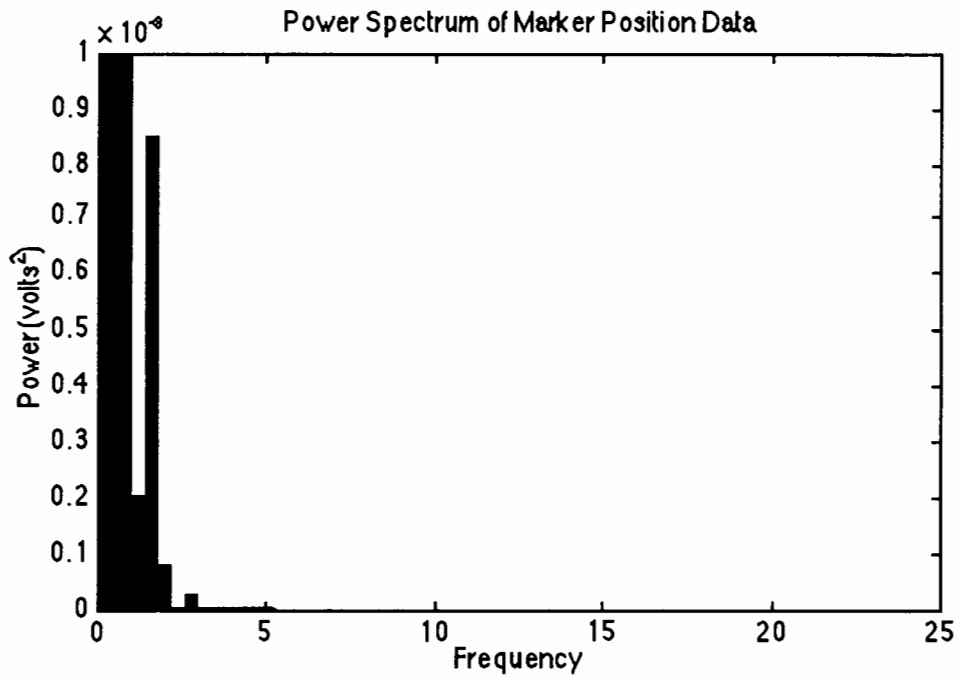
a	b	
1.000000000000000	0.00276126251838	e-05
-6.74753777266655	0.02209010014700	e-05
20.00402127588237	0.07731535051451	e-05
-34.02313166097544	0.15463070102903	e-05
36.30154206684909	0.19328837628629	e-05
-24.87559370070418	0.15463070102903	e-05
10.68892431516036	0.07731535051451	e-05
-2.63276494975526	0.02209010014700	e-05
0.28454749504166	0.00276126251838	e-05

# Marker Filter Design

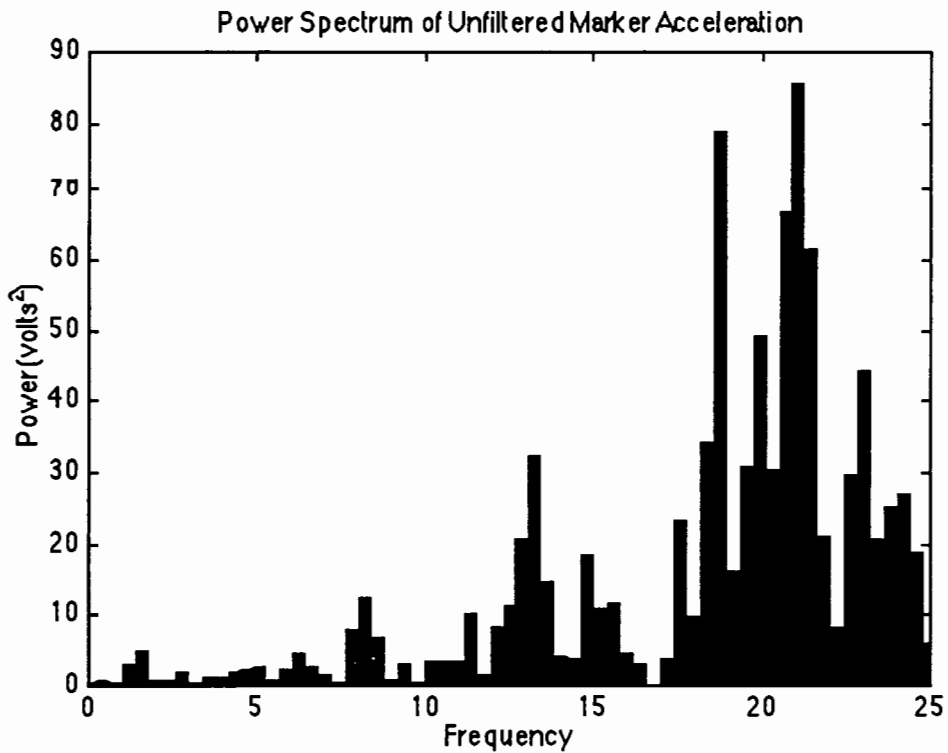
The marker position data error becomes significant when it is differentiated twice to calculate the acceleration data. Therefore, it is necessary to smooth the data before it is used to determine the acceleration. The following figure shows the power spectrum of the position data of a marker.



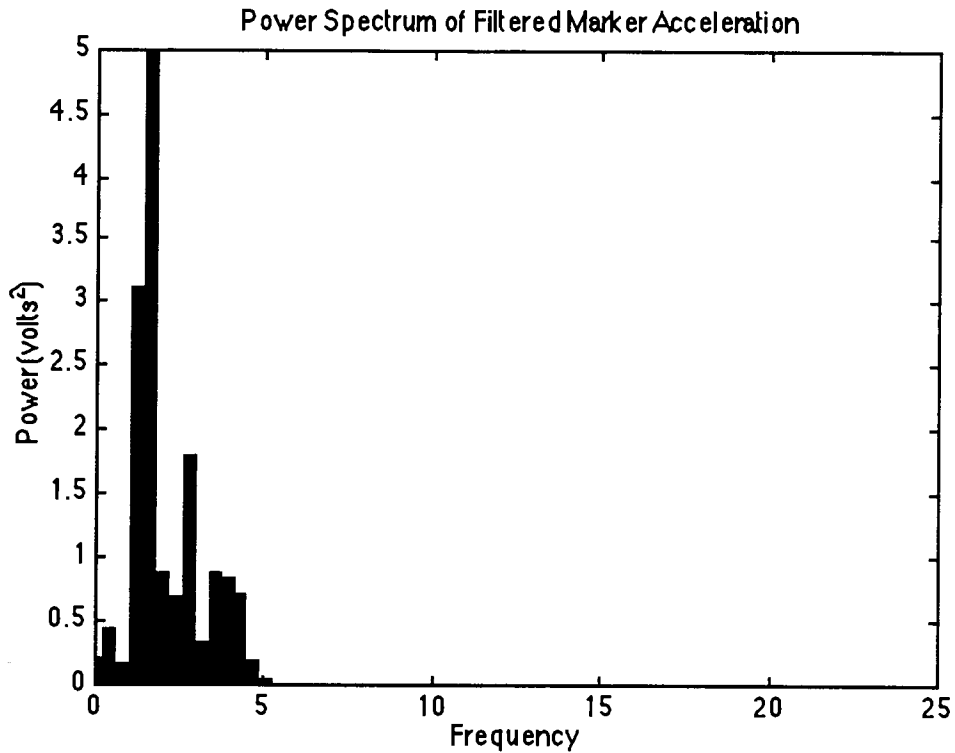
The previous figure shows that there are definitely low frequency signals. The following figure expands the y axis to make sure that there are not any higher frequencies that have a significant magnitude.



From the previous two figures we can conclude that there are not any significant signals above 3 Hz. If the unfiltered position data is differentiated twice to calculate the acceleration the power spectrum of the result would be as follows.



The previous figure shows that the higher frequencies dominate the signal. If the position data is filtered first and then used to calculate the acceleration then the signal would not have the higher frequency components. This is shown in the following figure.



A classic Butterworth filter was chosen as the filter design. To preserve the time sequence a double filtering technique is used that has zero phase distortion. The characteristics of the filter are shown below.

Pass Band: 0-3 Hz

Stop Band: 5 -  $\infty$  Hz

Maximum Attenuation in Pass Band: 0.01 dB

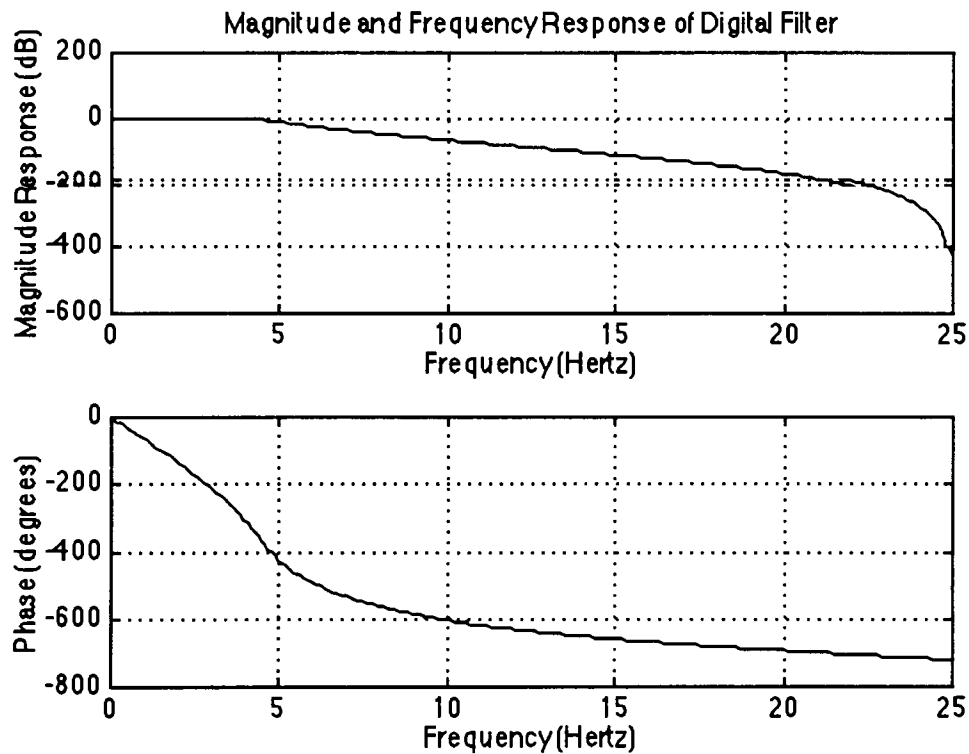
Minimum Attenuation in Stop Band: 10 dB

Filter Order: 8

Filter Natural Frequency: 4.4 Hz



The following figure shows the magnitude and frequency response of the filter.



The filter is applied using the following difference equation in the forward direction and then the data is reversed and the filter is applied again. This eliminates all phase distortion in the filtered signal.

$$y(n) = b(1)*x(n) + b(2)*x(n-1) + \dots + b(nb+1)*x(n-nb) \\ - a(2)*y(n-1) - \dots - a(na+1)*y(n-na)$$

The coefficients used in this filter are shown in the following table.

a	b * 1.0e-03
1.000000000000000	0.00982486102914
-5.17412639916459	0.07859888823312
12.06400450613629	0.27509610881591
-16.46278060825211	0.55019221763182
14.32829042946610	0.68774027203977
-8.12269786191790	0.55019221763182
2.92298398801270	0.27509610881591
-0.60945504380905	0.07859888823312
0.05629615395204	0.00982486102914

## Appendix B

### Monte Carlo Simulation m-file 'stderror'

```
function
[CoMstd,CoMa,STDResults,MinResults,MaxResults,CoMtrack]
    =stderror(t,xo,yo,mo,Io,Fx,Fy,T)

%   Inputs:
%       x = Matrix of x's
%       y = Matrix of y's
%       m = Matrix of actual masses
%       Fx = Actual Horizontal Reaction Forces
%       Fy = Actual Vertical Reaction Forces
%       T = Torque
%
%   Outputs:
%       CoMstd = Center of Mass Std for each position in time
%       CoMa = Actual Center of Mass Location
%       STDResults = Average Std
%       MinResults = Minimum Std
%       MaxResults = Maximum Std
%       CoMtrack = Record of each iteration's Center of Mass
%
%
g=9.80665;

%   Subtract the forces and moments associated with the table

tablemass=0.1264;
tablecm=0.79;
Fy=Fy-tablemass*g;
T=T-tablecm*tablemass*g;

%   Calculate the actual Center of Mass
```

```

xcm=(diff(xo'))'.*(ones(length(xo),1)*[43/80,1/2,1/2])...
    +xo(:,1:length(xo(1,:))-1);
ycm=(diff(yo'))'.*(ones(length(yo),1)*[43/80,1/2,1/2])...
    +yo(:,1:length(yo(1,:))-1);

```

```

CoMa=xcm*mo'/sum(mo);

```

```

len=length(CoMa);

```

```

seglength=sqrt(diff(xo(1,:)).^2+diff(yo(1,:)).^2);

```

```

%   Uncertainties in x and y, mass, and inertia

```

```

%   Marker Position (+/- 0.0005 m)
ux=0.0005;
uy=ux;
%   Skin Slipage (0-0.02 m)
uxslip=0.02;
uyslip=uxslip;
%   Center of Mass Location ([5,5,5])
%
uxcm=[5,5,5]/100;
lengthx=[0.36,0.43,0.39];
lengthy=[0.15,0.13,0.1];
%   Mass ([10.32,8.29,7.65])
%
um=mo.*[10.32,8.29,7.65]/100;
%   Moment of Inertia ([8.8,13.1,11.0])
uI=Io.*[8.8,13.1,11.0]/100;

```

```

[N, Wn] = BUTTORD(7/25,11/25, .1, 10);

```

```

[B,A] = BUTTER(N,Wn);

```

```

%   These variables are used to set the stability criteria in the
%       Monte Carlo Simulation
%   They are now set to get the loop started.

```

```

iterations=0;
CoMstdpast=0:100:9900;
conv=[];
CoMerror2=zeros(1,length(xo));

```

```

CoMerror=zeros(1,length(xo));
CoMtrack=[];
xcm40=[];
ycm40=[];

figure(2)
clf
hold

count=0;
tic

while max(abs(diff(CoMstdpast))) > 0.00001 & iterations<20000;
iterations=iterations+1;

% Calculate the orientation angle of the three segments
% clean data

thetasego=atan2(diff(yo)',diff(xo')));

% Set the error deviations

% Marker Position Error
dx=randn(size(xo))*ux/3;
dy=randn(size(yo))*uy/3;

% Skin Slippage Error
dxslip=ones(length(xo),1)*rand(1,length(xo(1,:)))...
-2).*(diff(thetasego')/(pi/2))*uxslip;
dyslip=ones(length(xo),1)*rand(1,length(yo(1,:)))...
-2).*(diff(thetasego')/(pi/2))*uyslip;

% Mass Error and Rescale the masses to match
% total sum of the mass
m=(mo+randn(1,3).*um);
m=m*(sum(mo)/sum(m));

% Moment of Inertia Error
I=Io+randn(1,3).*uI;

```

```

%    Add the Marker Position Error
x=xo+dx;
y=yo+dy;

%    Filter the Result
if ux > 0
    for k=1:length(x(1,:))
        x(:,k)=myfilt(B,A,x(:,k));
        y(:,k)=myfilt(B,A,y(:,k));
    end
end

%    Add the Skin Slippage Error
x(:,2:length(x(1,:))-1)=x(:,2:length(x(1,:))-1)+dxslip;
y(:,2:length(y(1,:))-1)=y(:,2:length(y(1,:))-1)+dyslip;

%    Calculate the orientation angle of the three segments
%    filtered data

thetaseg=atan2(diff(y)',diff(x)');

%    Calculate the Angular Acceleration
alphaseg=diff(diff(thetaseg))./.02^2;
alphaseg=[alphaseg(1,:);alphaseg;...
           alphaseg(length(alphaseg),:)];

%    Calculate the Center of Mass Location relative to the
%    first marker
xcml=(diff(x)').*(ones(length(x),1)*[43/80,1/2,1/2]);
ycml=(diff(y)').*(ones(length(y),1)*[43/80,1/2,1/2]);

%    Calculate the Center of Mass Location relative to the
%    global coord. system
xcm=xcml+x(:,1:length(x(1,:))-1);
ycm=ycml+y(:,1:length(y(1,:))-1);

%    Center of Mass Location Error
devxcm=(randn(1,3)/3.*uxcm).*lengthx;
devycm=(randn(1,3)/3.*uxcm).*lengthy;

%    Add the Center of Mass Location Error in Global

```

```

%   Coordinantes
xcmd=xcm+ones(length(thetaseg),1)*devxcm.*cos(thetaseg)...
-ones(length(thetaseg),1)*devycm.*sin(thetaseg);
ycmd=ycm+ones(length(thetaseg),1)*devycm.*cos...
(thetaseg)+ones(length(thetaseg),1)*devycm.*sin(thetaseg);

%   Store the Resulting Center of Mass Coord. for future
%   reference
xcm40=[xcm40;xcmd(40,:)];
ycm40=[ycm40;ycmd(40,:)];

if length(xcm40) >= 200
    count =count+1;

    figure(2)
    plot(xcm40,ycm40,['b','+'])
    disp(['Current Count is: ', num2str(count*200)])
    disp(['Time for last 200 was: ',num2str(toc)])
    disp(['Convergence is at (0.00001): ...
        ',num2str(max(abs(diff(CoMstdpast))))])
    disp(['Maximum and Minimum CoMstd for last 100',...
        ' iterations: ',num2str([max(CoMstdpast)...
        ,min(CoMstdpast)])])
    tic
    conv=[conv;max(abs(diff(CoMstdpast)))];
    xcm40=[];
    ycm40=[];
end

%   Calculate the Accelerations
ax=diff(diff(xcmd)).02^2;
axcm=[ax(1,:);ax;ax(length(ax),:)];
ay=diff(diff(ycmd)).02^2;
aycm=g+[ay(1,:);ay;ay(length(ay),:)];

%   Center of Mass
CoMx=xcmd*m'./sum(m);

```

```

%    Calculate the standard deviation of the center of mass
%    error
CoMstdpast(2:100)=CoMstdpast(1:99);
CoMerror2=CoMerror2+((CoMa-CoMx)').^2;
CoMerror=CoMerror+(CoMa-CoMx)';
CoMmean=CoMerror/iterations;
CoMstdpast(1)=mean(sqrt(1/(iterations)*(CoMerror2...
    -2*CoMmean.*CoMerror+iterations*CoMmean.^2)));
CoMtrack=[CoMtrack;CoMstdpast(1)];
end

```

```

iterations
convergence=max(abs(diff(CoMstdpast)))

```

```

%    Calculate the Standard Deviation

```

```

CMmean=CoMerror/iterations;
CoMstd=sqrt(1/(iterations-1)*(CoMerror2-2*CoMmean.*...
    CoMerror+iterations*CoMmean.^2));

```

```

%    Display results

```

```

STDResults=mean([CoMstd]);
MaxResults=max([CoMstd]);
MinResults=min([CoMstd]);
disp('([CoMstd])')
[STDResults;MinResults;MaxResults]

```

```

%    Plot Results

```

```

figure(1)
clf
hold
plot(t,[CoMa])
plot(t,[2*CoMstd+CoMa,-2*CoMstd+CoMa], '--')
title('Center of Mass and 2*STD error')

```

```

figure(2)
plot(xcm40,ycm40,['b','+'])
plot(xcm(40,:),ycm(40,:),['W','*'])

```



```
figure(3)
plot([(1:count)*200;iterations],[conv;convergence])
title('Convergence Plot of Maximum Difference in Previous 100
Iterations')
ylabel('Max Difference in STD (m)')
xlabel('Number of Iterations')
```